ANNUAL REPORT

"INVESTIGATION OF IN SITU PHYSICAL PROPERTIES OF SURFACE AND SUBSURFACE SITE MATERIALS BY ENGINEERING GEOPHYSICAL TECHNIQUES" Project

Fiscal Year 1965

N66 35966   **N66 35972**

(ACCESSION NUMBER)   (THRU)

185

(PAGES)

CR 65489

(NASA CR OR TMX OR AD NUMBER)   (CODE)

73

(CATEGORY)

FACILITY FORM 602

by

Joel S. Watkins, Jean Cl. De Bremaecker, Robert A. Loney, James H. Whitcomb, and Richard H. Godson

U. S. Geological Survey
Flagstaff, Arizona

GPO PRICE $ _____

CFSTI PRICE(S) $ _____

Hard copy (HC) ___3,95___

Microfiche (MF) ___1,35___

Work done on behalf of
National Aeronautics and Space Administration
Manned Spacecraft Center
Houston, Texas

NASA Contract T-25091 (G)

Annual Report

"INVESTIGATION OF IN SITU PHYSICAL PROPERTIES
OF SURFACE AND SUBSURFACE SITE MATERIALS BY
ENGINEERING GEOPHYSICAL TECHNIQUES" Project

Fiscal Year 1965

by

Joel S. Watkins, Jean Cl. De Bremaecker, Robert A. Loney,
James H. Whitcomb, and Richard H. Godson

U. S. Geological Survey
Flagstaff, Arizona

Contents

Part I

Annual Report for

"Investigation of In Situ Physical Properties
of Surface and Subsurface Site Materials by
Engineering Geophysical Techniques" Project

Fiscal Year 1965

by

Joel S. Watkins, Jean Cl. De Bremaecker, Robert A. Loney,
James H. Whitcomb, and Richard H. Godson

U. S. Geological Survey
Flagstaff, Arizona

SUMMARY OF OPERATIONS AND RESULTS

During FY-65 the In Situ Geophysical Studies project has prepared and submitted an engineering seismic experiment to NASA for consideration for inclusion on early Apollo missions, developed a technique for seismically detecting near-surface cavities, developed a technique for detecting shear waves in near-surface media, reconnoitered and geologically studied in varying degrees 11 test sites which have geologic structures analogous to those expected on the lunar surface, investigated attenuation of seismic energy in near-surface and unconsolidated media, developed improved empirical attenuation functions for those media and examined relationships between seismic velocity, attenuation and other physical properties of the media.

Results of these investigations have been the subjects of three papers presented orally before scientific societies and are the subjects of five manuscripts now in various stages of review within the Geological Survey. These manuscripts will appear as papers in scientific journals or publications of the Geological Survey probably within the next fiscal year.

Engineering Seismic Proposal

A proposal entitled "Examination of the Lunar Near-Surface Rocks by Engineering Seismic Techniques During Early Apollo Landings" by Joel S. Watkins, J. Cl. De Bremaecker, and Martin F. Kane was submitted to NASA during the report period for consideration for inclusion in the early Apollo missions.

The system, which will operate on less than 20 watts of power and which weighs less than 4.5 kg, basically consists of 3 transistorized amplifiers, a 4-channel tape recorder, 3 miniature detectors, and a low-energy shooting device which is designed to measure the velocity of propagation of the compressional seismic energy through rocks within 20 m of the lunar surface, measure the attenuation of seismic energy in these rocks, the frequency spectra and possibly the velocity of seismic shear waves through the material. Resultant data will be interpreted in terms of thickness of the fragmental layer of rocks on the lunar surface, degree of induration of the near-surface materials, probable bearing strength of the materials and possibly the in situ elastic constants of the materials.

Velocity, amplitude, attenuation and shooting efficiency data on which this proposal was based were collected by the in situ seismic field crew at sites reconnoitered, mapped and cored by the in situ geologic field crew.

Cavity Detection Techniques

Investigation of lava tunnels at two in situ project test sites and a cavity created by a nuclear detonation at the Nevada Test Site has shown that near-surface cavities can be seismically detected by virtue of vibrations of the cavity walls, anomalous attenuations of seismic energy recorded in the vicinity of the cavities, (and where applicable, the brecciated zones adjacent to the cavity), and delays of seismic energy in the vicinity of the cavity. Of these techniques, cavity vibrations are the most

unique and interesting. Although transient seismic waves generated by near-surface explosions are generally greatly attenuated within 0.5 seconds after the explosion, the vibrations of the cavity walls have been observed to persist for as long as four seconds after the blast.

The ease and simplicity with which these vibrations can be recorded make the technique an especially promising one for location of cavities on the lunar surface which would be used by the astronauts as natural shelters for themselves and their equipment. Terrestrial applications include damsite studies, investigations of illicit underground nuclear explosion sites and military applications.

Shear Wave Detection

Angular accelerometers appear to be far more effective for detection of shear waves generated by nearby explosions than conventional 3-component geophones. Angular accelerometers are relatively insensitive to the purely translational motion of reflected, refracted, and diffracted P-wave energy in the wave train following the onset of the head-wave, but are sensitive to the rotational component of the shear wave motion. The unwanted translational motion obscures shear wave motion recorded by the 3-component geophones.

Test Sites

Eleven sites were selected for geophysical experimentation carried out by the in situ project. Eight sites are in volcanic terrains; the other three sites consisted of a site on limestone terrain near Flagstaff, Arizona, project headquarters, which has been used to test procedures and equipment; a site on virtually unfractured and unweathered granite in the Sierra Nevada; and the Meteor Crater area which was selected for geophysical study of impact structures.

3

Data derived from observation of the lunar surface, empirical knowledge of cratering and other studies of lunar surface processes suggest that much of the mare surface consists of finely-broken rock fragments. The layer of broken rock fragments is thought to be of variable thickness and irregular contact with the underlying solid material. Test sites in volcanic terrains were selected to obtain a spectrum of data similar to that which might be obtained during exploration of the mare surface. Finer materials are represented by data from the Cinder Hills site near Flagstaff, Arizona, which consists of a thick accumulation of basaltic ash and cinders; the Mono Ash site immediately north of the Mono Craters in eastern California, which consists of a thick accumulation of rhyolitic ash and lapilli; and the Bishop Tuff site, which consists of several tens of meters of welded tuff overlying alternating layers of unwelded and welded tuffs. The coarser fractions of the lunar surface are represented by sites on S P flow near Flagstaff, Arizona, whose surface consists of blocks ranging in diameter from a few centimeters to a half a meter; the Southern Coulee site, which consists largely of broken blocks of rhyolitic pumice ranging in diameter from a few centimeters to blocks of several meters in diameter; and the Pisgah flow site, whose surface consists of roughly equal portions of aa and pahoehoe lava. The Kana-a flow consists of an aa lava flow covered with cinders ranging from 0 to 5 m in thickness. Massive rocks were investigated at the Sonora Pass and Amboy flow test sites where the outcrops consisted of massive, virtually unfractured and unweathered granite and pahoehoe lava, respectively.

The Kana-a flow site was our prototype site, selected principally for reasons of accessibility rather than for excellence as a lunar analog site. The report on the Kana-a flow data is now virtually complete and consists largely of seismic data found in reports E and F, geologic map cores, and petrography found in report D. Density, porosity, compressional strength,

4

tensile strength, P- and S-wave velocities, and magnetic susceptibilities have been determined from cores taken from this site but have not yet been incorporated into a report pending determination of physical properties from cores taken at other sites.

Similar studies will be completed on all test sites within the next 18 months, and reports prepared and made available to the scientific community. Table 1 summarizes the status of investigations at each of these sites.

Table 1

Site	Seismic Data	Geologic Map	Cores	Petrography	Phys. Prop.
Kana-a flow	X	X	X	X	X
Cinder Hills	X	0			
S P flow	X	X	/	/3	/3
Kaibab Limestone	X	0	/	0	/
Mono Ash	X	0			
Southern Coulee	X	X		/3	/3
Bishop Tuff	X	0			
Sonora Pass	X	0			
Amboy flow	X	/2	/	/2	/
Pisgah flow	X	/2		/2	
Meteor Crater	/1	X2	/	/2	

Explanation

X - complete

/ - partially complete

0 - not applicable

1 - gravity, magnetic and radiation surveys are also underway

2 - relatively complete reports available from other sources

3 - surface sample data, no core data as yet

Amplitude Attenuation and Velocity Data

We have obtained a spectrum of amplitude attenuation and velocity data similar to that anticipated for the fragmental

5

layer on the Moon's surface. These data, which have been collected at each of our 11 test sites, have qualitatively established a relationship between fracturing and amplitude attenuation. Investigation is under way to quantify this relationship.

Theoretical investigations have been carried out concurrently with analysis of field data and have contributed to improvement of field techniques as well as developed a better understanding of the mechanisms of propagation in near-surface and unconsolidated media. Data are currently being digitized and some programs have been written which will permit analysis of attenuation and velocity data faster and more efficiently than is currently possible.

Publication of Results

Partial results of the cavity investigations were presented as an invited paper at the National Speleological Society meetings in June 1965, and two papers dealing with aspects of velocity and amplitude attenuation data were presented at the American Geophysical Union during April 1965. We plan to present the results of cavity and shear wave investigations to the geophysical community at the Society of Exploration Geophysicists Annual Meeting in November 1965. Abstracts of these papers are included in reports B, C, E, and F. We have proposed presentation of certain aspects of the cavity investigation, shear wave investigation, attenuation investigations, and detailed geologic investigations of the Kana-a site at a symposium to be held at the dedication of the Branch of Astrogeology building, Flagstaff, Arizona, in September 1965.

Sufficient copies of the seismic experiment have been submitted to NASA to insure its circulation to interested parties of the scientific community. Reports B, C, D, E, and F consist of manuscripts of papers in varying stages of review within the Geological Survey prior to publication in scientific journals.

PART II A

EXAMINATION OF THE LUNAR NEAR-SURFACE ROCKS
BY ENGINEERING SEISMIC TECHNIQUES DURING
EARLY APOLLO LANDINGS

A PROPOSAL

by

1)   2)   1)
Joel S. Watkins   , J. Cl. De Bremaecker   and Martin F. Kane

1) U. S. Geological Survey

2) U. S. Geological Survey and
   Rice University, Houston, Texas

Technical Contact
E. M. Davin

EXAMINATION OF THE LUNAR NEAR-SURFACE ROCKS BY ENGINEERING

SEISMIC TECHNIQUES DURING EARLY APOLLO LANDINGS,

A PROPOSAL

by

Joel S. Watkins, J. Cl. De Bremaecker and Martin F. Kane

INTRODUCTION

Data derived from visual observations of the lunar surface, telescopic photometry, radiometry, and reflected microwave signals from the lunar surface, from empirical knowledge of cratering, cratering theory, meteoroid flux, and other studies of the lunar surface processes suggest that much of the mare surface consists of finely broken rock fragments. The layer of broken rock frag- ments is thought to be of variable thickness and in irregular contact with the underlying solid material. Thickness of the fragmented rock layer may vary from a few tens of meters to less than a millimeter. It is thickest where it covers floors of older craters and thinnest where walls of young craters cut through into the underlying solid rock of the mare surface. The average grain size probably decreases from the top of the layer where fragments will average much less than a millimeter downward to the bottom of the layer. Coarse, blocky rock may occur locally in the debris layer. Individual fragments may be extremely porous and spontaneously welded together.

Beneath the layer of fragmented rock, near-surface lunar rocks may be shattered and broken as a result of stresses created during the formation of larger craters. The contact between the underlying material and the fragmental layer probably has considerable relief.

Data on the presence or absence, thickness, strength and variation of physical properties with depth in the fragmental layer and in the solid rock of the mare where it is close to the surface are critical to a full interpretation of the fine structure of the lunar surface and the processes which have led to its formation. These same data are also of major importance in the evaluation of bearing strength and other engineering characteristics of the lunar surface which affect systems design and conduct of later lunar missions.

PROPOSED EXPERIMENT

The proposed experiment will measure the velocity of propagation of compressional seismic energy through rocks within 20 m of the lunar surface, attenuation of seismic energy in these rocks, frequency spectra of the energy and possibly the velocity of seismic shear waves through the material. These data will be interpreted in terms of thickness of the fragmental layer, the degree of induration of the near-surface materials, the probable bearing strength of the materials, and possibly the in situ elastic constants of the material.

The usefulness of active seismic surveys during early Apollo missions has been recognized by many scientists concerned with the Apollo program. However, hazards due to explosives deemed necessary for the experiment, and to a lesser extent the weight of the instrumentation, have been cited as reasons for delaying active seismic surveys until at least the fourth mission.

We have found that very small explosives (squibs and caps) and mechanical energy sources (hammer blows) on top of the ground induce enough energy in the ground for short seismic lines. Very small sources have the advantage that they do not create a hazard to an astronaut standing within two feet of the source. Weight of the proposed system is substantially less than that of a conventional system because of reduction of the number of detectors and amplifiers.

Elimination of hazards and reduced weight justify inclusion of the experiment on the first, second, and third Apollo missions on the basis of the engineering and scientific merit of the experiment.

Background. Use of refraction seismology to study both shallow and deep subsurface rock structure has been common for several decades. In recent years it has been used for in situ studies for dams, large buildings, and highways.

The role of refraction seismology in early phases of the lunar exploration program is being investigated by the writers

on behalf of the National Aeronautics and Space Administration in the form of a project entitled "Investigation of in situ physical properties of surface and subsurface site materials by engineering geophysical techniques." Project operations to date have consisted primarily of seismic studies of rock units which are thought to be analogous in structure or mineralogy to rocks of the lunar surface.

Units include basaltic and rhyolitic ash, which are thought to resemble the fragmented layer of the lunar surface; andesitic and basaltic lava flows, whose brecciated surface may resemble coarser parts of the fragmented layer. The interior of these lava flows, although not brecciated, are badly fractured and their structure probably resembles the shattered solid rock of the mare surface beneath the fragmented layer. Most velocities observed in the basaltic ash are between 240 and 370 mps (meters per second) and their mean Q (a measure of attenuation) is about average for unconsolidated materials which we have studied. Velocities in rhyolitic ash are slightly higher, ranging generally from 400 to 630 mps. The mean Q is lower than that observed in basaltic ash. The lava flows consist of two or three seismically distinct layers whose velocities increase with depth probably as a result of decreased fracturing and brecciation. Although laboratory measurements of velocities on core samples from these flows exceed 5000 mps in some cases, the in situ velocities generally range from 750 to 1200 mps for lower layers and no velocities

greater than 1550 mps have been observed to date. Velocities of surface layers (upper 2-3 m) are very low but data is inadequate to define the range. Velocities of lower layers in both flows have about the same range but the Q of the basaltic flow is much higher than that of the andesitic flow. Geologic study of outcrops and cores suggest that the higher attenuation (lower Q) in the andesitic flow may be caused by a higher degree of polygonal jointing in the andesite.

Data have also been collected from a welded rhyolitic tuff and a pumiceous rhyolitic flow. Structure of the welded rhyolitic tuff may be analogous to fine spontaneously (vacuum) welded material of the lunar surface, and pumiceous rhyolitic flow rocks are thought to be the best terrestrial analogs of extremely porous, vesicular lavas postulated by some investigators on the basis of rock melt behavior in a hard vacuum. Data from the welded rhyolitic tuff did not agree with our ideas formed during field reconnaissance of the site. The material seems uniform in texture and composition during hand specimen study, but the range of velocities and Q was very large. The only explanation we can suggest at the present time to account for the wide variation in Q is that the data include many multiple reflections from horizontal interfaces of welded and non-welded zones and from many near vertical fault planes; it appears necessary to postulate unrecognized lateral variations in texture to account for the variations in velocity.

Velocities observed in the pumiceous flow range from 300 to 2200 mps and Q also has a large range. This wide range of values is not surprising considering the wide range in densities and degree of brecciation observed in this material. This site as well as all other sites will be cored along seismic lines in order to establish the type and physical properties of rocks traversed by the seismic energy. As this proposal is being prepared, core data have been obtained for only the basaltic flow. However, all sites have been mapped and surface samples collected for study. A few shots recorded on a massive, glaciated granite outcrop yielded a uniform velocity of 5000 mps and a very high Q. These data represent the highest velocities and lowest attenuations which we have recorded.

Studies of energy coupling which we have conducted suggest that shot holes are not necessary for short traverses such as those described in this proposal if the noise level is no greater than the terrestrial noise level on a very quiet day.

Additional data will be collected during the remainder of fiscal year 1965 and during fiscal year 1966 from basaltic lava flows with pahoehoe surfaces, brecciated and solid rocks in and around Meteor Crater, Arizona, and from four to five sites consisting of unconsolidated, semiconsolidated and consolidated detrital rock. Rocks at these latter sites will be studied because of probable analogy to the fine-grained rocks of the lunar surface fragmental layer.

Quantitative analyses of energy spectra are not yet complete but qualitative examination of bandpass playback of records suggests that although modal frequency increases with velocity, the increase is not uniform. Variations in modal frequency variations seem to be related to variations in coupling of energy sources to media and are affected by both the nature of the sources and the media. Spectral studies are continuing in an effort to better understand this phenomenon. We are also studying means of generating shear waves in unconsolidated material which, if they are successful and do not require elaborate induction devices, may provide data for the calculation of in situ elastic constants of the lunar rocks.

These studies of potentially useful lunar seismic techniques will provide a broad range of data useful in the design and construction of the instruments for the proposed and other experiments, and for the interpretation of data obtained by astronauts during lunar exploration.

Description of the experiment. During a traverse on the lunar surface, an astronaut will emplace three seismometers at intervals of 50 m along a straight line extending away from the Lunar Excursion Module. The first seismometer will be emplaced approximately 10 m from the LEM and the most distant at about 110 m. Amplifiers and tape unit will remain in the LEM. After emplacement of the most distant seismometer, the astronaut will walk along the line of seismometers and induce energy into the ground

at intervals of 5 to 10 m by means of small explosions, an electro-mechanical device, or a mechanical device. The energy received by the detectors will be amplified and recorded on tape in the LEM along with the shot instant.

To initiate and record an energy pulse, the astronaut will start the tape transport from his location in the field; in approximately 4 sec, when tape transport is operating at a full speed of 4.5 cm per sec, the amplifiers will be turned on by a simple timer. Approximately 5 sec after the tape transport is started, the energy pulse will be automatically induced in the ground by a second timer on the induction device. Tape unit and amplifiers will remain in operation for an additional 5 sec (10 sec overall) before being stopped by the timer in the LEM. The 4 sec delay in turning on amplifiers allows the tape unit to attain full speed without exceeding combined power requirements of tape unit and amplifiers in their operating modes. The 5 sec recording time is adequate to record all refractions and near surface reflections.

Upon completion of the traverse, the astronaut disconnects the exterior equipment and abandons it. Total elapsed time will require an estimated 30 min. Tapes will be played back, digitized and analyzed upon return of the astronauts to the Earth.

Elapsed time between induction of energy and arrival of energy at the detectors is the most important property to be measured. These data permit determination of seismic velocities

of underlying materials provided that the velocity of the seismic energy does not decrease with depth. Available data concerning the fine structure of the lunar surface suggest that this assumption is justified for rocks within 20 m of the surface. Velocity data in turn permit determination of thickness of the surface layer and generalized estimates of its degree of induration and bearing strength. Other characteristics of the seismic energy such as Q, amplitudes of the various frequency components of the seismic energy, and, if detected, shear waves, Love waves and Rayleigh waves, may be used to calculate other physical properties of the material. Our research in these techniques has been discussed in previous paragraphs.

Equipment. Equipment characteristics can be stated with confidence on the basis of the available data. Data concerning the coupling of seismic energy to the ground, the attenuation of the seismic energy, and the spectra of the seismic energy at various sites as determined by our experiments suggest that the amplifiers should include automatic gain control, have a frequency band pass of approximately 15 to 150 cycles per second (cps), a dynamic voltage range of 120 db and an internal noise level of about 0.01 microvolts rms. The tape unit must have equal or less internal noise and frequency band pass characteristics but a dynamic voltage range of 40 db will be sufficient because of automatic gain control in the amplifiers.

State-of-the-art equipment exists which, with some modification, can be used for flight hardware. Maximum weights of modified equipment components for the experiment are as follows:

3 transistorized amplifiers	1.35 kg
4 channel tape recorder	0.90 kg
Wire to transmit signal from detectors to tape unit	1.15 kg
Shooting device, including explosives if explosive devices used rather than electromechanical or mechanical devices	0.90 kg
3 detectors	0.20 kg
Total weight	4.50 kg

Power requirements for the system will be less than 20 watts during warm-up and operation. Total operating time will be about 4 min in 10 sec increments. It is assumed that a power source will be available in the LEM for use by all the scientific experiments, hence, its weight is not included in the above tabulations. Shape is not a critical requirement and the system will occupy less than 7000 cm^3.

Although the proposed system is simple and streamlined to reduce weight, complexity and power requirements, data will be equivalent to data from a conventional array of 11 to 21 detector-amplifier-recorder systems with shots at each end and in the center.

Amplifiers exist which meet all of the requirements of the experiment with the exception of the weight requirements. Discussions with knowledgeable persons of the electronics industry

lead us to believe that the 1.35 kg weight for the three transistorized amplifiers is a conservative estimate of the maximum weight. Tape recorders designed to withstand the rigors of space flight and which require very little modification for the experiment have been developed by at least one commercial organization. Detectors are state-of-the-art.

The principal unknown is the shooting device which will require development and field testing in areas where rocks and terrain are analogous to those expected on the lunar surface. The device as described in previous paragraphs will be a relatively simple device consisting of an energy source, an ignition source and perhaps a piston-like transducer to couple the energy to the surface. The device is simple and hence design and fabrication problems should not be great.

Other factors.- A previous knowledge of amplitudes of lunar microseismic noise in the frequency band recorded by the proposed instrumentation would be of value in the determination of the minimum amount of seismic energy which we must induce in the ground to successfully complete the experiment. The proposed experiment, however, incorporates an adequate energy source to overcome any likely microseismic noise level encountered on the lunar surface.

The flight package will not be susceptible to radio frequency and magnetic interference, and in turn, will not produce radio

frequency or magnetic interference.

No telemetry is required for the experiment.

The Principal Investigator requires approximately ten days exclusive use time for the data.

PART II B

SEISMIC INVESTIGATION OF NEAR-SURFACE CAVITIES --
A PRELIMINARY REPORT

UNPUBLISHED MANUSCRIPT -
FOR OFFICIAL USE ONLY

by

Joel S. Watkins, Richard H. Godson and Kenneth Watson

U. S. Geological Survey
Flagstaff, Arizona

SEISMIC INVESTIGATION OF NEAR-SURFACE CAVITIES--A PRELIMINARY REPORT

by

Joel S. Watkins, R. H. Godson
and
Kenneth Watson

U. S. Geological Survey
Flagstaff, Arizona

ABSTRACT

Recent field investigations have successfully delineated two lava tunnels located a few feet below the surface of the ground and a cavity formed as a result of an underground nuclear explosion and subsequent collapse of the overlying rock at the Nevada Test Site. The top of the cavity at the Test Site was 25 m below the surface.

Three seismic phenomena--vibrations of the cavity walls, anomalous amplitude attenuations, and delays in arrival times-- have been observed in the vicinity of the cavities. Of these three phenomena, wall vibrations are the most diagnostic for location and delineation of cavities. Anomalous attenuations of amplitudes and delays in arrival times can be caused by local geological conditions other than cavities, but provide important supplemental evidence.

SEISMIC INVESTIGATION OF NEAR-SURFACE CAVITIES--A PRELIMINARY REPORT

by

Joel S. Watkins, R. H. Godson
and
Kenneth Watson

U. S. Geological Survey
Flagstaff, Arizona

INTRODUCTION

Recent seismic field investigations conducted by the U. S. Geological Survey have successfully delineated two lava tunnels a few feet below the surface of the ground and a cavity formed as a result of an underground nuclear explosion and subsequent collapse of overlying rock at the Nevada Test Site. The top of the cavity at the Nevada Test Site was 25 m below the surface of the ground. Seismic techniques developed and tested during these investigations show promise for location of cavities at much greater depths and in different geological environments.

The studies were undertaken on behalf of the National Aeronautics and Space Administration in order to test the feasibility of seismic location and delineation of cavities on the lunar surface during the Apollo manned landings because lava tunnels, if found on the lunar surface, could be used as natural shelters by astronauts. In certain instances, tunnels also might constitute a hazard to astronauts traversing the lunar surface on foot or in vehicles.

B-2

METHODS OF DETECTION

Three seismic phenomena--vibrations of the cavity walls, anomalous amplitude attenuations, and delays in arrival times-- have been related to the cavities, the associated brecciated zones and a chimney above one cavity during our investigations. Of these three phenomena, wall vibrations are the most diagnostic for location and delineation of cavities. Anomalous attenuations of amplitudes and delays in the arrival times, although they can be caused by local geologic conditions other than cavities, provide important supplemental data on cavity detection and delineation.

Free oscillations.- Although we originally thought that the waves detected over the cavities were standing waves formed when compressional waves traversed the air in the cavity and reflected off the borders of the cavity, calculations of the seismic impedance match between the rocks of cavity wall and air within the cavity suggest that it is unlikely that enough energy can be transferred from the wall to the air and back to the walls to account for the amplitudes which we observe. Therefore, it has been tentatively concluded that the phenomenon consists of vibrations of the cavity walls.

If the phenomenon does consist of free oscillations, it will be equally valuable for lunar and terrestrial surveys. Calculations are continuing and it appears that model studies may be necessary.

In the field, wall vibrations have been excited in cavities by direct and refracted waves initiated by an explosion near the surface of the ground. The seismic energy spectrum is sufficiently broad to induce wall vibrations in cavities whose dimensions range from a few feet to several hundred feet.

The vibrations propagate through the rock to the surface where they are sensed by conventional seismometers, amplified, and recorded on the seismograph. Figure 1 shows a recording made over a lava tunnel in the Pisgah lava flow in the Mojave Desert of southern California. Note that the initial ground motion generated by the explosion is greatly attenuated within 0.3 seconds after the explosion. Wall vibrations persist much longer and in some instances, have been recorded for as long as 4 seconds after the explosion. Note also that the waves are laterally coherent and that the dominant frequency is relatively uniform with time. These two characteristics of wall vibrations suggest that it will be possible to identify them by correlation techniques when their amplitudes are much lower than random noise amplitudes in the area.

Multiple geophone and multiple shot point configurations, which are common in reflection seismology, should also be useful in signal to noise enhancement of not only wall vibrations but other anomalous wave characteristics associated with the cavity and the adjacent brecciated zones.
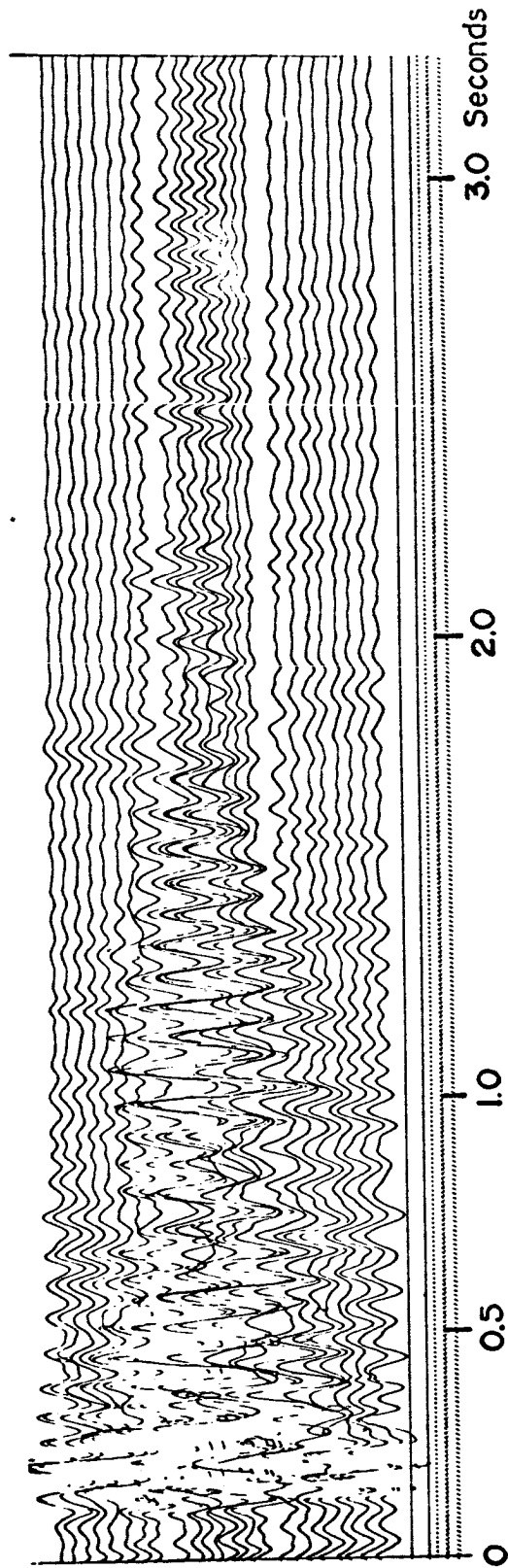
Figure 1. Portion of a seismogram recorded over a lava tunnel in the Pisgah lava flow, Mojave Desert, southern California. Note prominent in-phase cavity vibrations in center of seismogram.

Anomalous amplitude attenuations.- Studies conducted by the
U. S. Geological Survey on behalf of the National Aeronautics
and Space Administration during the past year of seismic amplitude
attenuation in near-surface rocks suggest that variations of
attenuation of amplitudes in unconsolidated or semiconsolidated
materials are primarily caused by absorption of energy by non-
elastic motion of uncemented or poorly cemented particles of the
rock, and by reflection and diffraction from joints and fractures
in the rocks. Decreased cementation or increased jointing or
fracturing increases attenuation of amplitudes of waves traversing
the material.

In the special case of a cavity, amplitudes of waves traversing
the cavity will generally be decreased as a result of reflections
at interfaces between the cavity and the surrounding rock, conver-
sion of a portion of the energy to wall vibrations, and, in the
case of a nuclear cavity, by reflection and diffractions in the
fractured zone adjacent to the cavity or chimney above the cavity.

In order to locate either the cavity, the jointed and frac-
tured region about the cavity, or the collapsed chimney above a
nuclear cavity by means of energy attenuation studies, it is
necessary that seismic waves traverse the cavity, the fractured
zone, or the chimney as they travel from the shot point to the
detectors.

Reflected waves have been successfully used (Cook, 1964)
to delineate solution cavities in salt beds and we have observed

B-6

anomalous reflection amplitudes over lava tunnels. A critical parameter in the use of reflected waves, however, is the existence of a good reflecting horizon below the cavity which, in our studies at the Nevada Test Site, did not exist.

Refracted waves which traverse the cavity and adjacent fractured and collapsed zones can be generated in most areas because surface materials generally have lower velocities than the rocks at depth. Even in massive igneous rocks, the propagation velocity of seismic energy increases as a function of pressure for depths up to several miles.

Surface waves and shear waves may also show anomalous amplitude variations in the vicinity of the cavity, the chimney or the jointed zone. Additional studies will be required to evaluate the usefulness of these arrivals, however.

In the nuclear cavity case, rocks on the surface of the ground directly above the focus of the explosion, are visibly fractured. These fractures should attenuate amplitudes of waves such as direct arrivals from nearby shot points which horizontally traverse the fracture zone. Field tests of this theory will be discussed in following sections.

Delays of arrival times.- Theoretically, waves traversing the cavity will be delayed because of the longer travel time required for the wave to go around the cavity. For deep cavities, however, wave paths exist in the vicinity of the cavity along

B-7

which the energy can propagate with an insignificant travel
time delay (that is, only a small fraction of the energy in the
wave front is delayed). The best opportunities to observe delays
of arrival times occur where cavities are near the surface or
where a large chimney is developed over a nuclear cavity. As
the top of the chimney approaches the surface of the ground, time
delays in the arrivals of the direct wave, refracted waves,
reflected waves, surface waves, and perhaps shear waves, become
progressively easier to identify. Without the benefit of a
high chimney, waves reflected from a discontinuity below the
cavity seem to offer the best possibility of success in detecting
a delay in the arrival times caused by deep cavities.

RESULTS OF FIELD STUDIES

Our first studies were conducted over a small lava tunnel in the Kana-a lava flow approximately 24 km northeast of Flagstaff, Arizona. The top of the tube is approximately 1.5 m beneath the surface of the ground and the diameter of the tube is about 2 m. The flow consists of two layers of basaltic lava which transmit the seismic energy at significantly different velocities. The upper layer consists of scoriaceous, vesicular, and fractured aa basalt. At depths ranging from 1.5 to 4.5 m below the surface of the flow, the flow rock changes abruptly to hard, dense, sparsely vesicular basalt which transmits seismic energy at a much higher velocity.

A linear array of 24 geophones was laid out perpendicular to and centered over the longitudinal axis of the tube. Shots of varying sizes were detonated along the seismic array and the projection of the array at distances ranging from 0 to 75 m from the axis of the tunnel. A pronounced anomaly in amplitudes of waves refracted through the dense lava at the base of the flow from a shot 75 m from the axis of the tunnel was observed directly over the tunnel and for a short distance along the seismic array on the side of the tunnel away from the shot point. These data are shown in figure 2. Small variations in amplitudes of reflected waves from horizons below the tunnel also were observed. A small delay was also noted in arrival times of the reflections but the
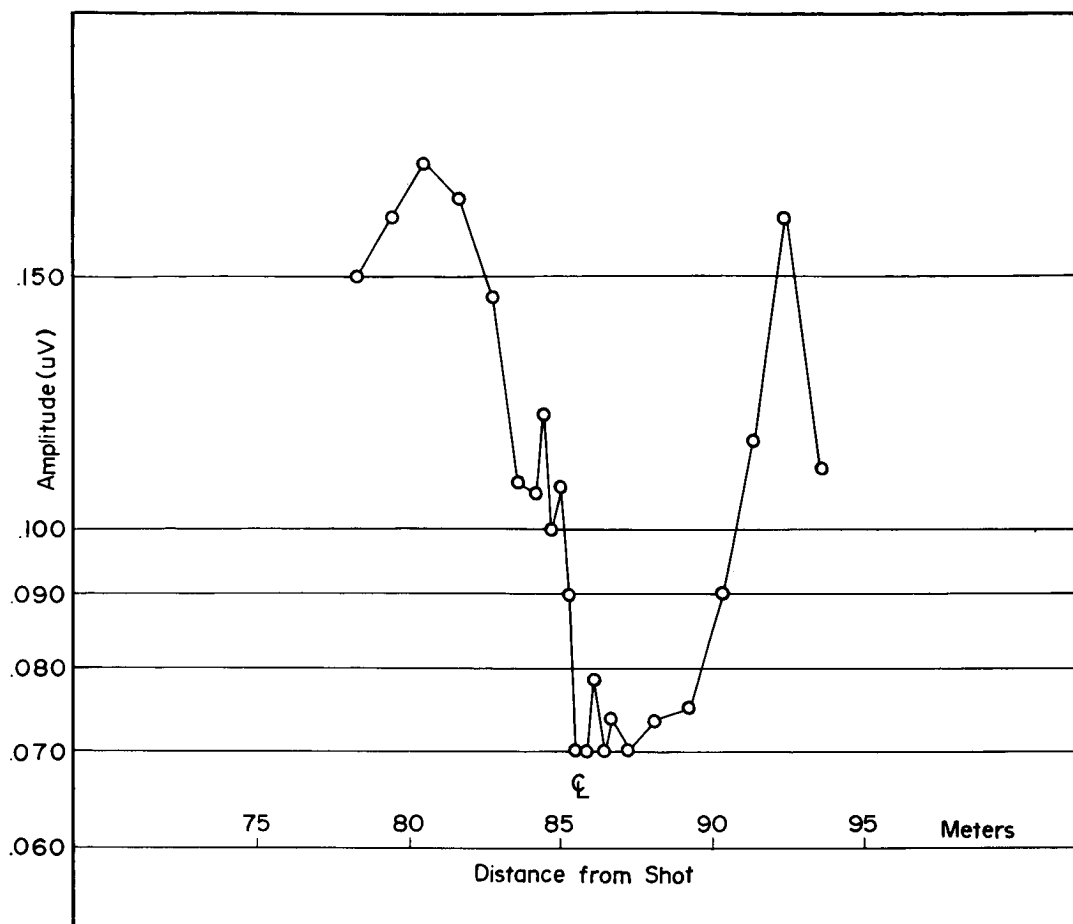
Figure 2. Amplitudes of first-arriving seismic energy
recorded over a lava tunnel in the Kana-a lava flow
near Flagstaff, Arizona. Dip of the emerging wave
front causes the amplitude anomaly to be most pro-
nounced on the side of the tunnel away from the shot.

noise level made it difficult to define the time delay with certainty. No time delays were observed in the refracted arrivals.

One interesting and singular phenomenon observed was the presence of an extremely high-frequency component in the direct arrival from a blasting cap detonated over the axis of the tunnel. It is thought that this high-frequency component represents vibrations induced in the relatively thin lava cap rock over the tunnel.

In retrospect, cavity vibrations can be identified on the Kana-a records. The frequency of the vibrations, 36 cps, is nearly the same as that of the many reflections recorded in the area. Hence, the vibrations were not as obvious as they were in other areas where frequencies differed significantly from those of background noise. Also, on records of shots which should show vibrations best, the amplifiers were overdriven.

The next experiments were conducted in much the same manner over a lava tunnel in the Pisgah flow in the Mojave Desert of southern California. Pisgah flow is a basalt flow located adjacent to and south of U. S. Highway 66, approximately 60 km east of Barstow, California. The flow surface is characterized by roughly equal portions of aa and pahoehoe lava, the tunnel being located in the area of pahoehoe lava.

The tunnel we studied was the largest tunnel which we found and it could be traced for at least 0.7 miles northward from the

base of the Pisgah cinder cone. During studies on the Pisgah
flow we first recognized wall vibration waves and developed
procedures for inducing strong oscillations. It was found that
shots fired several hundred feet away and buried 1 or two feet
below the surface in holes hacked out in the lava contained
enough energy at the proper frequency to induce strong waves in
the cavity.

Amplitudes of wall vibrations are high in those seismometers
immediately over the lava tunnel but are sharply attenuated in
seismometers not located over the cavity. A record showing
cavity vibrations is reproduced in figure 1.

The third area of investigation was centered about the shot
point for nuclear explosion U4B in Yucca Valley of the Atomic
Energy Commission's Nevada Test Site. The U4B shot consisted of
a low yield nuclear device placed approximately 440 m below the
surface of the ground. After the shot, an extensive chimney was
formed, rising to within 25 m of the surface of the ground.
Post-shot drilling revealed an open cavity at least 14 m high.
The exact diameter of the cavity is unknown but it is thought
to be 30 m or more. Figure 3 is a cross-section showing geology,
shot point, chimney, and seismic spreads on the surface. Data
were obtained from three seismic spreads of 24 detectors each
spaced at intervals of 10 m. Three detectors were overlapped
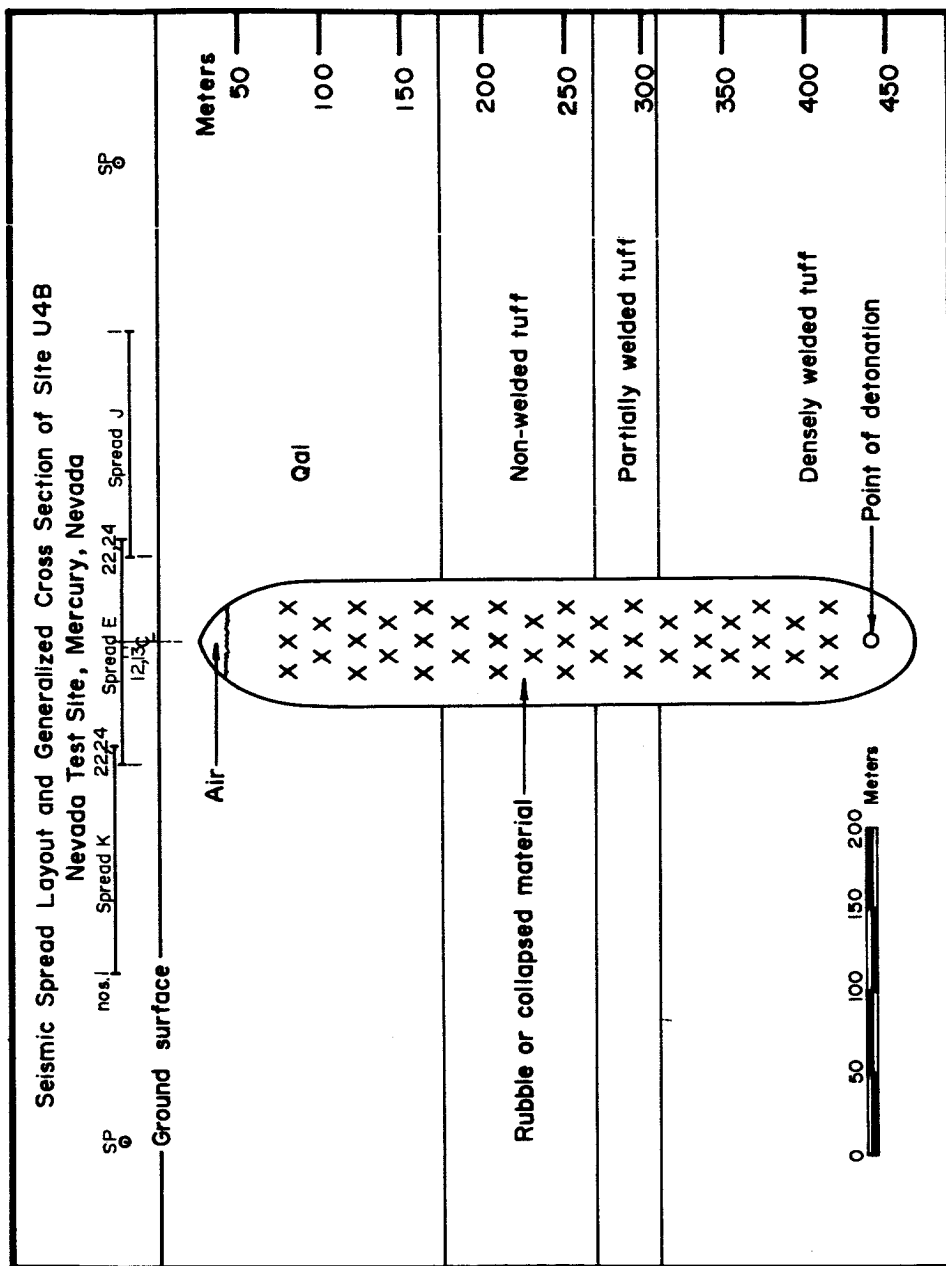on adjacent spreads in order to normalize amplitude variations

B-12

Figure 3. Geology of the U4B nuclear shot point and vicinity and locations of seismic lines.

B-13

caused by different shot hole conditions. Data from these spreads were composited and composite records showing energy received from both ends of the array are shown in figures 4 and 5. Wall vibrations can be clearly seen in the traces of the detectors immediately over the cavity in both figures 4 and 5.

Cavity vibrations shown on figure 4 are not as coherent as those in figure 1, but are easily identifiable. Examination of the earlier, noisier part of the record suggests that high amplitude waves are present and that correlation techniques could enhance signal to noise ratios.

Two pronounced later events are indicated in figures 4, 5 and 6 by darkening of one trough of the events. (Figure 6 is a replay of tape 39179 which also appears as the middle record of figure 4. The time base and filtering were varied in order to improve resolution of wall vibrations in figures 4 and 5 and of later events in figure 6.) The later events are indicated on figure 7 as B and C. Event A is the P head wave. The cause of event B is not entirely clear; however, it is thought that it may be a trapped wave in a low velocity layer within the alluvium.

Although arrival times of the first energy, A, show no anomalies in the vicinity of the cavity, arrival times of both events B and C are delayed in the vicinity of the cavity. This suggests that the first arriving energy traveled in the solid material above the cavity, but that significant quantities of energy of events B and C was at deeper levels where it traversed

Figure 5. Composite seismogram observed at the U4B nuclear shot site, Nevada Test Site from a chemical explosion south of the seismic lines. Note the cavity vibrations recorded by seismometers over the cavity in the center of the spread.

Figure 4. Composite seismogram observed at the U4B nuclear shot site, Nevada Test Site from a chemical explosion north of the seismic lines. Note the cavity vibrations recorded by seismometers over the cavity in the center of the spread.
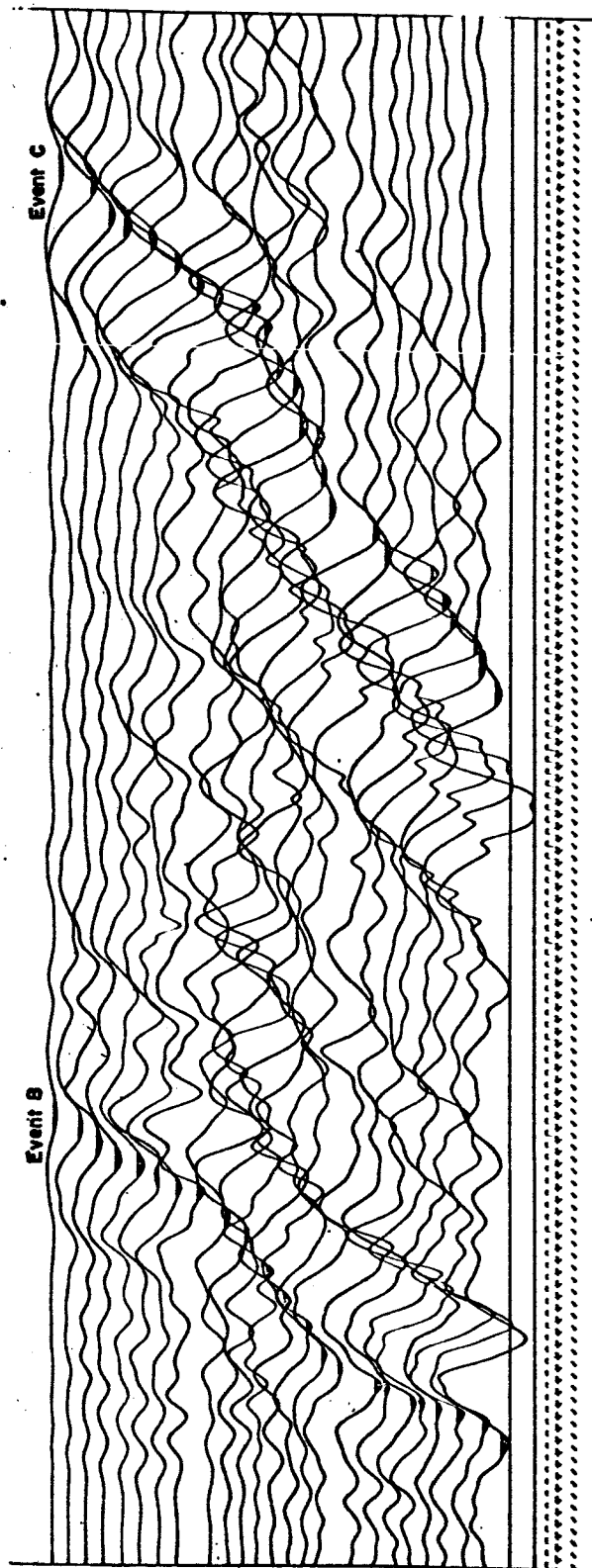
Figure 6. Replay of tape 39179 showing delays in events B and C in the vicinity of the U4B shot point. A trough of each event has been darkened for emphasis.

either the cavity or the chimney or both. The delay in event C,

which is thought to be a Rayleigh wave, is particularly significant

because of the ease with which Rayleigh waves can be generated in

unconsolidated or semi-consolidated alluvium overlying more rigid

strata. It should therefore be possible to detect chimneys

extending into the alluvium over other nuclear shot points with

relative ease. The delay in event B confirms the existence of

the chimney. The maximum depth to the horizon in which event B

is propagated can be estimated and this depth in turn will yield

a maximum depth for the top of the chimney. The width of the zone

in which the delay occurs probably represents a maximum width

of the chimney. Reduced travel time data are shown at the bottom

of figure 7 and are more distinctive than normal travel time data.

Examination of amplitudes of first arrivals (figures 8, 9

and 10) shows an anomalous decrease in amplitude over the cavity

and for a short distance on the side of the cavity away from the

shot. Plotted data in figure 8 were scaled from records shown

in figures 9 and 10, which are replays of tapes 39179 and 39178

shown in figures 4 and 5.

The empirical method used to reduce data shown in figure 8

is as follows. Data were normalized for shot point variations,

and an amplitude function, $A_e = ae^{-bd}$ (A_e = amplitude,

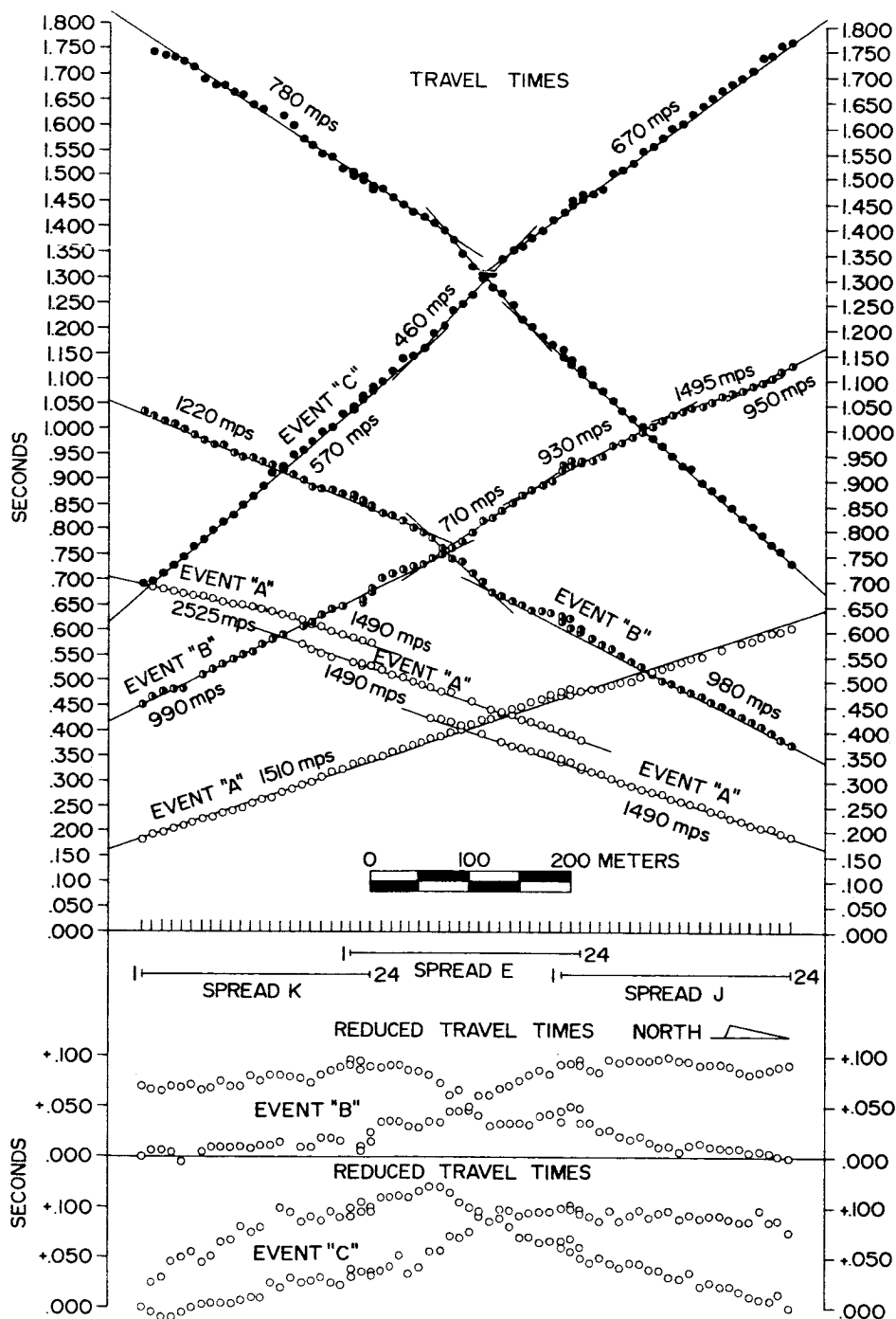d = distance from shot point, and a and b are arbitrary

Figure 7. Travel times of selected events recorded in the vicinity of nuclear test site U4B. Event A is the first arrival; event B is thought to be a trapped wave in a layer within the alluvium, and event C seems to be a Rayleigh wave. Note distinct flexures in reduced travel times ($t_r = t_o - x/v$) shown at bottom of figure.
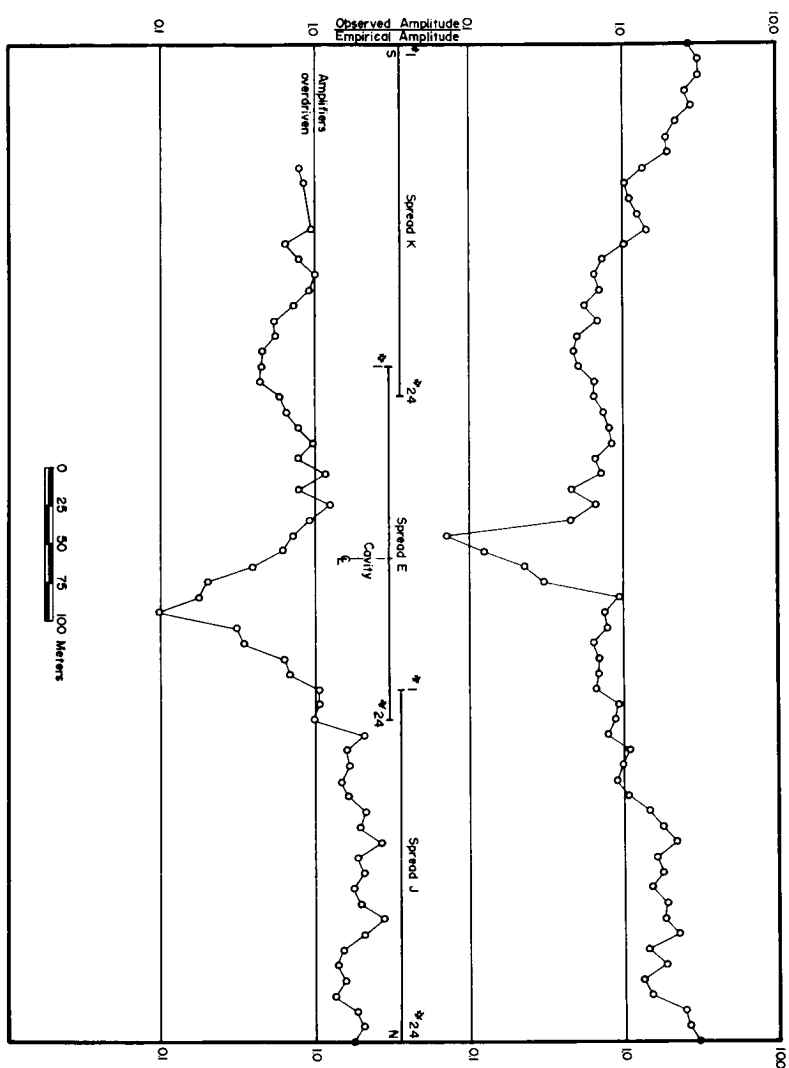
Figure 8. Ratio of observed amplitudes of first arriving seismic energy recorded in the vicinity of the U4B site at the Nevada Test Site to an empirical amplitude function, $A_e = ae^{-bd}$. Data in the upper part of figure were obtained from a shot south of the seismic lines; data in lower part of the figure are from a shot north of the lines. Differences in shot point locations cause asymmetry in amplitude anomalies.
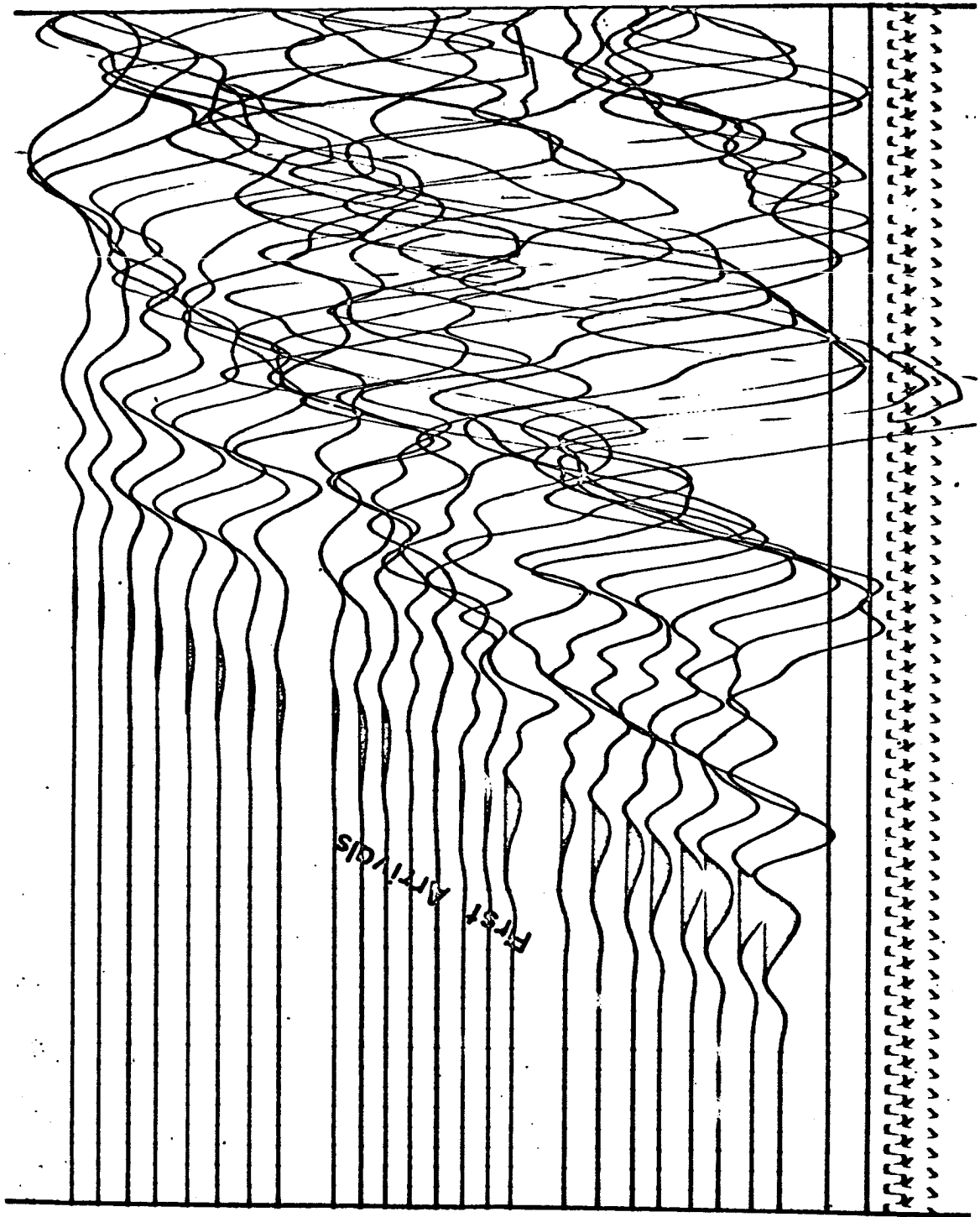
B-20

Figure 9. A portion of a seismogram recorded over the cavity at the U4B site showing attenuation of amplitudes of first-arriving energy from the north shot point.
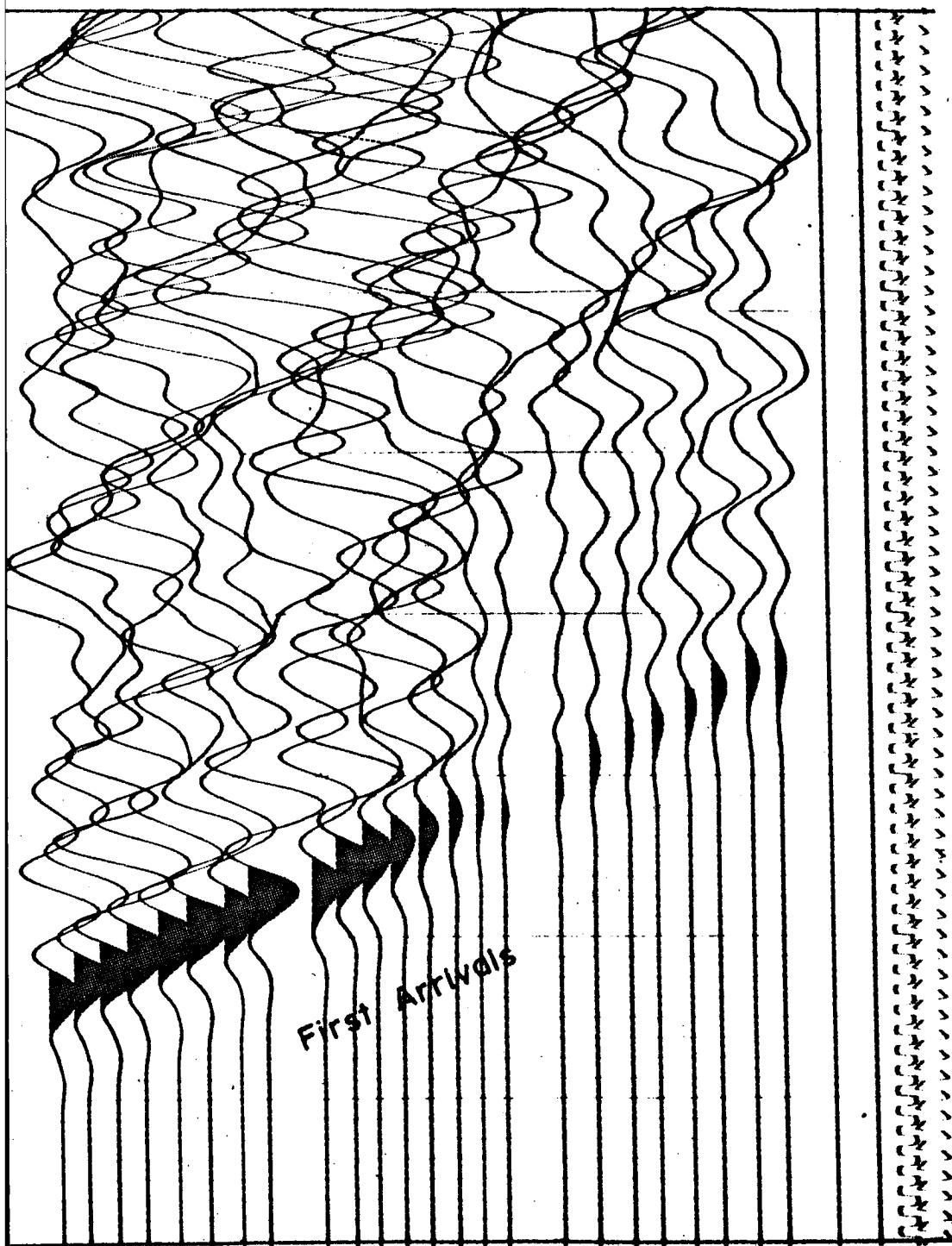
First Arrivals

Figure 10. A portion of a seismogram recorded over the cavity at the U4B site showing attenuation of amplitudes of first-arriving energy from the south shot point.

First Arrivals

constants), was found to fit the observed data. The ratio, A_e/A_o, (A_o = observed amplitude), was computed for each point and plotted as shown in figure 8.

Data in figure 8 show that amplitudes directly over the nuclear focus and on the sides of the nuclear focus opposite shot points are reduced by as much as an order of magnitude relative to the empirical function. The slight asymmetry with respect to the epicenter suggests that the axis of the cone of fractured material above the focus is inclined slightly to the north.

Anomalies in amplitudes of direct arrivals are probably the most useful of the amplitude anomaly data in terms of location of cavities caused by underground nuclear explosion. Direct arrivals are easy to generate, amplitudes are easy to measure, and jointing which causes the amplitude anomalies is thought to be developed over most of the underground nuclear-induced cavities, even though the jointing may not be obvious to the naked eye in every instance.

Reflection arrivals cannot be observed in some areas (we were able to observe only poor reflections in this area and were not able to use them for study of the cavity or chimney), and refracted arrivals, although possible to generate in all areas, often require large charges and deep shot holes. (We did not attempt deep refraction shots.)

We attempted no noise canceling seismometer arrays or shooting patterns although previous investigators in Yucca Valley have significantly enhanced signal to noise ratios of reflection data with these techniques.

A number of other seismic phenomena also seem promising, for example: (1) Waves traversing a cavity and/or a chimney should exhibit interference and diffraction patterns. (2) A mechanical energy source capable of generating variable frequency signals should improve resolution of cavity vibrations.

SUMMARY

Vibrations of cavity waves have been detected in a cavity 25 m below the surface. Large amplitudes and long duration of the signal suggest that the vibrations can be detected in cavities of similar dimensions at much greater depths. Detectable vibrations have also been generated in near surface cavities with dimensions of a few meters. Chimneys, where they exist, can probably be located by anomalous amplitudes and travel time delays in refracted, or reflected or surface waves. Jointing of the near-surface rocks caused by underground explosions causes significant anomalies in amplitudes of direct arrivals from small near-surface explosions.

REFERENCES

Cook, J. C., 1964, Seismic mapping of underground cavities
using reflection amplitudes [abs.]: Soc. Explor. Geophysicists
1965 Yearbook, p. 220.

PART II C

SHEAR-WAVE DETECTION

UNPUBLISHED MANUSCRIPT
- FOR OFFICAL USE ONLY -

by

James H Whitcomb

U. S. Geological Survey
Flagstaff, Arizona

SHEAR-WAVE DETECTION

by

James H. Whitcomb

U. S. Geological Survey
Flagstaff, Arizona

ABSTRACT

Shallow (less than 20 m) seismic refraction investigations of in situ materials showed that the SH-wave is usually immersed in a high noise level, presumably of P-wave nature, when recorded by 3-component geophones. Angular transducers record SH-waves while excluding all energy of a P-wave nature because the curl of the displacement of the P-wave is zero and that of the S-wave is not. Results of field tests of two angular accelerometers showed that angular transducers enable better SH-wave detection than 3-component transducers.

SHEAR-WAVE DETECTION

by

James H. Whitcomb

U. S. Geological Survey
Flagstaff, Arizona

INTRODUCTION

The problem of generation and detection of shear-waves (S-waves) "in situ" in near-surface materials has been under investigation during the majority of FY 1965. Various techniques of generation and detection of shear-waves (S-waves) in situ were tried using 3-component geophones arranged in different patterns to enable positive identification of the S-wave. Limited success was achieved in this work because the energy from the SH-wave (horizontally polarized S-wave), which is detected by the transverse-oriented geophones, was immersed in a high noise level. This noise presumably comes from side reflections and refractions of the earlier P-wave which, because of the short distances involved, is not widely separated in time from the SH-wave.

Our investigations indicated that an improved system of SH-wave detection which would exclude all P-wave energy such as a system of angular transducers was needed. The exclusion of P-waves by angular transducers is based on a mathematical characteristic of body waves; i.e., the curl of the P-wave displacement is zero and that of the S-wave is not. The angular transducer measures only rotational motion which is proportional to the curl of the displacement, and the unwanted P-wave motion is filtered out leaving only the S-wave motion.

ACCELEROMETER TESTS

<u>AA 17 Angular Accelerometer</u>.- A Statham model AA 17 angular accelerometer was obtained for the initial field trial of SH-wave angular motion detection. The accelerometer's frequency characteristics were those of a low-pass filter with a 3 db cutoff frequency of about 7 cps. Response to angular acceleration was 11.1 mv per rad per sec^2 and sensitivity to linear acceleration along any axis was about 0.050 mv per g.

The initial area chosen for the AA 17 trial was the Kaibab Limestone test site near Flagstaff, Arizona. The AA 17 was placed at successive 10 m intervals for a series of shots made at a common point. A buried dynamite cap was used for the generation of SH-waves because previous research with 3-component geophones indicated that SH-wave generation is associated with any type of explosive discharge in near-surface ground materials.

Figure 1 shows the composite of traces recorded from AA 17 for 8 locations at 10 m intervals using the same shot point. Arrival times of the P- and SH-wave first energies are marked on the traces; P-wave times were taken from traces of conventional vertical and radial geophones at corresponding stations. Because of the limitations imposed by the use of a single angular transducer, the variation of source energy and instrument settings for each shot produced traces of widely varying character and amplitude which prevented positive identification of the SH-wave past the fourth trace. A time-distance plot of P- and SH-wave arrival times is shown in
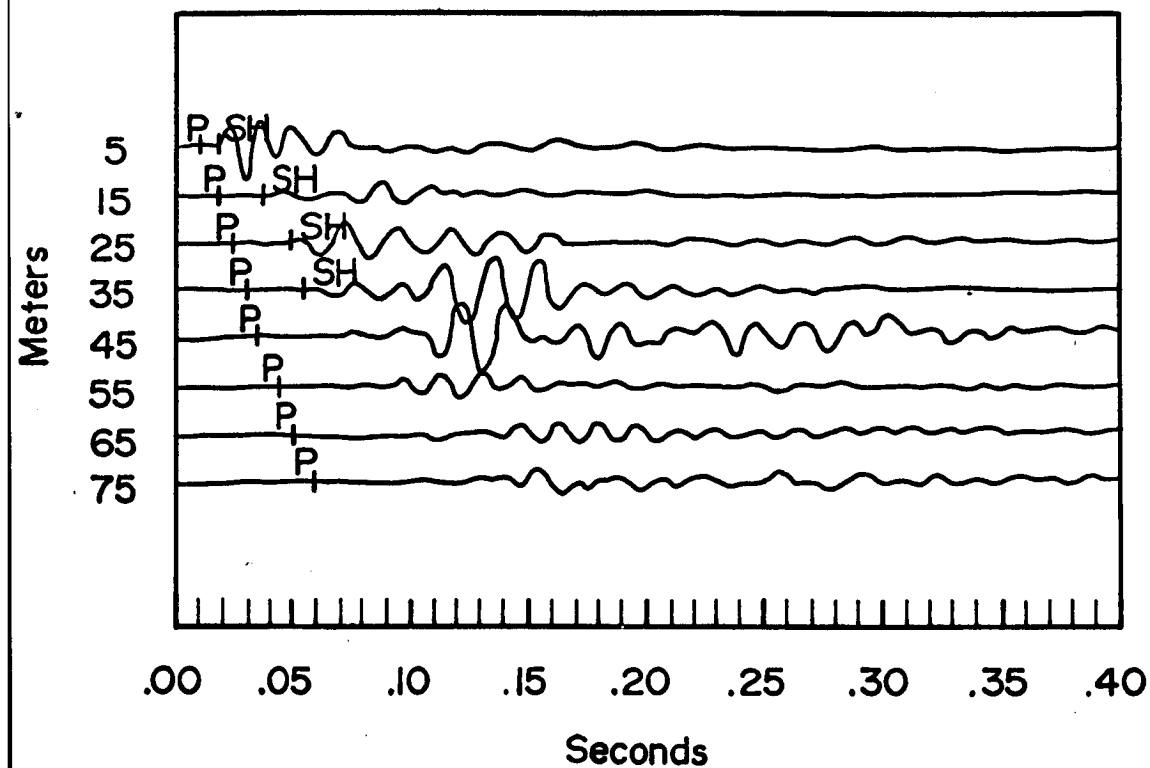
Figure 1. Traces from the AA 17 angular accelerometer recorded for 8 locations at the Kaibab Limestone test site using the same shot point. The source consisted of a buried dynamite cap.

figure 2 in which near-surface and refracted-apparent velocities have been calculated for slopes that were fitted to the arrival data by eye. Calculated depths to the refracting layer were 11 m using the SH-wave data and 13 m using the P-wave data. Core samples taken in the area at 3 m depth intervals showed a layer at 11 m depth with high SH- and P-wave velocities. It was concluded that SH-wave refraction calculations for short seismic spreads (less than 100 m) can be useful for obtaining velocity-layer depth data.

AA 14 Angular Accelerometer.- The frequency response of the AA 17 was out of the range of maximum energy produced by our seismic sources, therefore, we rented an angular accelerometer, a Stratham AA 14, having a more suitable frequency response. Its frequency characteristics were those of a low-pass filter with a 3 db cutoff frequency of about 15 cps. Response to angular acceleration was 1.4 mv per rad per sec^2 and sensitivity to linear acceleration along any axis was about 0.025 mv per g.

The Kana-a lava flow test site near Flagstaff, Arizona, was selected for testing the AA 14 accelerometer. The site consisted of variable thicknesses of loose volcanic ash and cinders over-lying a volcanic aa flow. It was thought that this area would be the most difficult in which to generate and detect SH-waves because of the nature of the surface materials, therefore positive results with SH-waves in this area would give support for applying the
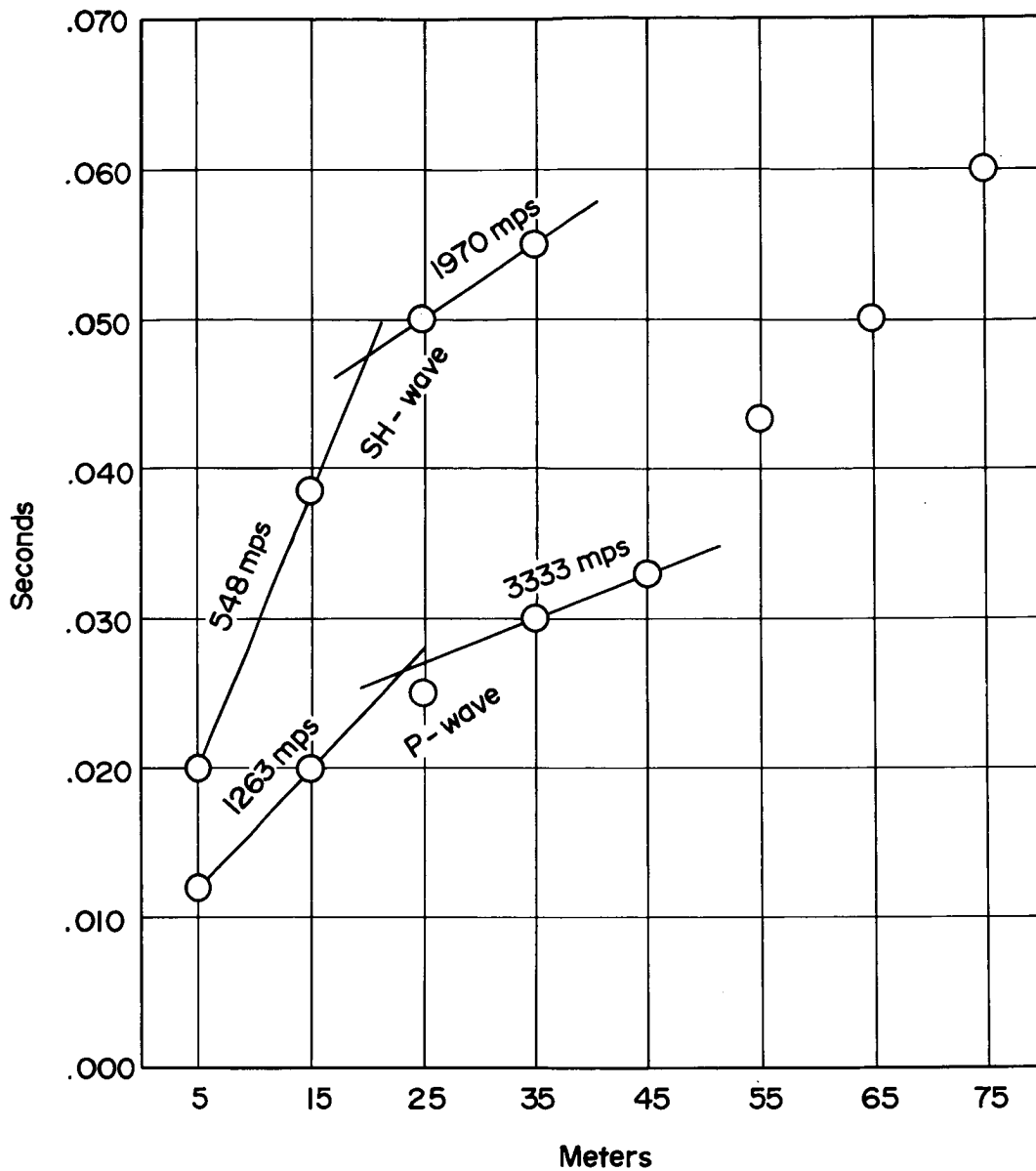
Figure 2. Time-distance plot of P- and SH-wave arrivals corresponding to the data of figure 1.

angular transducer technique to the remainder of our test areas. The investigation procedure for the AA 14 was the same as that followed for the AA 17. The composite of traces from 8 recording locations spaced at 5 m intervals is shown in figure 3. A unique problem encountered in this area was that the air velocity was slightly higher than the near-surface P-wave velocity so that the earlier air-wave energy has masked the P-wave arrivals. Air- and SH-wave arrivals are indicated (figure 3) along with a slower wave that may be a trapped wave. A time-distance plot in figure 4 illustrates apparent velocities of these waves for slopes fitted to the data by eye. Using the SH-wave to calculate the refracting-layer depth, a value of 6.9 m was found and was assumed to be the depth of the cinders. Drill hole data at a distance of 92 m north gave the thickness of cinders as 7.6 m and the cinders were underlain by a volcanic aa flow. This fact thus supports our depth calculations based on SH-waves.
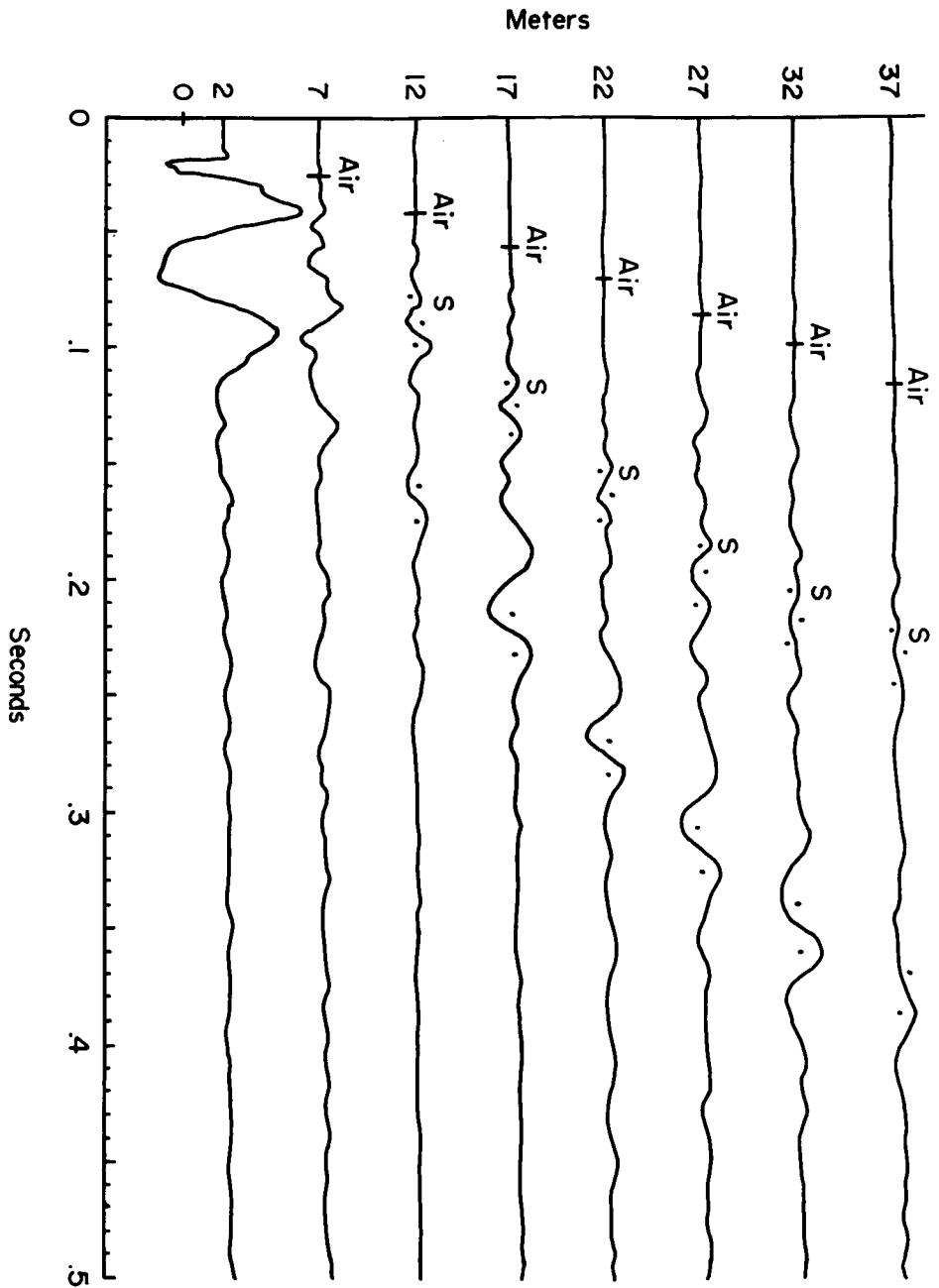
Figure 3. Traces from the AA 14 angular accelerometer recorded for 8 locations at the Kana-a lava flow test site using the same shot point. A buried dynamite cap was used for the source.
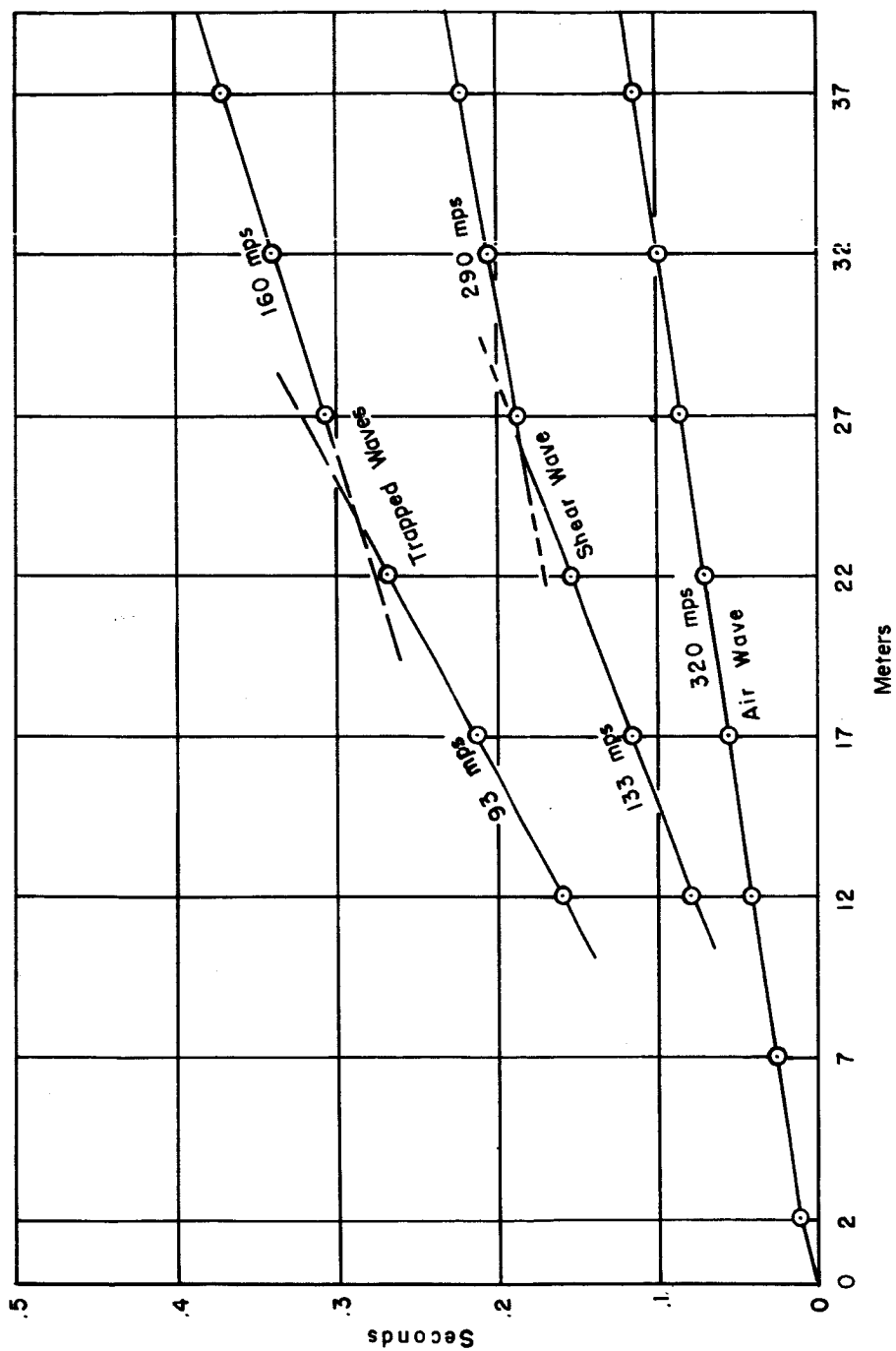
Figure 4. Time-distance plot of air- and SH-wave arrivals corresponding to the data of Figure 3. P-wave arrivals were masked by the earlier air-wave.

CONCLUSIONS

This investigation has shown that angular accelerometers are definitely more advantageous for the detection of S-waves than methods now in use. Because the technique provides a means of separating the P- and S-wave energy, much of the confusion in the interpretation of post first-arrival energy is eliminated in seismic refraction investigations. An array of 8 angular accelerometers will be used for study of SH-waves at all "in situ" test areas in FY-66 and for continued research in using the S-wave as a seismic tool.

PART II D

THE KANA-A FLOW,

AN ALKALI BASALT OF THE SAN FRANCISCO VOLCANIC FIELD,

ARIZONA

by

Robert A. Loney

U. S. Geological Survey
Flagstaff, Arizona

The Kana-a Flow,
an Alkali Basalt of the San Francisco Volcanic Field,
Arizona

by

Robert A. Loney

U. S. Geological Survey
Flagstaff, Arizona

ABSTRACT

The Kana-a basalt flow is a recent tongue of aa lava that
extends northeastward from the base of Sunset Crater, a cinder
cone in the eastern part of the San Francisco volcanic field,
about 25 km northeast of Flagstaff, Arizona. The flow is largely
mantled by a thin ash deposit that erupted from the top of the cinder
cone contemporaneously with the extrusion of the flow probably
from the base of the cone.

Six core holes drilled in the southeastern part of the flow
show this part of the flow to be 10.5 m thick and to consist of
4 structural units, which in descending order are (1) oxidized,
scoriaceous to highly vesicular unit, 1.5 to 2.4 m thick;
(2) moderately vesicular unit, 2.7 to 3.4 m thick; (3) massive,
sparsely vesicular unit, 3.1 to 4.0 m thick; and (4) highly
vesicular, slightly oxidized unit, which averages about 1.0 m
thick.

Petrographically only two types of basalt could be dis-
tinguished: a slightly glassy, oxidized basalt that forms the
outer crust of the flow, and a normal, holocrystalline basalt
that forms the bulk of the flow. Both consist largely of
andesine-labradorite, diopsidic augite, olivine ($Fo_{78}Fa_{22}$), and
magnetite. This mineral assemblage, together with three new
chemical analyses, indicates an alkali olivine basalt by most
modern classifications.

The Kana-a Flow,
an Alkali Basalt of the San Francisco Volcanic Field,
Arizona

by

Robert A. Loney

U. S. Geological Survey
Flagstaff, Arizona

INTRODUCTION

The Kana-a flow is a recent basalt flow, located in the

eastern part of the San Francisco volcanic field, about 25 km

northeast of Flagstaff, Arizona (figure 1). The flow extends

northeast for about 10 km from Sunset Crater, a contemporaneous

cinder cone in the Sunset Crater National Monument (figure 2).

The flow may have issued from a vent beneath the cone, but this

relation cannot be verified because of the thick ash deposits

immediately east of the cone. The rest of the flow, except for

a small bare patch at the toe, is mantled by a thin ash deposit,

through which project numerous small, jagged masses of the aa

crust of the flow (figure 3a). The ash supports a sparse growth of

pine and low bushes. The flow follows a narrow valley flanked

by ash deposits, older cinder cones and flows; its width ranges

from about .25 to 1.2 km.

The paper is based on field work and core drilling done in

1964 in connection with geophysical studies of the U. S. Geological

Survey on behalf of the National Aeronautics and Space Administration.

The core drilling and detailed field work were confined to a

small area at the western outcrop limit of the flow (figure 2),

although the entire flow and adjacent area were covered by
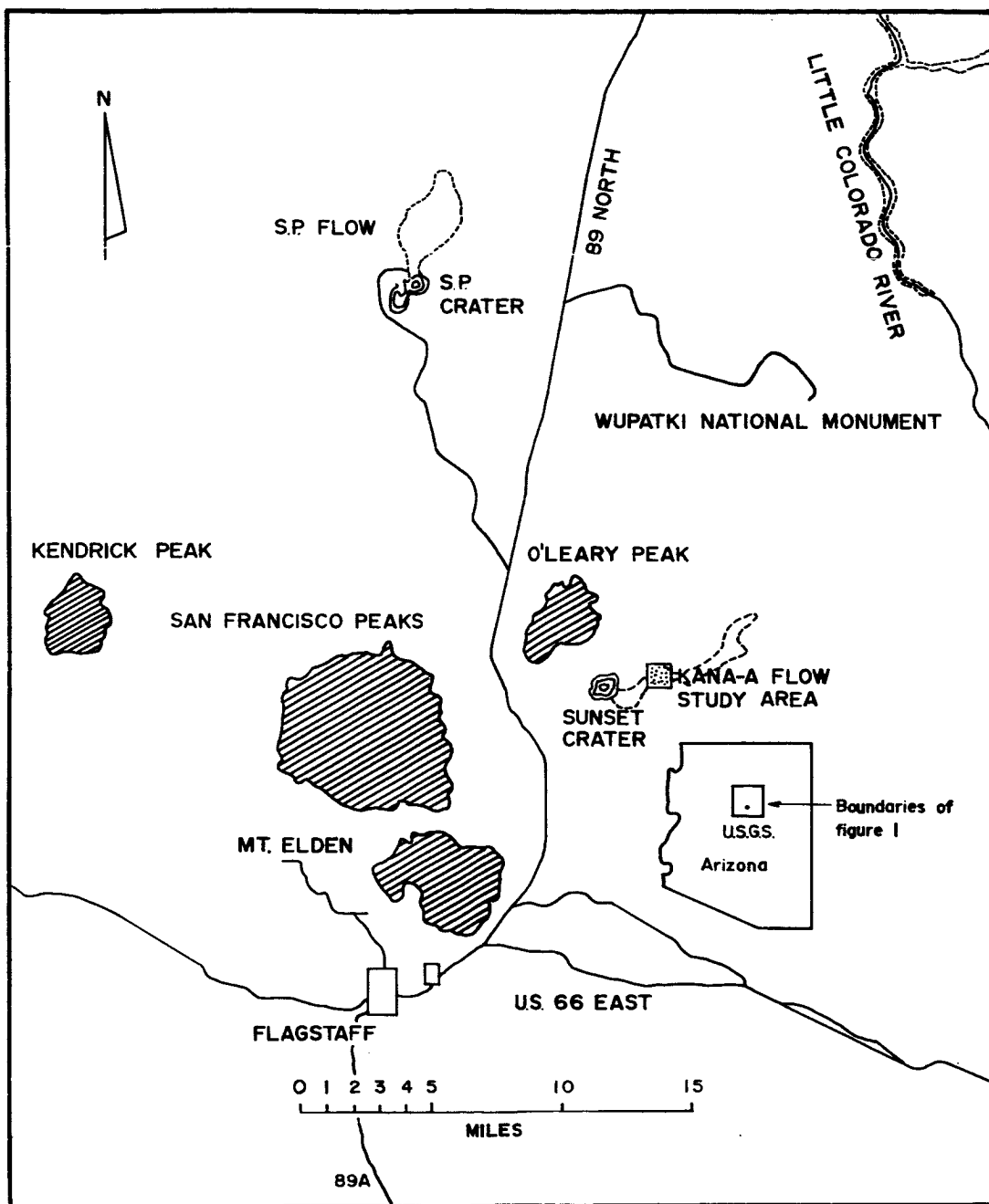
Figure 1. Location of study areas relative to prominent
terrain and cultural features of north-central Arizona.

Figure 2. Detailed map showing relationship of Kana-a flow to Sunset Crater cinder cone in Sunset Crater National Monument. Approximate core hole locations are indicated by dots.

Figure 3a. Jagged, tilted plates of aa lava projecting
through ash in Kana-a study area.

Figure 3b. Hornito in Kana-a study area. This cone sits
over a lava cave 50 feet long, 10 feet wide and from 2-15
feet high.

reconnaissance fieldwork. Because the flow is largely mantled by ash and is unbreached by erosion, these cores are the only source of information about the interior of the flow. In general, major varia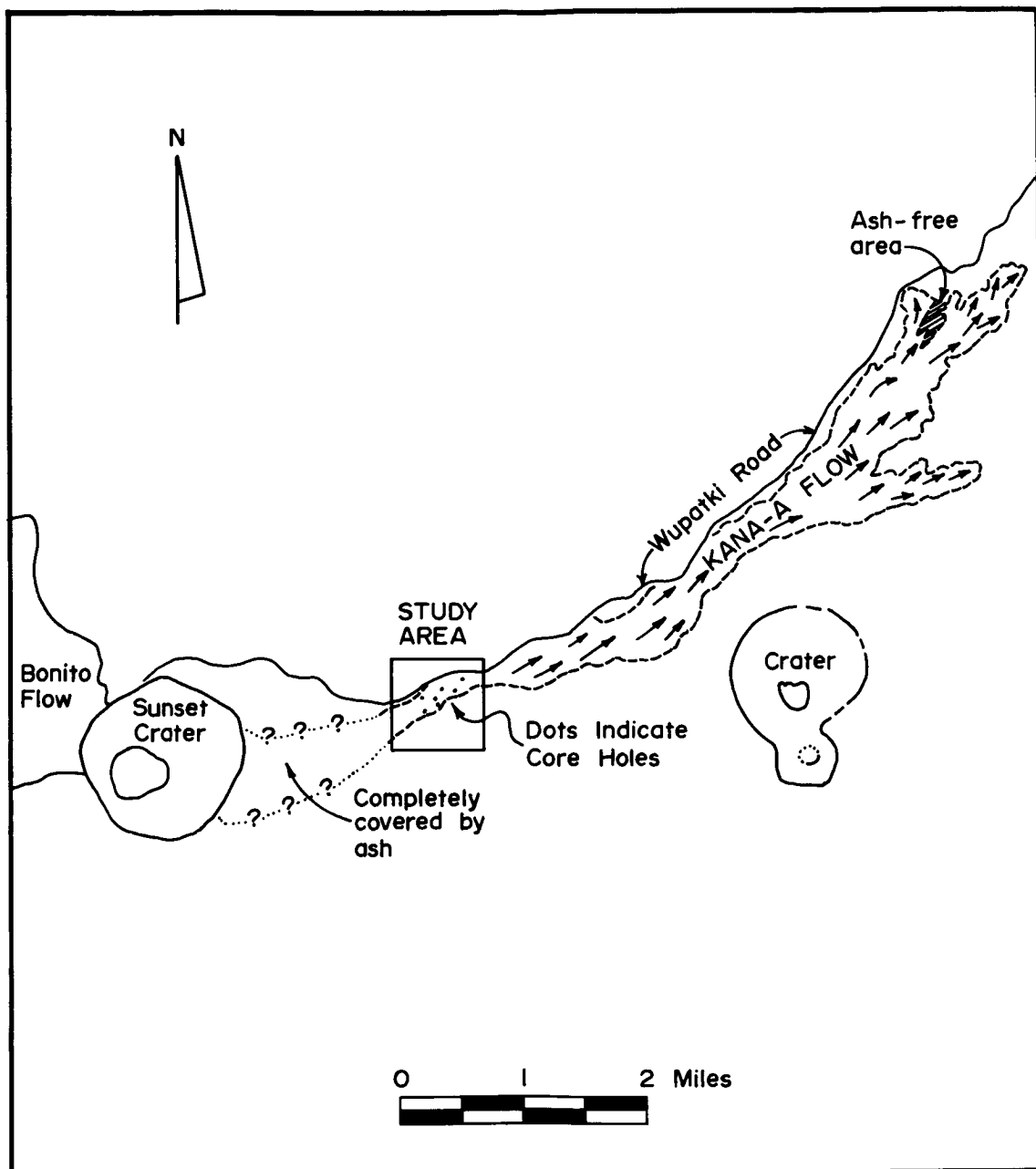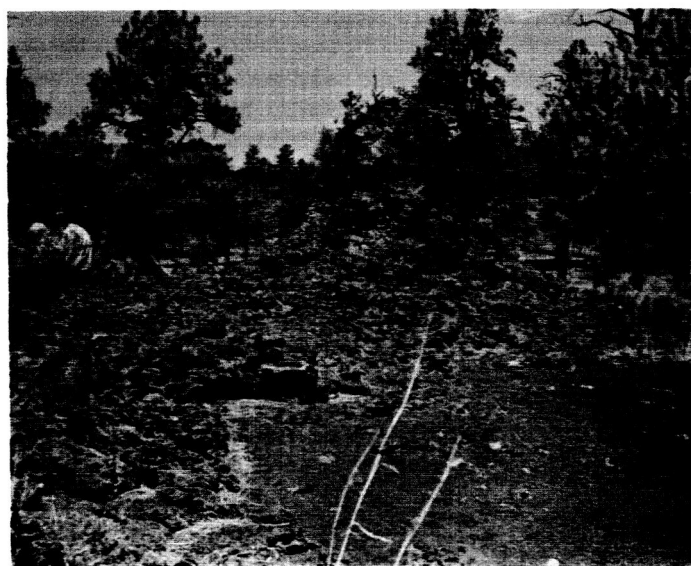tions are in vesicularity; little important variations in grain size, mineralogy, and chemical composition were found. Mineralogically and chemically the Kana-a flow is an alkali olivine basalt, as defined by several recent papers (Kennedy, 1933; Tilley, 1950; Kuno and others, 1957; Kuno, 1959, 1960; Yoder and Tilley, 1962; MacDonald and Katsura, 1964). However, the position of the flow in Yoder and Tilley's normative classification is somewhat ambiguous with respect to its modal mineralogy, and is discussed later in the paper.

The most comprehensive treatment on the San Francisco volcanic field remains that of Robinson (1913), who published many chemical analyses, but none of the Kana-a flow and very few on the widespread, basaltic flows of the third (and last) period of eruption, to which the Kana-a belongs. Colton's (1950) work is largely morphological and serves as a useful guide to the volcanic deposits of the field. The more recent work by Sabels (1960) gives partial analyses (potassium) of the Kana-a and other flows; his work sets up a geochronologic time scale of eruption based on a comparison of thermoluminescence of various flows with that of the Bonito flow of the Sunset Crater National Monument. The Bonito flow was dated at 900 years by dendrochronology (Smiley, 1958). According to Sabels, the Kana-a flow

is 1500 years old. Hodges (1960; 1962) presents a petrographic

and morphologic comparison of the Kana-a, Bonito, and S P flows,

which contains a brief petrographic description of the Kana-a.

ASH DEPOSITS

In general, the ash mantle of the Kana-a flow thins north-
eastward away from its probable source, Sunset Crater (Colton,
1950, p. 33) and is continuous with similar ash deposits on both
sides of the flow. This thinning, however, is complicated by
numerous local irregularities. The ash-free area near the north-
east end of the flow is considered by Hodges (1960, p. 67) to be
an indication that the lava and ash eruptions were contemporaneous.
In her view, the ash-free toe of lava was produced by a final
drainage of lava from the largely solidified flow after the close
of the ash eruption. Hodges' interpretation is supported by the
similarity of Sabels' (1960, p. 192) thermoluminescence age of
the Sunset Crater (cinder cone, 1400 years) to that of the Kana-a
flow (1500 years). Contemporaneity of lava and ash eruptions
would insure that the original surface of the Kana-a flow is
virtually untouched by erosion.

The grain size of the ash mantle in the study area ranges
from .05 to more than 4.0 mm, but more than 75 percent lies in
the range .25 to 4.0 mm, and may be classified as coarse ash;
coarser grains (lapilli) are rare (less than 1 percent). Hodges
(1960, p. 63) states that the grain size becomes finer to the
northeast away from Sunset Crater, averaging about .25 to .50 mm
in diameter at the toe of the flow and about 3 mm near the crater.
This statement appears generally true, but the grain size variation

is complex because the ash occurs in beds from .015 to more than 1 m thick in which the grain size grades markedly upward from coarse to fine in each bed.

The ash is predominantly dark gray but contains scattered, slightly weathered, yellowish brown grains. In a few places, gas activity has oxidized the ash to various hues of red. In general, the ash grains are rounded and scoriaceous; they consist chiefly of a very fine mesh of plagioclase laths (An45-50) and clinopyroxene, and sparce larger grains of plagioclase (about An50) and olivine. The composition is probably close to that of the Kana-a basalt.

KANA-A FLOW

Surface Features

The Kana-a flow itself is typical aa lava (Wentworth and MacDonald, 1953, p. 57-63) and the surface that projects above the ash consists of jagged, spinose, vesicular, clinkery blocks and plates, which are commonly tilted up at various angles (figure 3a). Small breached domal structures and hornitos (or remnants thereof) are common on the flow, especially in the study area. One nearly perfect hornito about 3 m high, composed of welded reddish agglomerate piled around an open, cylindrical vent sits astride a lava cave in the western part of the area of study, north of Wupatki Road (figure 3b). The lava cave is about 18 m long, 3 m wide, and 1 to 5 m high, and trends NE roughly parallel to the direction of flow. The ceiling of the cave is studded with lava stalactites as much as 15 cm long. In places small, groove "pushups" project one or two meters above the flow. In general, outcrops of lava and linear features within the outcrops are elongate parallel to the direction of flow and in spite of the ash mantle, give an indication of the structural grain of the flow. Figure 2 shows the principal flow directions as based on the above linear outcrops. The highly irregular surface of the Kana-a flow beneath the ash is generally firmly attached to the underlying more massive part of the flow.

Description of Cores

The study area was penetrated by 6 core holes, the lithology and correlation of which are shown in figure 4. Core holes 1, 2, and 6 are located in the medial, thicker part of the flow, whereas core holes 4, 5, and 7A are located near the margins. A maximum thickness of 10.5 m of flow was encountered in core hole 6.

The most striking variation in the cores is in the degree and kind of vesicularity, and hence in porosity. Grain size variation is not noticeable megascopically, and the basalt of the flow is generally fine grained. However, large phenocrysts of olivine and enstatite as much as 2 cm long are scattered very sparsely through the rock. The basalt is generally a uniform medium gray, except for small patches of red and dark reddish gray in the outer parts of the flow. Four units based on megascopic characters have been distinguished in the cores from the medial part of the flow, and are listed below in descending order as follows:

1. A unit composed of the uppermost part of the flow and ranging from 1.5 to 2.5 m thick in the medial cores (figures 5a and 5b). It consists of scoriaceous to highly vesicular, fine-grained basalt that is generally medium gray, but is oxidized in places to various shades of red. The normal weathered surfaces are dark

Figure 4. Correlation of core holes.

D-12

Kana—a Flow
Core Hole 2
5 Feet

0   1   2 cm

Figure 5a.   Core hole 2, depth 5 feet; scoriaceous to
   highly vesicular basalt oxidized red; near top of
   unit 1.

Kana—a Flow
Core Hole 2
10 Feet

0   1   2 cm

Figure 5b.   Core hole 2, depth 10 feet; highly vesicular
basalt vesicles slightly flattened horizontally; base
of unit 1.

gray. The vesicles make up from 25 to 40 percent of
the rock, and range from 1 to 20 mm in length.
Spheroidal vesicles dominate, but irregular ones are
also common. Flattened, uniformly alined vesicles are
rare. Recurring oxidized zones and broken cores suggest
that the unit may be fragmental in places.

2. A moderately vesicular unit, uniformly medium gray and
   fine grained, that ranges from 3 to 4 m thick in the
   medial core holes (figures 6a and 6b). Spheroidal
   vesicles dominate in the upper few meters of cores
   2 and 6, and throughout most of core 1. The vesicles
   tend to become flattened and irregular downward in all
   cores, and in 2 and 6 the lower part of the unit con-
   tains almost exclusively fine flattened vesicles that
   form discontinuous layers one vesicle thick (figure 6b).
   The vesicle layers, which average about 1 mm thick,
   anastomose and divide the rock into lenses. This type
   of vesicle is nearly lacking in core 1 and predominant
   in core 6. In places the layers are inclined at steep
   angles to the core. In the unit as a whole, vesicles
   form from 10 to 20 percent of the rock.

3. A massive, sparsely vesicular unit in which the vesicles
   average about 1 mm in length and form less than 5 percent

Kana—a Flow
Core Hole 2
15 Feet
0   1   2 cm

Figure 6a. Core hole 2, depth 15 feet; moderately
vesicular basalt, vesicles moderately flattened
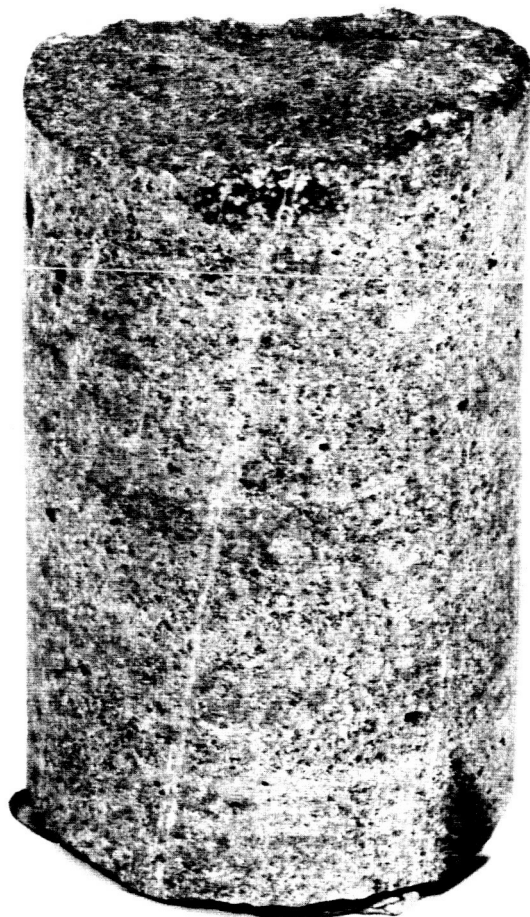horizontally; middle of unit 2.

D-16
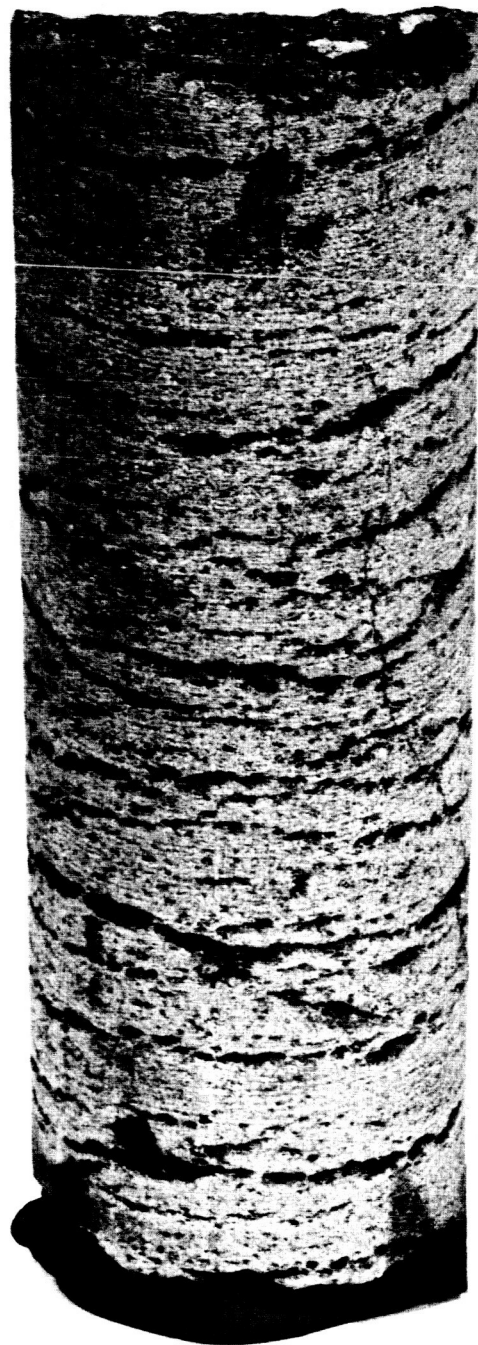
Kana–a Flow
Core Hole 6
20 Feet

0   1   2 cm

Figure 6b. Core hole 6, depth 20 feet; moderately
vesicular basalt, vesicles flattened into thin
layers; middle of unit 2.

of the rock (figures 7a and 7b). In the medial core
holes the unit ranges from 3 to 4 m thick, and consists
of uniformly medium gray, fine-grained basalt. The
vesicles in core 2 are largely spheroidal, whereas in
core 6 they form flattened layers similar to those in
unit 2 of the same core.

4. A lowermost unit that consists of moderately to highly
    vesicular fine-grained basalt (figure 8). The unit
    averages about 1 m thick in the medial core holes, and
    is generally medium gray mottled with reddish oxidized
    zones. The vesicles form from 15 to 30 percent of the
    rock, and tend to be elongate tubes whose greatest
    cross section dimensions range from 1 to 10 mm and
    average about 3 mm.

Cores 4 and 5 probably represent the edges of the flow, where
a relatively thin, highly vesicular, oxidized, and partly frag-
mental zone is to be expected. Core hole 7a is located in deep
ash deposits just beyond the northern margin of the flow. Core
hole 3a may lie beyond the southern margin of the flow. Although
the sequence of units in core 3a is similar to those described
above, the upper scoriaceous unit (unit 1) is missing and only
the bottom few feet of unit 2 is present at the top of the core.
This relation suggests that unit 1 and the upper part of unit 2
have been removed by erosion, and thus the upper part of this

Kana—a Flow
Core Hole 2
20 Feet

0   1   2 cm

Figure 7a.   Core hole 2, depth 20 feet; sparsely
  vesicular basalt, vesicles not noticeably flattened;
  near top of unit 3.
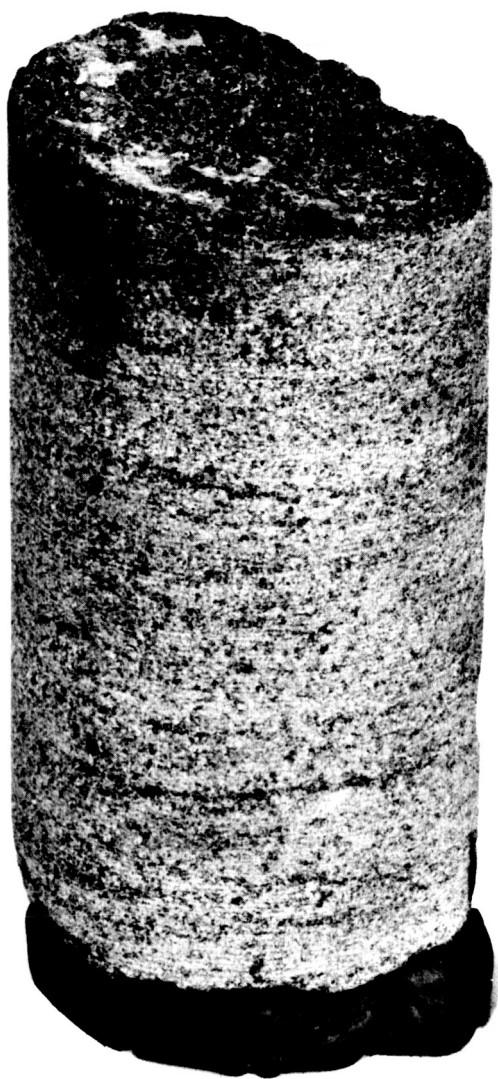
Kana—a Flow
Core Hole 6
28 Feet
0   1   2 cm

Figure 7b. Core hole 6, depth 28 feet; very sparsely
  vesicular basalt, vesicles in thin flat layers; upper
  part of unit 3.

Kana—a Flow
Core Hole 2
30 Feet
0   1   2 cm

Figure 8.   Core hole 2, depth 30 feet; moderately vesicular
basalt, vesicles flattened horizontally; middle of unit 4.

core would represent an older eroded flow. An alternative
interpretation is that core hole 3a, as core holes 4 and 5,
is located in the chaotic marginal part of the Kana-a flow and
that the sequence is disturbed.

Petrography

Microscopically only two lithologic phases can be dis-
tinguished: (1) an oxidized phase that comprises the outer
crust of the flow and includes megascopic units 1 and 4; and
(2) a normal phase that comprises the interior part of the flow
and includes units 2 and 3.

Both phases have a fine-grained texture composed of elongate
labradorite laths between which lie equant to stubby prismatic
grains of olivine, clinopyroxene, enstatite, and equant grains
of magnetite (figure 9). In the holocrystalline normal phase
the texture is intergranular, and the angular interstices between
the labradorite laths are filled with small prisms of clinopyroxene
and a lesser amount of equant grains of olivine and magnetite.
In the oxidized phase the interstices are commonly filled with
murky, partially devitrified glass; where this occurs the texture
is intersertal. The elongate labradorite and mafic minerals
commonly have a marked subparallel flow alinement (figure 9)
that is best developed in the main part of the flow (units 2 and
3) and least developed in the oxidized parts (units 1 and 4).

Figure 9. Photomicrograph of normal phase basalt showing marked flow alinement of labradorite laths (plain light, X10).

In the oxidized phase, magnetite is concentrated in anhedral masses as much as .5 mm across in the vicinity of vesicles. Hematite after magnetite is scattered sparsely throughout the normal phase, but is much more abundant in the oxidized phase, where its local abundance imparts a reddish hue to the basalt. The olivine in the oxidized phase generally contains abundant magnetite inclusions, especially near vesicles. In addition, the pyroxene grains of the oxidized phase commonly have a brownish yellow coating that also seems most abundant near vesicles.

The grain size of the normal phase averages about .2 mm, and appears to be nearly uniform throughout. The oxidized phase averages between .1 and .15 mm in granularity. There is no distinct groundmass in either phase and an almost complete gradation in the size of plagioclase and olivine exists between .01 and .8 mm. The only true phenocrysts are sparse, large, generally corroded grains of plagioclase and olivine that range from 1 to 20 mm in length. Enstatite also occurs as very sparse, highly corroded grains that are probably xenocrysts.

In general, the vesicles show no marked influence on the rock fabric. The flattened, irregular vesicles common in the middle parts of the flow in some cores show no influence on the orientation of minerals adjacent to the vesicles (figure 10a). However, the labradorite laths in the upper part of the flow

Figure 10a. Photomicrograph showing flattened vesicles in middle part of flow; note how the vesicles cross-cut the rock fabric with no apparent influence on it (crossed nicols; X10).
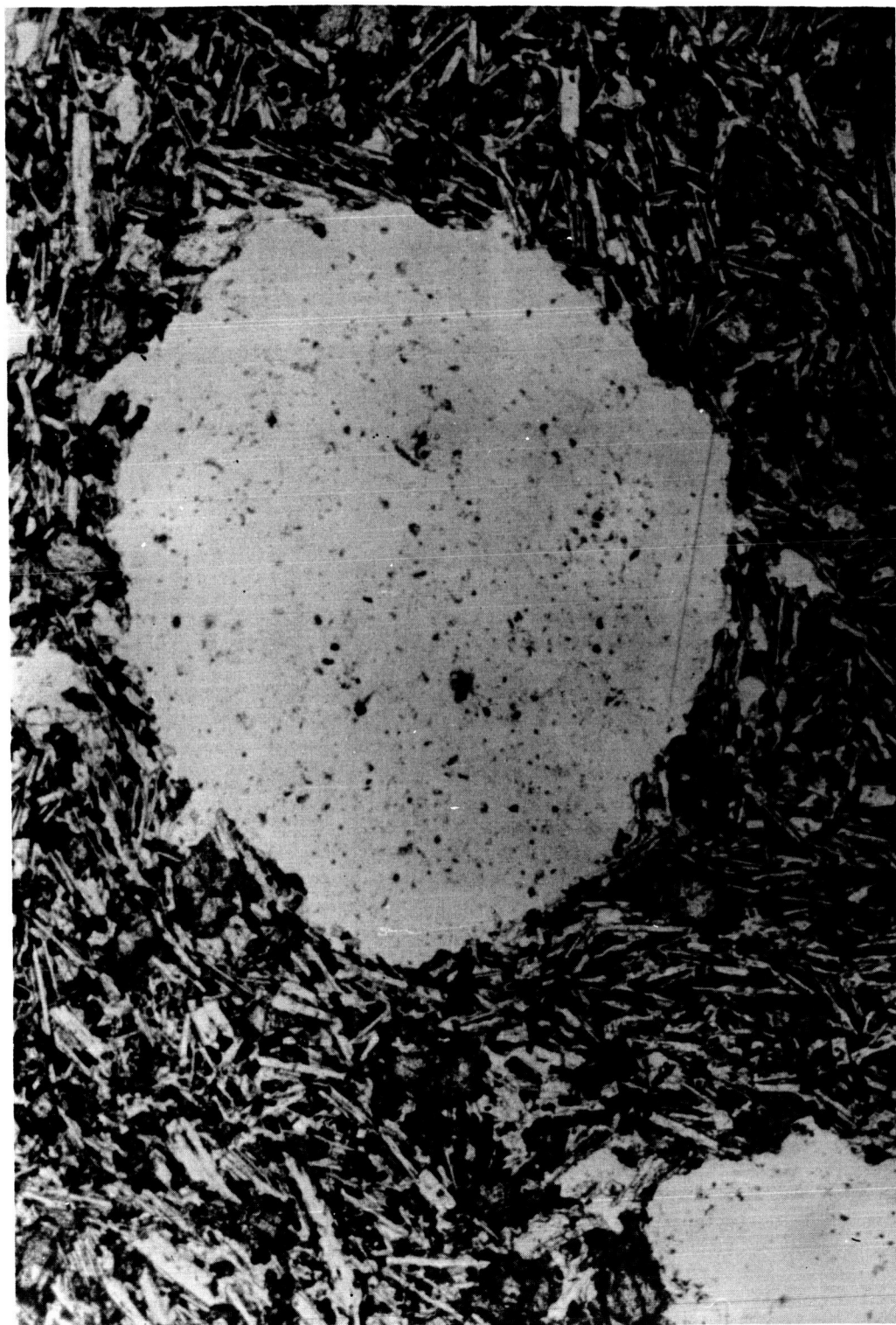
Figure 10b. Photomicrograph showing spheroidal vesicles in upper part of flow; note slight tendency for labradorite laths (light gray) to lie subparallel to vesicle walls (plain light, X10).

show a slight tendency to be subparallel to the walls of the

spheroidal vesicles common in that part of the flow (figure 10b).

The following table shows representative modal analyses

(in percent volume) for the normal (lower part, unit 3) and

oxidized (upper part, unit 1) phases.

Table 1. Comparison of modal analyses (point counts) of the
phases of the Kana-a basalt.

	normal phase		oxidized phase	
	(with vesicles)	(without vesicles)	(with vesicles)	(without vesicles)
labradorite (An_{48}-An_{64})	47	50	25	34
olivine	29	29	12	16
pyroxene	14	14	17	24
magnetite (and associated hematite)	7	7	13	17
glass	0	0	7	9
vesicles	3		26	

The more pronounced preferred orientation of plagioclase

laths in the normal phase prevents a close comparison of the

modal analyses of the two phases. For this reason an average

of the two modes given above is used in Table 2, in which the

mineralogical data are summarized. In general, the modal per-

centages (less vesicles) indicate that the total percentage of

mafic minerals (including magnetite) is about the same in the

two phases. There is probably more olivine in the lower part

of the flow, but the difficulty of reliably distinguishing small

Table 2.-- Summary of modal mineralogical data, Kana-a basalt

%*	Mineral	Size mm	Composition	Optical Data	Description
43	plagioclase	.05-.1	An_{48} to An_{52}		Fresh, laths, multiple twinning, unzoned.
		.1 -2	An_{64}(core to An_{48}(rim)		Fresh, laths, multiple twinning, normal zoning.
26	olivine	.01-.8 rare 1-20	$Fo_{78}Fa_{22}$ (Deer and others, 1962, v.1, fig. 11)	$2Vx=86°+2°$; $Y_D=1.696$ ($\pm$.003)	Colorless, equant grains and stubby crystals; iddingsite on margins and in fractures. Both in groundmass and as larger crystals. (010) cleavage well developed and locally (100) cleavage well developed.
21	augite	.05-.08	Diopsidic probably with Al & Na Winchell and Winchell, 1951, fig. 306)	$2V_z=66°-71°$; $Y_D=1.691 \pm .003$) $Z\Lambda c\approx40°$	Pale olive green, stubby crystals in groundmass, interstitial to plagioclase; larger crystals very rare.
10	magnetite (and associated hematite)	highly variable	Possibly with titanium	Opaque	Equant euhedra & irregular grains; much is derived from alteration of olivine.
tr	enstatite	1-1.8	$En_{88}Fs_{12}$ (Deer and others, 1963, v.2, fig. 10)	$2Vz=82° \pm 2°$	Colorless, large, highly corroded xenocrysts; well-developed exsolution lamellae (100); reaction rims of fine plagioclase and augite grains, also sieved with these minerals.

* less vesicles

grains of olivine from those of pyroxene prevents a more certain statement. The oxidized phase is probably enriched in magnetite at the expense of olivine, owing to the greater degree of replacement of olivine by magnetite in the oxidized phase.

Chemical Composition

Chemical analyses of the Kana-a lava (Tables 3 and 4) show it to be a basalt near the composition of the "normal alkali basalt" of Nockolds (1954, Table 7), but somewhat richer in alumina. The analyses of the three samples of the lava are nearly identical, except for the ratio of ferrous to ferric iron, and even here the total iron is nearly the same. The lowest oxidation state of iron obtains in the massive, lower part of the flow (Table 3, column 3) and the highest oxidation state obtains in the upper crust (Table 3, column 2). Obviously these variations in oxidation state relate to the cooling conditions of the flow and have little petrogenetic significance.

Robinson (1913, p. 151-152) gives a single analysis as representative of his third period basalt flows, to which the Kana-a flow belongs. This analysis - from a basalt flow near Kendrick Peak, about 20 miles west-northwest of Sunset Crater - shows about 47 percent silica, 16 percent alumina, and 3.2 percent total alkali ($Na_2O + K_2O$). Except for the slightly lower alkali content, these figures suggest a basalt similar in composition to the Kana-a (Table 3). However, further comparison

Table 3.-- Major oxides, Kana-a and S P flows
(Rapid rock analyses by Paul Elmore, Sam Botts, and Lowell Artis of the U.S. Geological Survey.)

| | Chemical Analyses | | | | | | | CIPW Norms | | | | | |
	1	2	3	4	5	6		7	8	9	10	11	12
SiO_2	47.7	47.4	47.6			57.2	g	----	----	----	----	----	6.04
Al_2O_3	16.5	16.4	16.4			14.7	or	4.08	4.02	4.25	4.08	4.02	13.59
Fe_2O_3	3.7	5.0	2.0	2.0	2.0	2.3	ab	27.91	28.75	25.25	26.60	25.51	32.14
FeO	7.3	6.2	9.0	8.9	9.0	4.2	an	28.12	27.48	27.81	28.17	27.48	16.27
MgO	8.1	8.2	8.2			5.2	ne	----	----	1.44	0.72	1.77	----
CaO	9.8	9.8	10.0			7.4	di	13.65	14.05	14.93	13.83	14.40	12.64
Na_2O	3.3	3.4	3.3			3.8	hy	1.45	0.92	----	----	----	11.50
K_2O	.69	.68	.72			2.3	ol fo	10.08	9.98	11.14	11.19	11.25	----
H_2O^-	.05	.05	.00			.18	ol fa	4.29	2.54	7.45	7.41	7.48	----
H_2O^+	.39	.32	.32			.92	mt	5.36	7.25	2.90	2.90	2.90	3.33
TiO_2	1.7	1.7	1.7			.89	il	3.23	3.25	3.23	3.23	3.23	1.69
P_2O_5	.48	.48	.48			.67	ap	1.14	1.14	1.14	1.14	1.14	1.58
MnO	.13	.14	.18			.15	cc	0.11	0.11	0.11	0.11	0.11	0.11
CO_2	.05	.05	.05			.05							
Sum	100.oo	100.oo	100.oo			100.oo							
Fe^{+++}	3.1	4.1	1.6										
Fe^{++}	6.9	5.4	7.9										

Table 3 Continued

1. Specimen K2-7; medium gray, very sparsely and finely vesicular, fine-grained basalt from middle of unit 3; normal phase, Kana-a basalt.

2. Specimen K6-1; medium gray streaked with reddish brown, highly vesicular, fine-grained basalt from top of unit 1; oxidized phase, Kana-a basalt.

3. Specimen K6-11; medium gray, sparsely vesicular, fine-grained basalt from base of unit 3; normal phase, Kana-a basalt.

4 and 5. Recalculated Fe_2O_3 and FeO for analyses 1 and 2 respectively on basis of ratio of Fe^{++} to Fe^{+++} in analysis 3.

6. Analysis of specimen 64L-23; augite andesite, S.P. flow.

7, 8, 9. Norms of analyses 1, 2, and 3 respectively.

10 and 11. Norms of analyses 1 and 2 respectively using recalculated Fe_2O_3 and FeO values of columns 4 and 5 respectively.

12. Norms of analysis 6, Specimen 64-L-23; S.P. andesite.

Table 4.-- Minor elements, Kana-a and S P flows
(Quantitative spectrographic analyses by J. D. Fletcher,
U.S. Geological Survey.)

	[1] PPM	[2] PPM	[3] PPM	[4] PPM		[1] PPM	[2] PPM	[3] PPM	[4] PPM
Pb	<10	<10	<10	10	Ti	860	860	860	600
Ag	< 1	< 1	< 1	< 1	Be	< 2	< 2	< 2	< 2
Cu	87	150	63	87	Nb	40	50	40	40
Ga	22	23	23	18	Sc	25	25	25	22
Mn	1,060	925	925	555	La	<50	<50	<50	90
Cr	180	220	215	105	Mo	< 2	< 2	< 2	7
B	<10	<10	<10	10	Y	32	36	35	26
Co	40	45	45	20	Zr	140	135	150	225
Ni	95	110	120	65	Li	9	9	8	14
Ba	580	860	790	1,350	Cs	2	2	2	2
Sr	400	1,100	860	600	Rb	7	8	6	24
V	108	180	130	82					

Elements looked for but not found: Au, Hg, Ir, Pt, W, Ge, As, Sb, Sn,
Bi, Zn, Cd, Tl, Th, Ta, U, and P.

1. Specimen K2-7 (see table 1), Kana-a basalt.

2. Specimen K6-1 (see table 1), Kana-a basalt.

3. Specimen K6-11 (see table 1), Kana-a basalt.

4. Specimen 64L-23 (see table 1), S P andesite.

is unwarranted because Robinson's weight percentages and molecular numbers are based on the percentage of modal augite in the rock instead of 100, and are hence dependent on his ability to distinguish augite from olivine. The above percentages are my conversions based on 100 percent of Robinson's figures.

The only other analysis from a third flow (1300 years, Sabels, 1960) known to me is one from the S P flow, made during the present investigation (Table 3, column 6; Table 3, column 4). The S P flow is a thick flow (more than 60 m) of block lava that extends north about 4.5 miles from the base of S P Mountain, a contemporary cinder cone about 30 km northwest of the Kana-a flow. The S P flow is an andesite or a doreite (Nockolds, 1954) that has an average modal composition as follows: andesine (An_{40-48}; 26 percent), diopsidic augite ($2Vz = 56°-62°$; $X_D = 1.692 \pm .003$; $Y_D = 1.712 \pm .003$; 24 percent); olivine (2 percent); brown glass ($n_D = 1.540 \pm .003$; 36 percent); vesicles (12 percent), and magnetite (trace). Also present are scattered, rounded quartz grains that amount to less than 1 percent and are probably xenocrysts from the underlying Coconino Sandstone.

Discussion of Magma Types

Since the classic work on magma types at Mull (Bailey and others, 1924), petrologists have tended to give the modal mineral composition of basalt precedence over chemical composition in

characterizing the various magma types. As more work has been
done, many instances of ambiguous or obscure modal mineralogy
relative to the classic magma types have arisen. Chemical data
have generally been invoked to solve the problem and as chemical
and experimental data have increased, some geologists have tended
to place chemical criteria above mineralogical ones. It is
obvious that both are but facets of the same problem, but, as
will be apparent from the following discussion, at present there
seems to be a rather poor correlation between the two criteria.

Mineralogical classification.- The modal mineralogical
composition of the Kana-a basalt is that of an alkali olivine
basalt, as defined by modern authors (Kennedy, 1933; Tilley,
1950; Kuno and others, 1957; Kuno, 1960; Yoder and Tilley, 1962;
Macdonald and Katsura, 1964). Table 5 gives a comparison of the
modal mineralogy of Kana-a and modal mineral phases considered
characteristic of alkali basalt and tholeiite by the above authors.
As can be seen, there is no general agreement, but certain cri-
teria, namely: the type of pyroxene, presence or absence of
olivine in groundmass, reaction relation of olivine and ground-
mass, and the nature of the interstitial material have been
accepted by most of the authors. Of these, the first two are the
most important from the standpoint of reliability, widespread
occurrence, and ease of identification. The other criteria are
less useful because they are less widespread, difficult to identify,

Table 5. Comparison of the modal mineralogy of the Kana-a basalt and some modern published characteristic modal mineral phases of alkali basalt and tholeiite.

Kana-a basalt	alkali basalt	tholeiite
diopsidic augite	calcic or diopsidic augite, or titanaugite 1,2,3,4,5,6	pigeonite or hypersthene or both 1,2,3,4,5,6
olivine in groundmass and as phenocrysts; no reaction rims	olivine in groundmass and as phenocrysts; no reaction rims 3,4,5,6	groundmass olivine rare; 3,4,6 olivine has reaction rims of pigeonite 2,3,4,5,6
plagioclase: smaller crystals: An 48 - An$_{52}$	andesine in groundmass 4,5	labradorite to bytownite in groundmass 4
larger crystals: An 64 (core) to An 48 (rim)	andesine to labradorite as phenocrysts 4	bytownite to anorthite as phenocrysts 4
generally no interstitial material; only top crust is glassy	interstitial alkali feldspar or zeolite--no quartz; glass rare 1,2,3,4,5,6	interstitial glass and silica mineral-feldspathic material 1,3,4,5,6

References to data:

1. Kennedy (1933)
2. Tilley (1950)
3. Kuno and others (1957)

4. Kuno (1960)
5. Yoder and Tilley (1962)
6. Macdonald and Katsura (1964)

or of questionable validity. Because of the problem of using
modal mineralogical criteria and the lack of general agreement
on validity of some of them, the most important relative to the
Kana-a basalt are discussed briefly below.

Pyroxene. The presence of diopsidic augite in the
groundmass of the Kana-a basalt agrees with one of the
most generally and unequivocally accepted alkali basalt
criteria. Further, the probable Na_2O and Al_2O_3 enrichment
of the augite, as indicated by the refractive index (Y_D)
and the large optic axial angle (Winchell and Winchell,
1951, figure 306), agrees with statements by Yoder and
Tilley (1962, p. 355) regarding the pyroxene composition
of alkali basalts. Kuno (1960) lists calcium-rich augite
for both groundmass and phenocrysts, but the other authors
either state groundmass or do not specify. The large, rare,
enstatite crystals of the Kana-a basalt generally show
strong reaction relations to the groundmass and are probably
xenocrysts not petrogenetically related to the basalt.

Olivine. The olivine of the Kana-a basalt occurs both
in the groundmass and as phenocrysts. All authors since
Kuno and others (1957) have considered groundmass olivine
to be a reliable characteristic of alkali basalts.

The olivine shows no reaction relations with
clinopyroxene. All authors since Tilley (1950) have stated

that olivine in tholeiites shows reaction relations with
subcalcic augite or pigeonite. However, there is a
considerable range of opinion as to whether this reaction
is widespread enough to be useful. Kuno (1960) feels that
it "invariably" occurs wherever olivine occurs in the
groundmass of tholeiitic rocks, whereas Yoder and Tilley
(1962) state that tholeiites with olivine "not infrequently"
show reaction with the groundmass. Macdonald and Katsura
(1964) state that reaction rims of lime-poor pyroxene is
a certain indication of tholeiite basalt, but the rims are
seldom seen. Thus the absence of the reaction rim can
hardly be used by itself as an indication of an alkali
basalt. It seems probable that the rim criteria is meant
to apply to olivine phenocrysts and not to groundmass
olivine.

The experimental work of Schairer and Yoder
(1960, p. 281-282; 1964, p. 71) indicates that the reaction
of olivine with the liquid of alkali rocks (tephrites,
basanites, melilite basalts, and possibly olivine
nephelinites) to produce diopside is likely. The reaction
has not been reported in natural alkali basalts, but its
possibility weakens the reaction rim criteria. Perhaps
the diopsidic nature of the reaction rims of olivine in
alkali basalt could be used to distinguish them from the
pigeonitic rims of olivine in tholeiite.

Plagioclase. The composition of the plagioclase of

the Kana-a basalt agrees closely with Kuno's (1960) plagio-

clase composition for alkali basalt (Table 5). However,

the other authors make no such sharp distinction between

the plagioclase of alkali basalt and tholeiite. Yoder and

Tilley (1962), for example, give An_{50} zoned toward anortho-

clase for plagioclase of alkali basalt and also give An_{50}

for plagioclase of tholeiite.

Interstitial material. Except for the slightly glassy

upper crust, the Kana-a flow is holocrystalline, and

generally lacks interstitial material in the sense of very

fine, last-to-crystallize, mineral phases. The finer-

grained plagioclase, olivine, augite, and magnetite, which

form the bulk of the rock, appear to have crystallized

together. The holocrystalline nature is considered by

Yoder and Tilley (1962, p. 355) to be almost universal

for alkali basalts, as is interstitial glass for tholeiites.

However, Macdonald and Katsura (1964, p. 89) feel that glass

does occur in many alkali basalts and hence its presence or

absence cannot be used alone to separate tholeiites from

alkali basalts.

Chemical classification.- Although there is no general

agreement among the previously listed authors as to the location

of the chemical compositional boundary between alkali basalt and

tholeiite, the chemical composition of the Kana-a basalt lies well within the field of alkali basalt in all classifications except that of Yoder and Tilley (1962). Because of this difference of opinion as to the compositional limits of alkali basalt and tholeiite, a brief discussion of the most recent classifications is given below.

It has been widely held that alkali basalts are undersaturated with silica and tholeiites are saturated or oversaturated (Kennedy, 1933; Kuno, 1959; Macdonald and Katsura, 1964). In other words, the presence or absence of normative olivine is taken to be critical as to whether a basalt is alkalic or tholeiitic. By this criterion the Kana-a basalt is clearly an alkali basalt (Table 3).

However, in the normative classification of Yoder and Tilley (1962, p. 352-356) the undersaturated basalts are divided into two groups: (1) the undersaturated basalts with normative nepheline; (2) the undersaturated basalts without normative nepheline. This classification is illustrated by figure 11, in which the plane Cpx-Opx-Pl is the plane of saturation, separating oversaturated rocks to the right from undersaturated rocks to the left. Those undersaturated rocks that have normative hypersthene lie in tetrahedron Cpx-Opx-Ol-Pl and are called the olivine tholeiite group, whereas those that lie in tetrahedron Cpx-Ol-Ne-Pl have normative nepheline but no normative hypersthene and are called
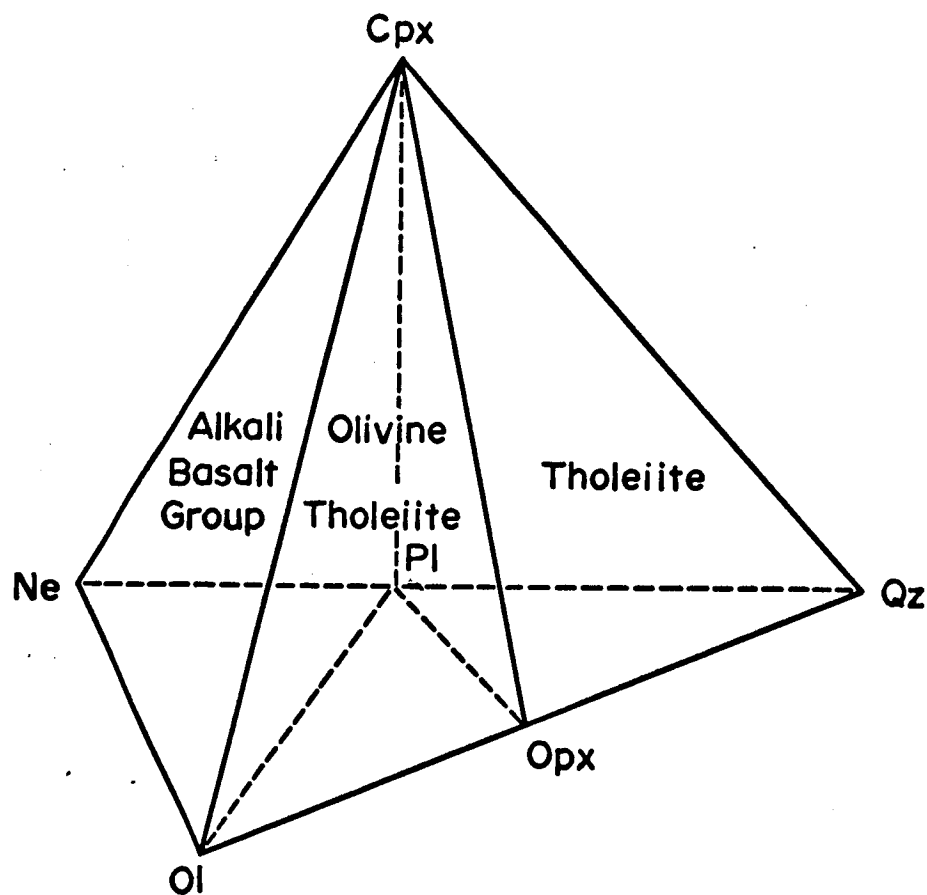
Figure 11. Tetrahedron representing normative classification of
basalts of Yoder and Tilley (1962, figure 1 and 2); CIPW
normative phases on diagram: Cpx- clinopyroxene, Ne -
nepheline, Ol- olivine, Opx- orthopyroxene (hyperthene),
Pl- plagioclase, Qz- quartz.

the alkali basalt group. The name olivine basalt is restricted to those rocks whose normative composition lies on plane Cpx-Ol-Pl and hence have neither normative hypersthene nor nepheline.

With respect to the Yoder and Tilley classification, the Kana-a basalt lies very nearly on the olivine basalt plane. It is evident from the norms of the three analyses of the Kana-a basalt (Table 3) that the norms of analyses 1 and 2 have a small amount of normative hypersthene and lie in the tetrahedron of olivine tholeiites, whereas the norms of analysis 3 have a small amount of normative nepheline and no hypersthene and lie in the tetrahedron of the alkali basalt group. The only appreciable difference among the three analyses is in the oxidation state of iron. Columns 4 and 5 of Table 3 show the recalculated norms of analyses 1 and 2 respectively, in which the ratios of ferrous to ferric iron have been adjusted to that of analysis 3, which has the lowest oxidation state. The recalculated norms are nearly identical to that of analysis 3 and show a small amount of nepheline and no hypersthene. Thus the basalt of analyses 1 and 2 can be made either tholeiite or alkali basalt by simply changing the oxidation state of iron in the analyses.

Yoder and Tilley (1962, p. 353) foresaw the above difficulty and state that the mode is given preference over the norm when ambiguities arise. Therefore, it seems justified to classify

the Kana-a as an alkali basalt on the basis of its typical alkali

basalt mineralogy. As observed by Macdonald and Katsura (1964,

p. 86), the use of the presence or absence of normative hypersthene,

which is closely related to the oxidation of iron, seems an inap-

propriate basis by which to classify basalts, in which the oxida-

tion state of iron is known to vary markedly within a single flow.

The "olivine tholeiite" tetrahedron of Yoder and Tilley probably

contains other basalts of alkalic modal mineralogy.

The ratio of total alkali ($Na_2O + K_2O$) to silica has been

used by Tilley (1950), Kuno (1959), and Macdonald and Katsura

(1964) to show that alkali basalts are richer in alkali content

than tholeiites for a given silica content. Figure 12 shows the

boundaries between the alkali basalt and tholeiite fields for two

major volcanic provinces: Japan (Kuno, 1959) and Hawaii (Macdonald

and Katsura, 1964). Although the boundary between the two fields

is in a different position for the two provinces, the alkali : silica

ratio of the Kana-a basalt lies clearly within the alkali basalt

field of both. According to Kuno's boundary curve, which he extends

into more silicic compositions, the S P andesite also belongs to

the alkali series.

Both of the above curves were determined from chemical analyses

of rocks that were identified as alkali basalt or tholeiite on the

basis of modal mineralogy. It is evident from the different posi-

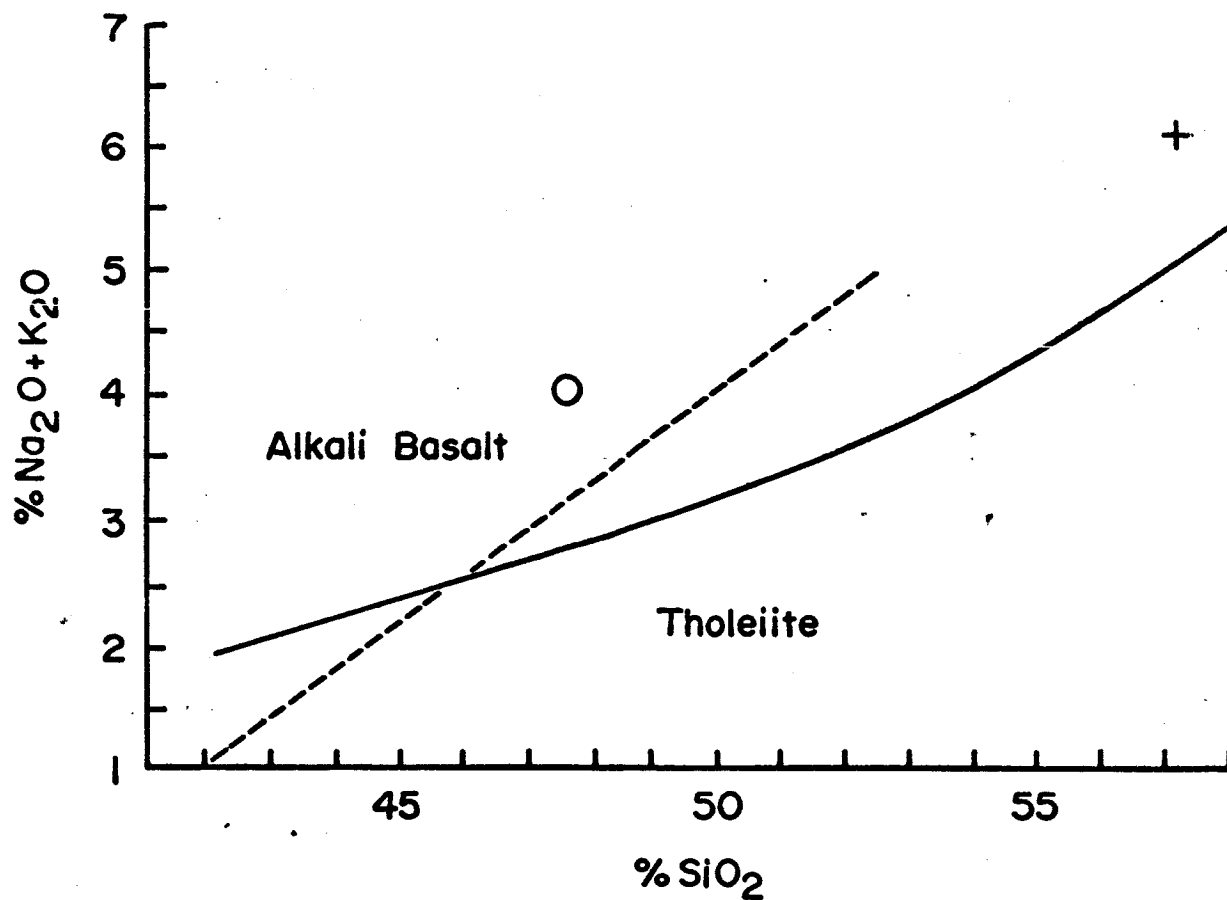tions of the curves that it is hazardous to use a curve established

Figure 12. Total alkalis : silica diagram showing the relation
of the Kana-a basalt (circle) and S P andesite (cross) to the
fields of alkali basalt and tholeiite; solid line from Kuno
(1959, figure 2) and broken line from MacDonald and Katsura
(1964, figure 1).

in one volcanic province to classify basalts in another province that are glassy or in which the mineralogical criteria are obscure or otherwise nondiagnostic. The reason for this marked divergence of the two curves is difficult to evaluate without more data. Perhaps it reflects a chemical compositional gradation from one type of basalt to the other that is not detected in the conventional optical mineralogical work. It is not clear from published work whether the above chemical transition involves a gradual or an abrupt change from typical tholeiite mineralogy to typical alkalic mineralogy. Only careful optical work coupled with chemical analyses of the mineral phases of the chemically transitional rocks can cast light on this important transition.

Kuno (1960), in an effort to show the relation of high alumina basalts to tholeiites and alkali basalts, produced a series of diagrams in which alumina is plotted against total alkali for a given range of silica composition (figure 13). For both silica ranges indicated, the Kana-a basalt lies well within the alkali basalt field.
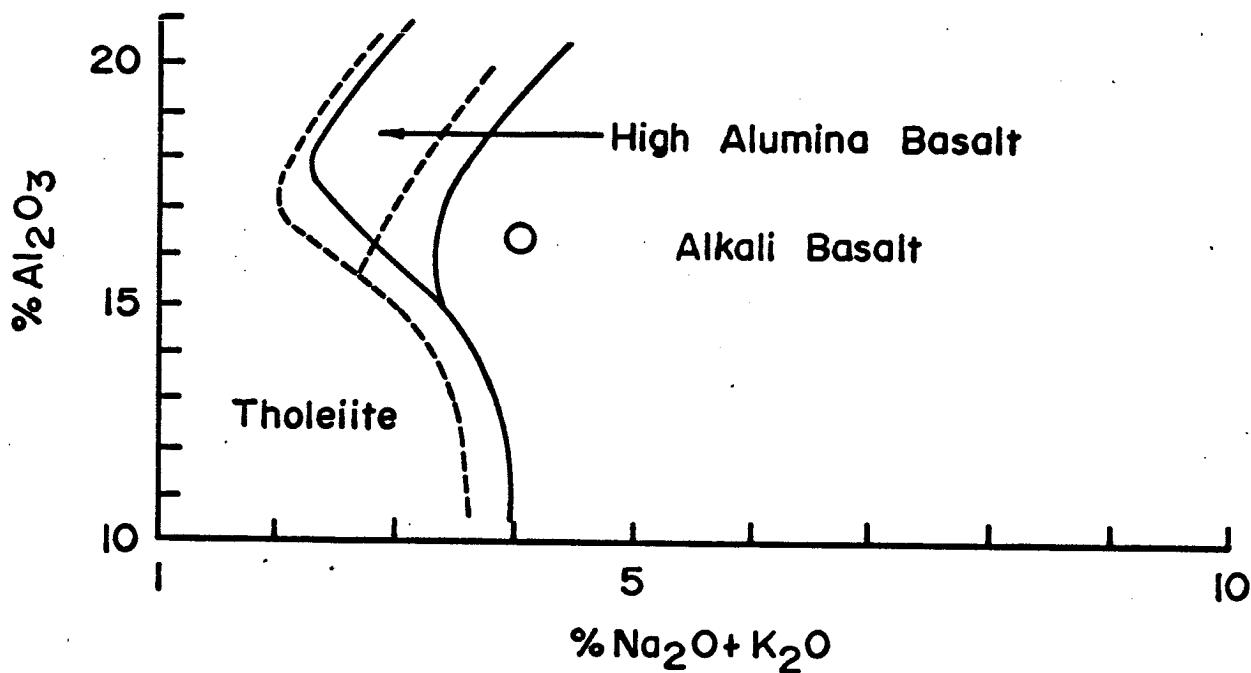
Figure 13. Alumina: total alkalis diagram showing the relation
of the Kana-a basalt (circle) to the fields of alkali basalt,
high alumina basalt, and tholeiite; solid lines are boundaries
of fields for 47.50-50.00% silica and broken lines are for
45.00-47.50% silica; adapted from Kuno (1960).

SUMMARY

The present work has shown that the Kana-a flow has four distinct structural units, based primarily on differences in the degree of vesicularity. These units cannot be distinguished petrographically, and the flow, except for the thin oxidized crust, is homogeneous mineralogically and texturally. (It may be slightly richer in olivine in the lower part, but this could not be proved with the available data.)

Mineralogically and chemically the Kana-a lava is an alkali olivine basalt by most modern classifications except in the recent normative classification of Yoder and Tilley (1962), where it appears to be transitional between their olivine tholeiite and alkali basalt groups. The modal mineralogy of the Kana-a basalt, however, agrees with their conception of the mode of an alkali basalt. Lack of agreement between their modal and normative classifications results from the effect which the oxidation state of iron has on the normative mineral composition. The oxidation state of iron varies widely in the three analyses of the Kana-a basalt, as is common in volcanic rocks, and this variation caused differences in the normative mineral compositions for the three analyses that are critical to the normative classification of Yoder and Tilley. The use of a normative classification of volcanic rocks in which the oxidation state of iron is critical is therefore open to question.

REFERENCES

Bailey, E. B., and others, 1924, The Tertiary and post-Tertiary geology of Mull, Loch Aline, and Oban, Geol. Survey Scotland Mem.

Colton, H. S., 1950, The basaltic cinder cones and lava flows of the San Francisco Mountain volcanic field, Arizona: Mus. Northern Arizona Bull. 10 2d ed., p.1-49.

Deer, W. A., Howie, R. A., and Zussman, F., 1962, Rock-forming minerals, v. 1, Ortho and ring silicates: London, Long-mans, Green and Co., Ltd., 379 p.

Deer, W. A., Howie, R. A., and Zussman, F., 1963, Rock-forming minerals, v. 2, Chain silicates: London, Longmans, Green and Co., Ltd., 333 p.

Hodges, C. A., 1960, Comparative study of S P and Sunset Craters and associated lava flows, San Francisco volcanic field, Arizona: Univ. of Wisconsin, unpublished master's thesis, 129 p.

Hodges, C. A., 1962, Comparative study of S P and Sunset Craters and associated lava flows: Plateau, v. 35, No. 1, p.15-35.

Kennedy, W. Q., 1933, Trends of differentiation in basaltic magmas: Amer. Jour. Sci., 5th ser., v. 25, p.239-256.

Kuno, H., 1959, Origin of Cenozoic petrographic provinces of Japan and surrounding areas: Bull. Volcanologique, 2d ser., v. 20, p.37-76.

Kuno, H., 1960, High alumina basalt: Jour. Petrology, v. 1, p.121-145.

Kuno, H., Yamasaki, K., Iida, C., and Nagashima, K., 1957, Differentiation of Hawaiian magmas: Jap. J. Geol. Geogr. v. 28, p.179-218.

Macdonald, G. A., and Katsura, T., 1964, Chemical composition of Hawaiian lavas: Jour. Petrology, v. 5, p. 82-133.

Nockolds, S. R., 1954, Average chemical compositions of some igneous rocks: Bull. Geol. Soc. Amer., v. 65, p.1007-1032.

Robinson, H. H., 1913, The San Franciscan volcanic field:
    U. S. Geol. Surv. Prof. Paper, 76, 213 p.

Sabels, B. E., 1960, Late Cenozoic volcanism in the San Fran-
    cisco volcanic field and adjacent areas in north-central
    Arizona: Univ. of Arizona, unpublished doctor's thesis.

Schairer, J. F. and Yoder, H. S., Jr., 1960, The nature of
    residual liquids from crystallization with data on the
    system nepheline-diopside-silica: Amer. Jour. Sci.,
    v. 258A, p. 273-283.

Schairer, J. F., and Yoder, H. S., Jr., 1964, Crystal and
    liquid trends in simplified alkali basalts: Ann. Rpt.
    Dir. Geophys. Lab. for 1963-1964, p. 65-74.

Smiley, T. L., 1958, The geology and dating of Sunset Crater,
    Flagstaff, Arizona: New Mexico Geol. Soc. Guidebook,
    9th Field Conf., Black Mesa Basin, northeastern Arizona.

Tilley, C. E., 1950, Some aspects of magmatic evolution:
    Quart. Jour. Geol. Soc. London, v. 106, p. 37-61.

Wentworth, C. K., and Macdonald, G. A., 1953, Structures and
    forms of basaltic rocks in Hawaii: U. S. Geol. Survey
    Bull. 994, 98 p.

Winchell, A. N., and Winchell, D. H., 1951, Elements of optical
    mineralogy, pt. 2, 4th edition; New York, John Wiley &
    Sons, Inc., 551 p.

Yoder, H. S., Jr., and Tilley, C. E., 1962, Origin of basalt
    magmas: Jour. Petrology, v. 3, p. 342-532.

PART II E

Attenuation measurements in the field

by

J. Cl. De Bremaecker*, Richard H. Godson+ and Joel S. Watkins+

* Geology Dept., Rice University, and Branch of Astrogeology,
  U. S. Geological Survey, Flagstaff, Arizona

+ Branch of Astrogeology, U. S. Geological Survey, Flagstaff, Arizona

ATTENUATION MEASUREMENTS IN THE FIELD

by

J. Cl. De Bremaecker*, Richard H. Godson+ and Joel S. Watkins+

* Geology Dept., Rice University, and U. S. Geological Survey, Flagstaff, Arizona.

+ U. S. Geological Survey, Flagstaff, Arizona.

ABSTRACT

The amplitudes of the P head wave were measured on an aa lava flow, on unconsolidated cinders and on compact limestone. The data are satisfied by the equation $A = N\ d^{-2} \exp(-\pi d Q_\alpha^{-1} \nu \alpha^{-1})$, where A is the amplitude, d the distance, Q_α the attenuation coefficient for P waves, ν the frequency and α the P wave velocity. This equation results from the assumption of a complex shear modulus μ^* but a real λ, which also yields $Q_\alpha/Q_\beta = 0.5\ \alpha^2/\beta^2$. ($\beta$=shear wave velocity.) This formula is in reasonable agreement with published data.

Introduction

As part of the preparation for active seismic experiments on the Moon, the U. S. Geological Survey carried out a series of short range seismic refraction profiles on sites north of Flagstaff, Arizona. The present paper deals with some geophysical aspects of the problem, geological descriptions will be published in subsequent papers.

One site was on an aa flow (American Geological Institute, 1960) which is covered with a thickness of cinder and ash ranging from 0 to 3 m; it is designated Kana-a; three profiles, A_1A2, BC, and DE were shot. The second site, designated Cinder Hills, was on a gentle slope of a cinder-and-ash layer approximately 20 m thick; two profiles, AB and CD, were shot. The third site was on Kaibab Limestone at least 25 m thick; one profile was shot.

Instrumentation and procedure

Records were taken with a field system with a uniform response for frequencies between 5 and 500 cps and as little filtering as possible. Geophones were vertical 4.5 cps instruments, and were spaced 15 m apart. Each shot was recorded with twelve geophones. After each shot the shot point was moved 15 m, and a new series of records was taken. Charges consisted of electric blasting caps or dynamite primed with caps; dynamite charges ranged from 0.05 to 0.7 kg. On the limestone charges were fired on the surface;

on the lava flow and on the cinders they were buried in shallow holes (depth equal to or less 1 m).. This had to be done in order to suppress the air wave whose velocity often exceeded that of the P wave in the cinders. The amplitudes of the first wave were measured by a method similar to that of Kovach et al. (1963), i.e., reading the distance from the first peak to the first trough. Although this method is open to objections the large amount of data, their scatter, and the absence of magnetic tape records, appeared to make this the best choice.

In order to compare the amplitudes due to the various shots in each profile, we proceeded as follows. We used one shot as a reference, usually with the shot point 300 ft away from the nearest geophone. Let the readings of the geophones for this shot be R_{300}, R_{350}...R_{850}. Consider now another shot, and let its readings be e.g. A_{100}, A_{150}...A_{650}. We then multiplied each A_i by a constant c determined by the relation.

$$\sum_{300}^{650} R_i = c \sum_{300}^{650} A_i \qquad (1)$$

i.e., we let the "overlapping averages" coincide. This method was carried out for each profile, and the points were plotted on log-log paper so as to make a law of the type $A = N\, d^{-a}$ clearly visible.

(A: amplitude, d: distance). Figures 1, 2 and 3 show the composite profiles of the amplitude versus the distance. It may be seen that the scatter is large in all profiles. Such a scatter is often observed in amplitude work, and makes the use of amplitudes greatly more difficult than that of arrival times.

At any given site all the arrivals used fall on the same branch of the travel-time curve.

Restrictions on the interpretation

Any interpretation should explain the following facts, the first three of which are directly relevant to the data, the last one being less directly connected with it.

1) A law $A = N\,d^{-a}$ appears satisfactory from an experimental standpoint but has no theoretical justification, because a varies
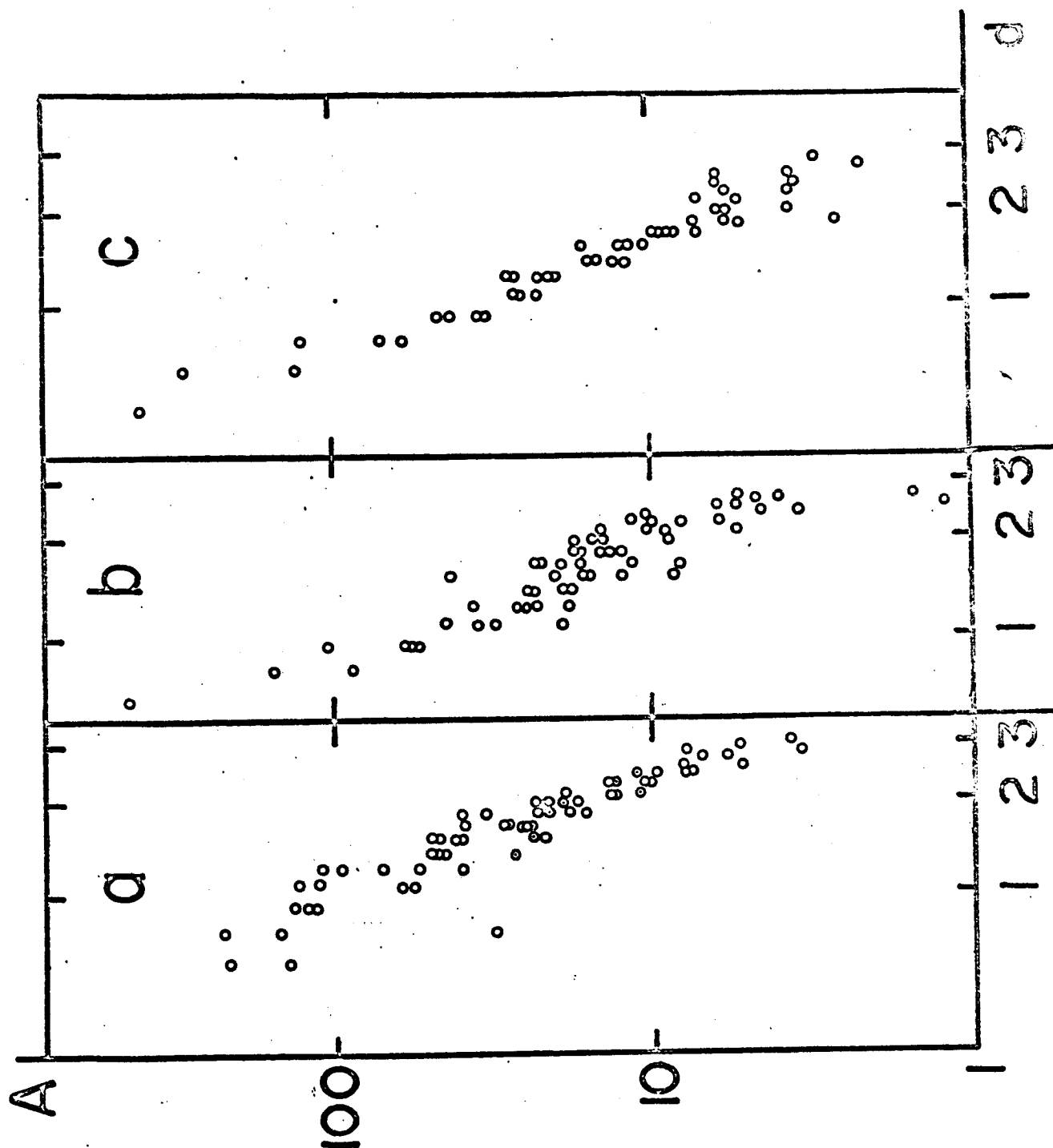
Figure 1. Amplitudes versus distance, Kana-a site (d in hundreds of meters); Profile BC, Profile A_1A_2, and Profile DE.
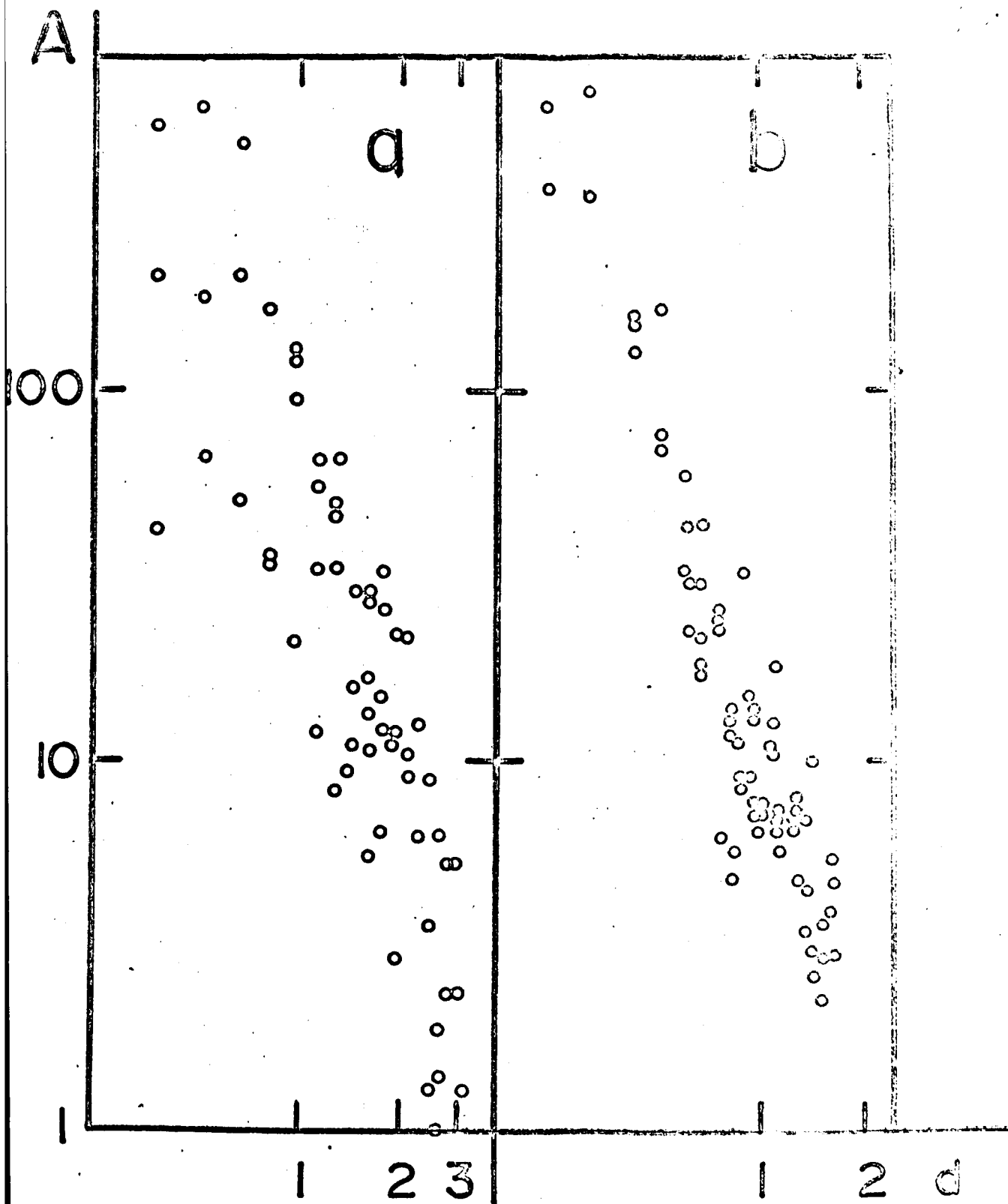
Figure 2. Amplitudes versus distance, Cinder Hills site (d in hundreds
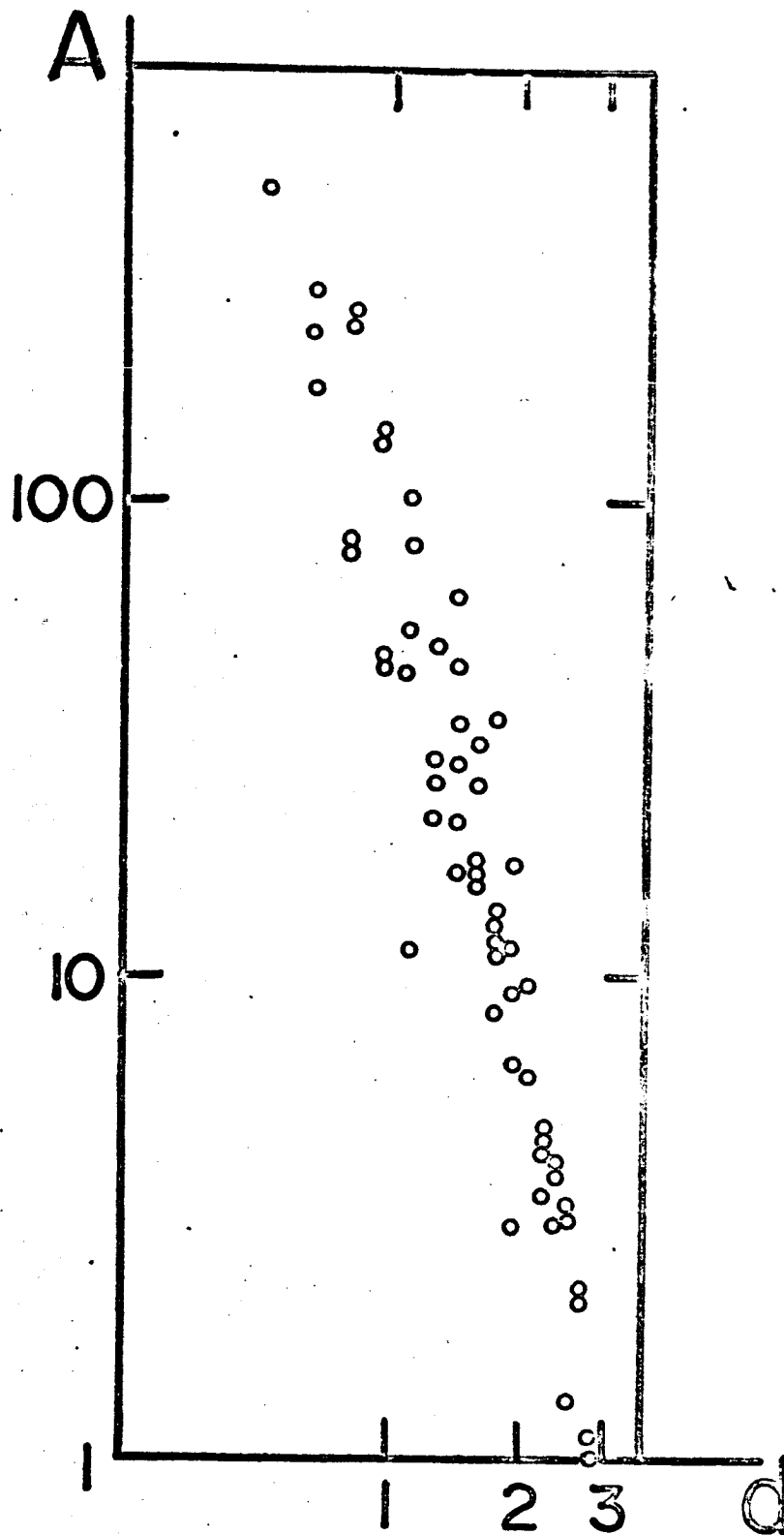of-meters); Profile AB and Profile CD.

Figure 3. Amplitudes versus distance, Kaibab site (d in hundreds of meters).

greatly from profile to profile and is larger than 2, which is the theoretical spreading factor for head waves. The excess can be attributed to dissipation processes.

2) The attenuation of P waves in the Kaibab Limestone is much greater than in Cinder Hills and still greater than on Kana-a. This fact appears surprising because the Kaibab Limestone is hard and compact, whereas the surface of Cinder Hills crumbles under foot (although it is somewhat more compact at depth). The Kana-a flow appears to be a typical aa basalt flow.

3) The attenuation law found by Kovach et al. (1963) is $A = N d^{-2.3}$ on alluvium, while a rough estimate of a in the Kaibab Limestone gives a value of 4, thus almost twice as great.

4) In addition, any explanation must be compatible with the fact that the S wave attenuation in sediments near the surface is approximately nine times greater than that of the P wave (White and Sengbush, 1963); it must also agree with other data in the literature (e.g. Vasil'yev and Gurevich, 1962; also Anderson et al., 1964).

Interpretation

It is well-known that the behavior of real bodies is very complicated (Kolsky, 1953, ch. 5). It appears, however, that when the period of waves is short compared to the relaxation time of

a Maxwell solid, a Voigt solid is a fairly good approximation to the actual situation. (Ewing, Jardetzky and Press, 1957, p. 277). It must be understood that this assumption is only valid in a more or less restricted band of frequencies: a range of two orders of magnitude is probably reasonable.

In such a restricted frequency band, an isotropic Voigt solid can be represented by making both of Lamé's constants complex, or by an equivalent assumption (see e.g. Kolsky, 1953, ch. 5). We will write

$$\lambda^* = \lambda + i\lambda' \qquad\qquad \mu^* = \mu + i\mu'$$

In this case the wave number $k^* = k + ik'$, becomes complex, resulting in an attenuating P head wave of amplitude

$$A = N \, d^{-2} \exp(-k'_\alpha \, d) \qquad\qquad (2)$$

where d is the distance. The attenuation k'_α is related to the attenuation coefficient for P waves, Q_α, by the relation

$$k'_\alpha \, Q_\alpha \, \alpha = \pi \, \nu \qquad\qquad (3)$$

where α is the P wave velocity and ν is the frequency. Q_α is supposed to be independent of frequency.

Before attempting to reconcile formula (2) with the experimental law

$$A = N \, d^{-a} \qquad\qquad (4)$$

it should be observed that a formula of the type

$$A = N (d-f)^{-3/2} \ d^{-1/2} \ \exp \ (-k_\alpha' d)$$

where f is the minimum distance of arrival of the head wave, is
probably more correct (Ryall and Stuart, 1963). In the present
case, however, the scatter of the data makes this further refine-
ment of dubious value.

Least square solution

We will later show that formulae (2) and (4) are compatible
within the limits of experimental error, but first we will use the
experimental data to determine the constants in equation (2). In
this equation we observe that the value of N is not relevant to the
present problem. On the other hand the determination of k_α' by a
least square process is not immediate, because the standard method
leads to a system of non-linear equations. We may, however, obtain
a system of linear equations by taking the logarithm of both sides;
thus:

$$\ln A = \ln N - k_\alpha' \ d - 2 \ \ln d \ . \tag{5}$$

The determination of k_α' from (5) is a simple least square problem.
However the "best" k_α', as found from (5), is not the "best" k_α' for
equation (2).

It is well-known that in such a case one obtains the best fit
for the original equation by solving the transformed equation, but

weighting the measurements by the inverse of the square of the derivative of the transformation, evaluated at each point (Guest, 1961, p. 335). In the present case (logarithmic transformation) the weights are thus proportional to the squares of the amplitudes.

It should be observed that the standard deviation, s, thus computed, depends on the absolute amplitude rather than on the relative one. Since we had to adjust the measurements to a common reference profile before the least square fit, the computed standard deviation is probably not meaningful in the present case.

We determined the "best" k_α' both directly from equation (5) without weights, and from equation (5) with weights, i.e. in essence from equation (2). The results for each profile are shown in table 1, where we have also given the velocity in mps, the standard deviation, s, of each k_α', and the corresponding Q_α(table 2). The latter was obtained from α and the dominant frequency (100 cps).

The question now arises which of the two k_α' is actually best. In the literature, the determination of a in equation (4) (which is analogous to that of k_α' here) appears always to have been made after a logarithmic transformation. No justification of this process appears to have ever been given, and from what has been said, it might appear incorrect. On closer examination it may perhaps be suggested that the choice between the two depends on the data: if these are obtained in such a way that the relative amplitude of the error (noise) compared to the signal is substantially constant, then a fit from (5) is best. If it is the absolute

E-11

Table 1

Attenuations at various sites

Site	Profile	α mps	10^4 k'_α/m from (2)	$10^4 s$	Q_α	10^4 k'_α/m from (5)	10^4	Q_α
Cinder Hills	AB	305	85	69	121	74.4	15.4	138
	CD	305	44	88	234	30.5	13.8	338
Kana-a	A_1A_2	760	149.2	59	28	29.5	11.02	140
	BC	760	0.111	39	37000	33.8	7.2	122
	DE	760	180	85	23	32.8	8.5	126
Kaibab		2,440	43.6	59	29	115.7	8.9	11.1
Kovach et al.		610	14.1	32	14.6	2.79	2.5	74

Table 2

Least-square fit of formulae (2) and (5) to a power law ($d^{-\underline{a}}$)

	From (2)	From (5)	
$\underline{a}$	$10^4 k'_\alpha$	$10^4 k'_\alpha$	$10^4 s$
2.5	50.5	30.8	1.74
2.75	79.3	46.2	2.59
3.0	110.2	61.6	3.48
3.25	143.3	77.0	4.33
3.5	177.7	92.5	5.18
3.75	213.1	107.9	6.03
4.0	249.5	123.3	6.92
4.25	286.9	138.7	7.77
4.5	324.3	154.4	8.62
4.75	362.0	169.8	9.51
5.0	400.0	185.2	10.39

amplitude of the error which is constant, then a fit from (2) must be used. In the present case we believe that (5) is slightly closer to reality, at least for most points. A much more detailed investigation than the present one would be needed to settle the question. Another reason for using (5) rather than (2) has been given when discussing the standard deviation.

The values obtained from (5) are not very well determined: s is the order of 20% of k'_α except in the Kaibab site where it is less than 10%. This is to be expected because of the homogeneity of the last material; it confirms the visual impression about the relatively small scatter in this case.

The values of Q_α obtained from (5) range from approximately 340 (Cinder Hills, CD) to approximately 11 (Kaibab). Evison (1953) suggested a value of 0.03 for the attenuation per wave length, which corresponds to $Q_\alpha = 105$; this is in the range covered by our values. The fact that the attenuation in the Kaibab Limestone is by far the largest is surprising, and we will revert to this later.

We now apply the same technique to the measurements made in alluvium by Kovach et al. (1963). From the data on their figure 3, from the 4 cps dominant frequency in their figure 4, and assuming, for lack of data, $\alpha = 600$ mps, we find the results given in the last line of table 1. Note that k'_α is very poorly determined in this case ($s \approx k'_\alpha$). The most interesting result is Q_α from (5) i.e. 74 a result comparable to ours in Kana-a and Cinder Hills.

This also shows that the exponent in equation (4) is meaningless, because it does not take into account the frequency or the velocity. The third fact is thus explained.

The results of Kovach et al. on granite are probably not head waves ($a<2$), and will not be discussed.

It should be noted that our results refer only to material near the surface.

Compatibility of formulae (2) and (4)

In order to show that formulae (2) and (4) are compatible within the limits of experimental error we computed the values of A from (4) every 15 m from 60 m to 300 m for values of a ranging from 2.5 to 4.5 in steps of 0.25. We then used the same technique as previously to fit a least square curve corresponding to either (2) or (5). The results are shown in table 2.

The standard deviation of k_α' for equation (2) is not given: it is meaningless because it depends on the absolute amplitudes, and N in equation (4) is arbitrary.

The best fit of equation (5) to d^{-a} yields $s <0.1 k_\alpha'$. This is a substantially better fit than is obtained from the experimental data. We thus conclude that the data are too scattered to permit us to differentiate between a law in d^{-a} and a law in $d^{-2} \exp(-k_\alpha' d)$. We further observe that k_α' computed from (5) is approximately half that computed from (2), but such a relation does not hold for the experimental data due both to the different scatter, and to the variable number of measurements at different distances.

The attenuations of P and S

So far we have only examined the attenuation of P waves. We now turn to the question of the relative attenuations of P and S, and to their relation with the appearance of the material. As mentioned before, the latter intuitively suggests a larger attenuation in Cinder Hills than in Kaibab, but one is left in doubt whether one's intuition refers to P or S waves.

In a general Voigt solid both λ and μ are complex. However, there is some indication that in sedimentary rocks λ' is substantially smaller than μ', so that $\lambda' + 2\mu' \approx 2\mu'$; D. L Anderson (private comm. 1964) found that in the Pierre shale $\lambda' = 0.16 \mu'$. As an approximation, therefore, we propose to set $\lambda' = 0$. Note that this corresponds to $\varkappa' = 2/3 \mu'$, whereas a more common assumption has $\varkappa' = 0$ which gives $\lambda' = -2/3\mu'$. As Kolsky (1953, p. 109) points out, the latter assumption does not appear to be generally true. We will show that $\lambda' = 0$ leads to more nearly correct results, although we must emphasize that it is only an approximation.

If, thus, we let

$$\mu^* = \mu + i\mu'$$

then

$$\beta^* = \beta + i\beta' = (\mu + i\mu')^{\frac{1}{2}}\rho^{-\frac{1}{2}}$$

and

$$\alpha^* = \alpha + i\alpha' = (\lambda + 2\mu + 2i\mu')^{\frac{1}{2}}\rho^{-\frac{1}{2}}.$$

Squaring and dividing we obtain

$$\alpha\alpha' = 2\beta\beta' \tag{6}$$

hence

$$k'_\alpha = -2\pi\nu\alpha' \, (\alpha^2 + \alpha'^2)^{-1}$$

E-16

We may assume that in the earth $\alpha^2 \gg \alpha'^2$, hence

$$k'_\alpha \approx -2\pi\nu\alpha'\alpha^{-2}$$

and similarly

$$k'_\beta \approx -2\pi\nu\beta'\beta^{-2}.$$

Thus,

$$k'_\beta/k'_\alpha \approx \beta'\alpha^2\beta^{-2}/\alpha'$$

and using (6)

$$k'_\beta/k'_\alpha \approx 0.5 \, \alpha^3/\beta^3 \tag{7}$$

or

$$Q_\alpha/Q_\beta \approx 0.5 \, \alpha^2/\beta^2 \tag{8}$$

or, in terms of Poisson's ratio σ

$$k'_\beta/k'_\alpha \approx 0.5 \, [\, 2(1-\sigma)/(1-2\sigma) \,]^{3/2} \tag{9}$$

or

$$Q_\alpha/Q_\beta \approx (1-\sigma)/(1-2\sigma).$$

On the other hand, if we assume that the imaginary part of the compressibility is zero, we find

$$Q_\alpha/Q_\beta = 0.75 \, \alpha^2/\beta^2. \tag{10}$$

Poisson's ratios as high as 0.42 to 0.47 have been reported in unconsolidated sedimentary material (Heiland, 1946, p. 468), while a value of 0.41 is reported in ignimbrite near the surface (Evison, 1956). A value of $\sigma = 0.45$ leads to $k'_\beta/k'_\alpha = 18.2$, while $\sigma = 0.4$ gives $k'_\beta/k'_\alpha = 7.3$. White and Sengbush (1963) give the values $\alpha = 2.15$ km/sec, $\beta = 0.86$ km/sec, $k'_\beta/k'_\alpha = 17.4/2.06 = 8.4$; equation (7) gives $k'_\beta/k'_\alpha = 7.8$. The agreement is thus excellent in this case. The same values are also given in McDonal et al. (1958).

In their paper summarizing most measurements on attenuation and propagation velocities Vasil'yev and Gurevich (1962, see figure 4) remark that equation (1) does not agree with most of the experimental data. It may be noted that they write this equation under the equivalent form

$$\Delta_p/\Delta_s = 1.33\ \beta^2/\alpha^2 \qquad\qquad (11)$$

where Δ_p is the logarithmic decrement of the P wave, hence $\Delta_p/\Delta_s = Q_\beta/Q_\alpha$. (There is an evident misprint in their equation 27). Our figure 4 is similar to the one shown in their paper, but shows both equations (8) and (10). It is clear that (8) is more nearly correct than (10), even though it is only an approximation. On the other hand we should remark that the data shown in this figure have been obtained by a large number of investigators at frequencies ranging from 0.05 cps to 1 Mcps, and for substances ranging from water-saturated clays to dry granite. (Vasil'yev, 1962). We propose the approximation $\lambda' = 0$ only for sedimentary material near the surface. With this restriction in mind it appears that our assumption is in reasonable agreement with published data, although a case could clearly be made for a larger value of k', i.e. for a positive value of λ'.

Reverting to our own measurements we now seek to explain the relatively high attenuation in the Kaibab Limestone compared to that in other materials, despite their field appearances. In the Kaibab $k'_\alpha \approx 35$; moreover in limestone $0.18 < \sigma < 0.26$ (Birch, 1942, p. 76) thus $k'_\beta/k_\alpha = 2.0 \ldots 2.7$ and $k'_\beta = 70 \ldots 95$. In Kana-a
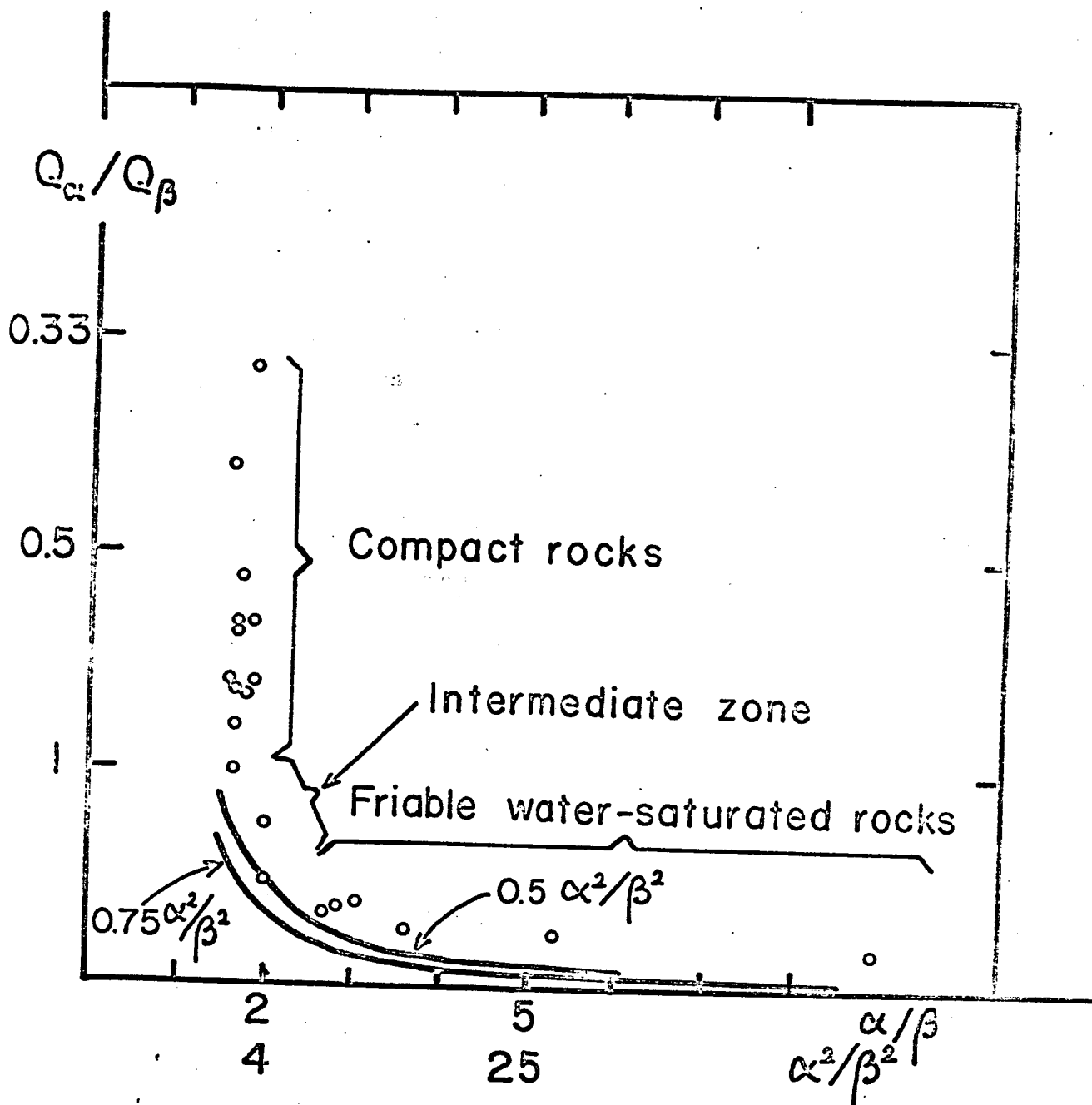
E-18

Figure 4.   Measurements and range of Q_α/Q_β versus α^2/β^2, after Vasil'ev and Gurevich (1962), and curves corresponding to $Q_\alpha/Q_\beta = 0.75 \, \alpha^2/\beta^2$ and to $Q_\alpha/Q_\beta = 0.5\alpha^2/\beta^2$.

and Cinder Hills $k'_\alpha = 10...20$; presumably $k'_\beta/k'_\alpha = 7.0 ... 18$, thus k'_β might range from perhaps 70 to 360, with a smaller range rather more likely. It is thus barely possible for the attenuation of the S waves in the Kaibab to be smaller than in the other materials, but it is still surprisingly high. Don Tocher (personal comm., 1965) has suggested that this result is due to the downward deflection of energy by a low velocity bed underlying the Kaibab Limestone. We hope to investigate this possibility at a later date. Meanwhile we note that more recent measurements at this site appear to give a smaller value of the attenuation.

It should be added that our own efforts to measure β in situ have not, so far, been successful; we have used explosives and some variation of the weight dropping technique (hammer blow, etc.). The latter method should produce shear waves, as was first shown by Lamb (1904) and as recorded in the field by White and Sengbush (1963). Unfortunately the field record is too confused to permit any definite measurement of velocity or of amplitude.

In this connection it is, of course, realized that it is incorrect to use ray optics in the present case where the layers have dimensions comparable to the wavelengths, but it is thought that the first arrivals of both P and S should not be very much distorted. Furthermore, the complexity of the seismograms does not appear to permit a more involved analysis.

Conclusions

The assumption of a complex shear modulus μ^*, but a real λ, appears to furnish an adequate explanation of both published and new data on the attenuation of P wave with distance; it also explains the greater attenuation of S waves, and relates the attenuations to the relative velocities of P and S.

Acknowledgements

REFERENCES

American Geological Institute, 1960, Glossary of geology and
   related sciences, with supplement.

Anderson, D. L., and Archambeau, C.B., 1964, The anelasticity
   of the earth: Jour. Geophys. Research, v. 69, pl 2071-2084.

Birch, Francis, 1942, Elasticity, in Birch, F., Schaifer, J. F.,
   and Spicer, H. C., eds., Handbook of physical constants:
   Geol. Soc. Am., Spec. Paper, v.36.

Bullen, K. E., 1963, An introduction to the theory of seismology,
   3rd ed.: Cambr. Univ. Press, 381 p.

Evison, F. F., 1953, An improved electromechanical seismic source
   tested in shattered rock: New Zealand Jour. Sci. and Tech-
   nology, v. 35, p. 4-13.

_____, 1956, The seismic determination of Young's modulus
   and Poisson's ratio for rocks in situ: Geotechnique, p.
   118-123.

Ewing, W. M., Jardetzky, W. S., and Press, Frank, 1957, Elastic
   waves in layered media: New York, McGraw Hill Book Co.,
   380 p.

Guest, P. G., 1961, Numerical methods of curve fitting: Cambr.
   Univ. Press, 422 p.

Heiland, C. A., 1946, Geophysical exploration: New York, Prentice-
   Hall, 1913 p.

Kolsky, H., 1953, Stress waves in solids: Oxford, Clarendon Press,
   211 p.

Kovach, R. L., Lehner, Francis, and Miller, Roy, 1963, Experimental
    ground amplitudes from small surface explosions: Geophysics,
    v. 28, p. 793-798.

Lamb, H., 1904, On the propagation of tremors over the surface of
    an elastic solid: Phil. Trans. Roy. Soc. London, vol. A, no.
    203, p. 1-42.

McDonal, F. J., Angoma, F. A., Mills, R. L., Sengbush, R. L., Van
    Nostrand, R. G., and White, J. E., 1958, Attenuation of shear
    and compressional waves in Pierre shale: Geophysics, v. 23,
    p. 421-439.

Ryall, Alan, and Stuart, D. J., 1963, Travel times and amplitudes
    from nuclear explosions, Nevada Test Site to Ordway, Colorado:
    Jour. Geophys. Research, v. 68, p. 5821-5835.

Vasil'yev, Yu. I., 1962, Dve svodki konstant zatukhaniya uprugikh
    kilebaniy v gornykh porodakh [Two sets of constants of attenu-
    ation of elastic oscillations in rocks]: Akad. Nauk SSSR
    izv. Ser. Geofiz., no. 5, p. 595-602.

Vasil'yev, Yu. I., and Gurevich, G. I., 1962, O sootnoshenii
    mezhdu dekrementami zatukhaniya i skorostyami rasprostraneniya
    prodol'nykh i poperechnykh voln [Relationship between the
    decrements of attenuation and the velocity of propagation of
    longitudinal and transverse waves]: Akad. Nauk SSSR Izv.
    Ser. Geofiz., no. 12, p. 1695-1716.

White, J. E., and Sengbush, R. L., 1953, Velocity measurements in

near-surface formations: Geophysics, v. 18, p. 54-69.

White, J. E., and Sengbush, R. L., 1963, Shear waves from explosive

sources: Geophysics, v. 28, no. 6, p. 1001-1019.

PART II F

VELOCITIES AND ATTENUATIONS OF HEAD-WAVE AMPLITUDES

OBSERVED IN LUNAR ANALOG ROCKS

UNPUBLISHED MANUSCRIPT
FOR OFFICIAL USE ONLY

by

R. H. Godson, J. S. Watkins and R. A. Loney

U. S. Geological Survey
Flagstaff, Arizona

VELOCITIES AND ATTENUATION OF HEAD-WAVE AMPLITUDES
OBSERVED IN LUNAR ANALOG ROCKS

by

R. H. Godson, J. S. Watkins and R. A. Loney

U. S. Geological Survey
Flagstaff, Arizona

INTRODUCTION

During the fiscal year 1965 seismic investigations were carried out at 11 selected sites. Five sites, Kaibab, Kana-a flow, S P flow, Cinder Hills and Meteor Crater are located within 80 km of Flagstaff, Arizona (see figure 1). The other 6 locations are situated in eastern and southern California: Pisgah and Amboy flows between Amboy and Barstow in the Mojave desert (see figure 2); Southern Coulee and Mono Ash close to Lee Vining; Sonora Pass about 80 km northwest of Lee Vining in the Sierra Nevada Range; and Bishop Tuff near Bishop, California (see figure 3). A total of 512 recordings at 220 spread locations were made at the above sites. Several experimental recordings were made in preparation for astronaut training studies at the Nevada Test Site and Meteor Crater, as well as cavity location feasibility studies at U4B Crater at NTS, and shear wave studies at Kana-a, Kaibab and in the Mojave desert.

VELOCITIES AND ATTENUATIONS OF HEAD-WAVE AMPLITUDES

OBSERVED IN LUNAR ANALOG ROCKS

by

R. H. Godson, J. S. Watkins and R. A. Loney

U. S. Geological Survey
Flagstaff, Arizona

ABSTRACT

Seismic data collected at 11 sites each having structural and lithologic similarities with those inferred for lunar near-surface materials indicate that P head wave amplitude attenuation is strongly affected by fracturing. Velocity seems dependent on porosity and degree of cementation. The data have formed the basis for an estimate of amplitude attenuations on the lunar surface and were incorporated into the design of a proposed lunar engineering seismic experiment.
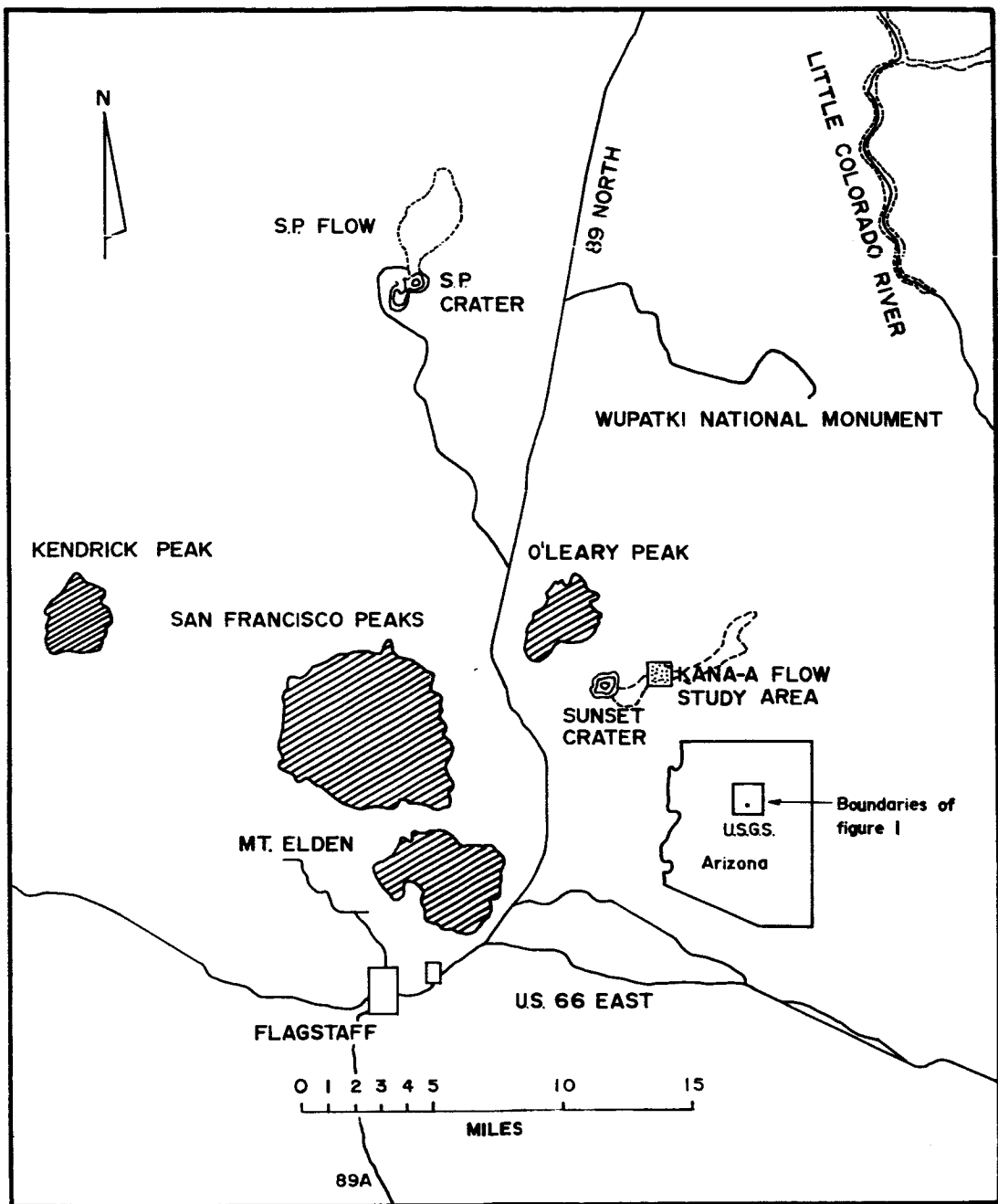
Figure 1. Locations of study areas relative to prominent terrain and cultural features of north-central Arizona.
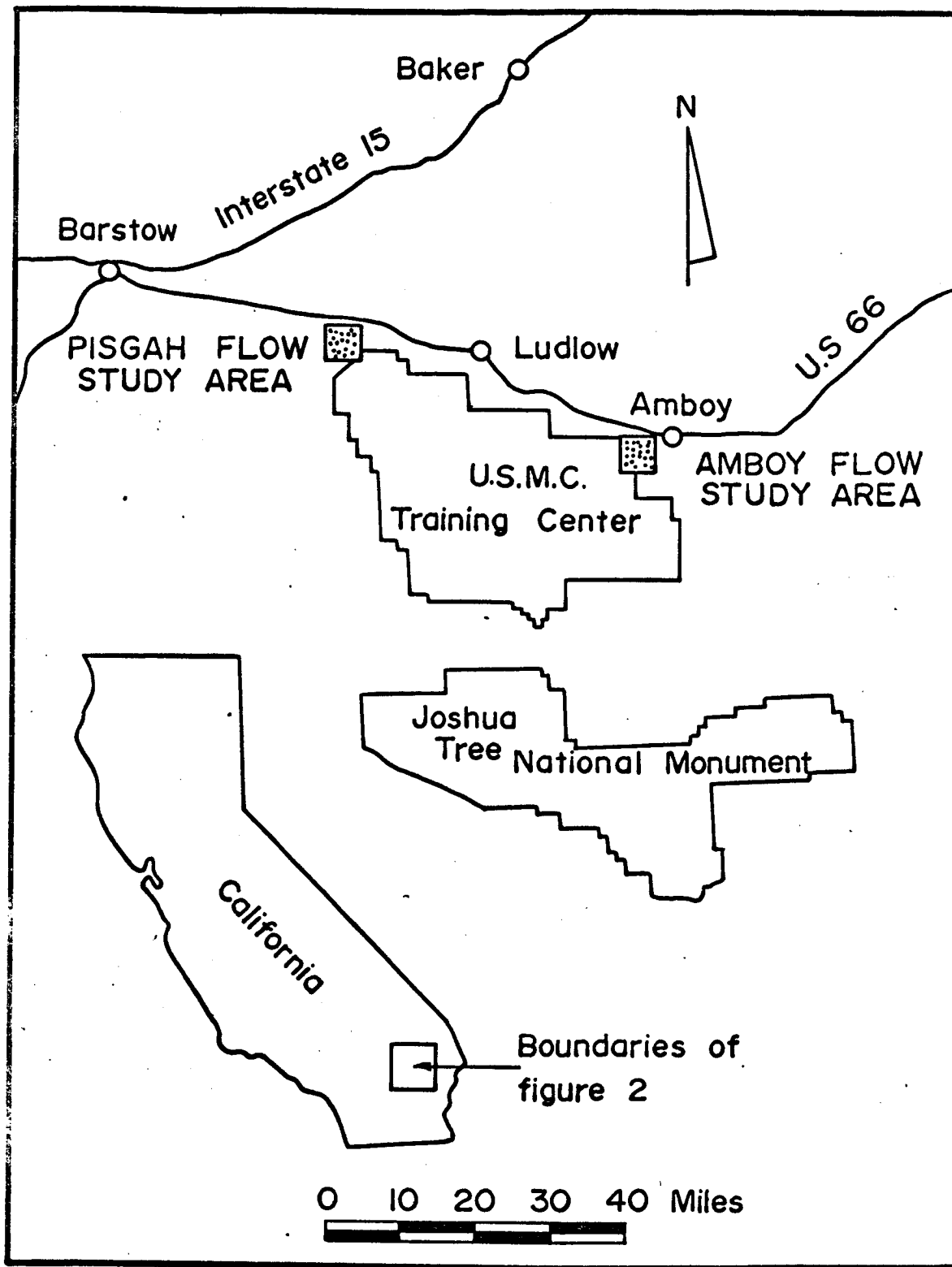
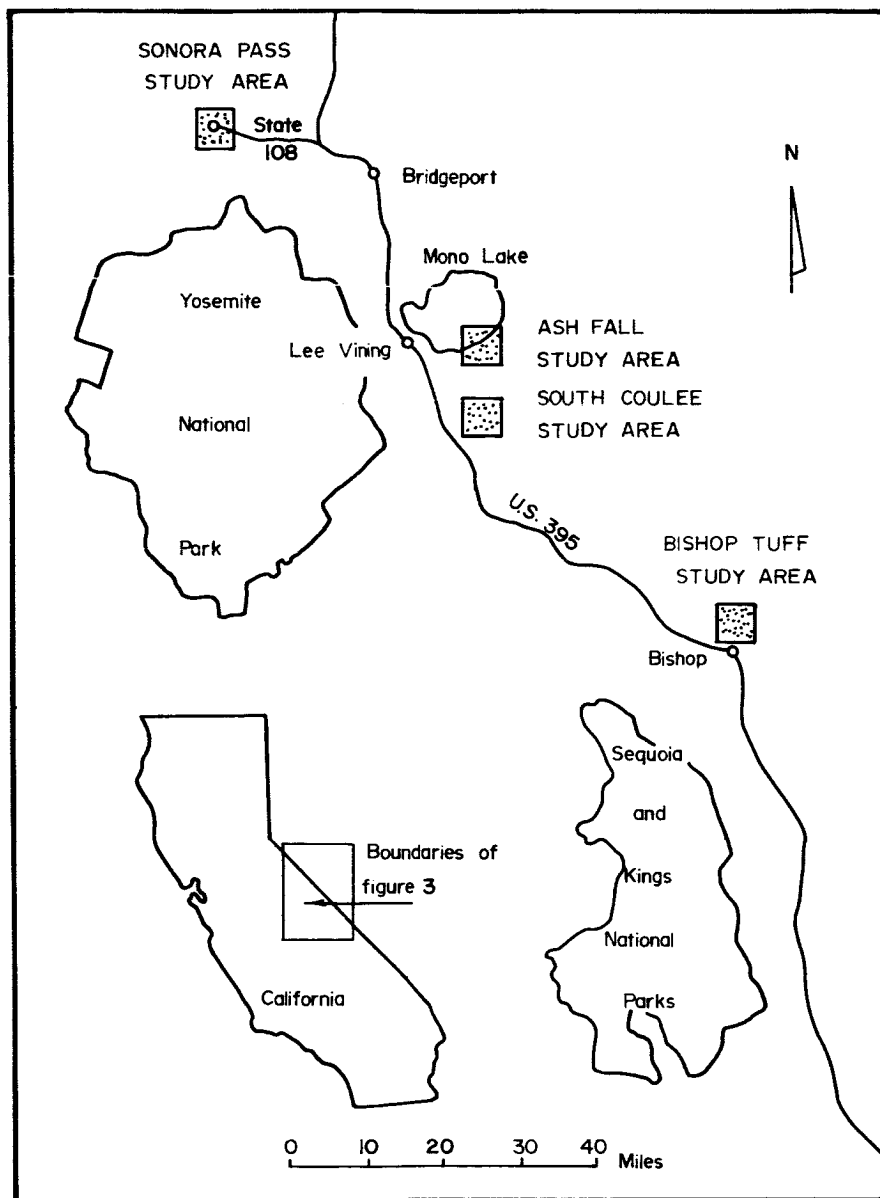Figure 2.   Map showing study areas in southern California.

Figure 3. Map showing study areas in east central California.

General Field Procedures

The following is a description of field methods used for attenuation studies:

1) When possible, all spread locations were chosen so that the spread and shot points would be approximately level.

2) All seismometers were leveled and buried to minimize the effect of the wind.

3) One vertical geophone and two horizontal geophones with their axes at right angles were mounted on one base plate.

4) All recordings were made on magenetic tape with fixed gain and the filters out-out.

5) At most sites three cables of lengths of 175, 70 and 35 m were laid out. Each cable has eight takeouts so the geophone intervals were 25, 10 and 5 m, respectively. The number eight group of each cable was common.

6) As a general rule, the 175 m cable was recorded using charge sizes varying from 5 to 10 lbs of dynamite at an offset distance of 30 m; the 70 m cable recorded with 1/8 lb of dynamite at offset distances of six and nine meters and the 35 m cable recorded using an electric blasting cap at offset distance varying between 3 and 9 m.

Rock Type Descriptions of Study Areas

S P flow.-The flow is a recent basaltic lava flow, whose surface consists of loosely packed, angular, equant, polygonal blocks of lava that range from 20 cm to 2 m across and average about 0.3 m in diameter.

The porosity of the loosely packed rubble is estimated to range between 20 and 35 percent.

The blocky basalt is dark gray to grayish-black and weathers to a mottled dark-reddish and yellowish-brown. It is fine grained and finely vesicular; the vesicles being generally tube-like and distinctly flattened. The vesicularity of the rocks at the surface ranges from less than 5 to as much as 50 percent and averages about 15 percent. Small phenocrysts of plagioclase, pyroxene and rarely olivine which average about 1 mm in length, are sparsely scattered through the rock.

The rock has a porphyritic hyalopilitic texture mainly composed of elongate laths of plagioclase and stubby prisms of pyroxene set in a base of brown glass. The plogioclase laths in general show a distinct fluidal orientation that beds and swirls around the phenocrysts, which are mainly pyroxene. The grain size ranges from .01 mm to 5.0 mm and averages about .07 mm. The plagioclase is mostly calcic andesite, indicating that the rock is probably a basaltic andesite or an andesitic basalt.

Kana-a flow.-This recent olivine basalt flow is a typical aa-type lava. The flow is covered with 0 to 6 m of ash through which project jagged, spinose, vesicular, clinkery blocks and plates of lava which are commonly tilted up at various angles.

The lava is medium gray to medium dark gray and weathers dark gray. It is fine grained, though distinctly coarser than S P and is very sparsely and finely prophyritic. Olivine and plagioclase phenocrysts occur in about equal amounts but the larger (average about 2 mm in diameter) rounded, glassy

green olivine crystals are much more conspicuous. The flow is much more vesicular than S P with the vesicles ranging in diameter from less than 1 mm to more than 20 mm and averaging about 5 mm. The vesicularity ranges from 10 to 50 percent and averages about 25 percent.

Cinder Hills.-This area, which lies north-northeast of Sunset Crater, consists of thick accumulations of ash. The ash is deposited in beds that range from 15 cm to more that a meter in thickness. The grain size in these beds varies markedly from bed to bed with some suggestion of grading upward from coarse to fine. The range in grain size within a meter or so varies from ¼ to 3 mm in diameter.

Kaibab.-This area near S P Crater consists of a relatively thick sequence of limestone beds and interbedded limestone-clastic beds of Permian age. The thickness in the study area is in excess of 80 feet.

Sonora Pass.-This granite is coarsely prophyritic, pale pink and characterized by abundant large euhedral phenocrysts of pink potassium feldspar, which average about 5 cm long and in places are as much as 10 cm long. Megascopically, the groundmass consists of small (average about 3 mm in diameter) grains of pink potassium feldspar, white plagioclase, and glassy quartz through which are scattered fine grains of biotite and hornblende.

The granite is generally unweathered except for the upper inch or two. It is nearly homogeneous and sparsely jointed; only a few 2 to 5 cm thick, aplite veins are present.

South Coulee.-The top of this coulee is a chaos of spires, crags and

loosely piled angular blocks of pumice and obsidian. Three distinct litho-logic units are recognized; each has a characteristic range in density and distinctive physical characteristics. No compositional differences have been recognized--differences are related to degree and character of visicu-larity. The unit of lowest density ranges from .51 to .78 g per cc, the intermediate layer has a density of 1.20 g per cc and the unit of highest density, where obsidian is more abundant ranges from 1.37 to 2.07 g per cc.

The rock of the coulee is predominantly layered pumice (density 0.53 to 2.01 g per cc) that generally lacks microscopically visible crystals. Obsidian, a minor but ubiquitous constituent of all units, occurs as lenses and laminae in the pumice. The obsidian lacks visible phenocrysts but contains sparse spherulites that range in diameter from less than 1 mm to more than 40 mm, and average about 2mm. X-ray diffraction indicates that the spherulites are composed of sanidine and well-ordered cristobalite.

Glass of the pumice and obsidian is fresh and lacking in devitrifica-tion products, except the sparse spherulites in the obsidian. A few minute crystals of sanidine have been seen microscopically, but these are extremely rare and do not noticeably affect the whole-rock x-ray diffraction patterns, which are characteristic of pure glass.

Mono Ash.-This area lies northeast of the northernmost of the main mass of the Mono Craters and consists of a thick layer of white pumiceous ash and lapilli that is level and free of vegetation. The ash shows a higher degree of crystallinity than the flow rocks; quartz, plagioclase, biotite and possibly potassium felspar have been identified by x-ray diffraction.

<u>Bishop Tuff</u>.- The rock of this large area is partially welded rhylite tuff of Pleistocene age between 30 and 60 m thick. The upper 10 or 15 m is welded, hard and dense but below this layer it is unwelded and less dense to an unknown depth. In general, regardless of the degree of welding, the tuff is a well indurated rock. It is tightly jointed into polygonal columns about 0.7 m across.

The tuff is composed of fragments of porphyritic pumice, which contain abundant phenocrysts of quartz, sanidine, and lesser amounts of plagioclase and biotite sprinkled at random through a matrix of fine vitric tuff. The matrix also contains crystals similar to the pumice of South Coulee. Crystals compose about 10 percent of the tuff. The color of the tuff is pink to reddish brown at the surface but white layers stratigraphically below the pink tuff crop out along the southern edge of the deposit.

DATA RESULTS

Data from 8 sites, Kaibab, Kana-a flow, S P flow, Cinder Hills, Southern Coulee, Mono Ash, Sonora Pass and Bishop Tuff, have been analyzed for velocities of head-waves, amplitudes of first full cycle of arriving seismic energy and modal frequency of the first cycle of energy.

Amplitudes of the first cycle were measured and compared with amplitudes on records taken with known input voltages thereby obtaining the output for each geophone on a spread (see figure 4). The measured voltages were then plotted against distance from shot point to geophone on semi-log paper; voltage on the log scale and distance on the linear scale. A straight line estimate of the best fit of the data was drawn through the plotted points and the slope of this line calculated from the formula $A = N \exp{(-\pi d Q_\alpha^{-1} \nu \alpha^{-1})}$ where A is the amplitude, d the distance, Q_α the attenuation coefficient for P-waves, ν the frequency, and α the P-wave velocity.

The above formula was selected after comparison of results obtained using $A = N d^{-n}$ and $A = k d^{-2} \exp{(-\pi d Q_\alpha^{-1} \nu \alpha^{-1})}$. The results using the latter of the two above formulas were scattered only slightly more than results based on the formula which we selected.

Graphs showing arrival time of the head-wave as a function of distance and amplitude of the head-wave as a function of distance are shown in figures 5-10, inclusive. These figures also

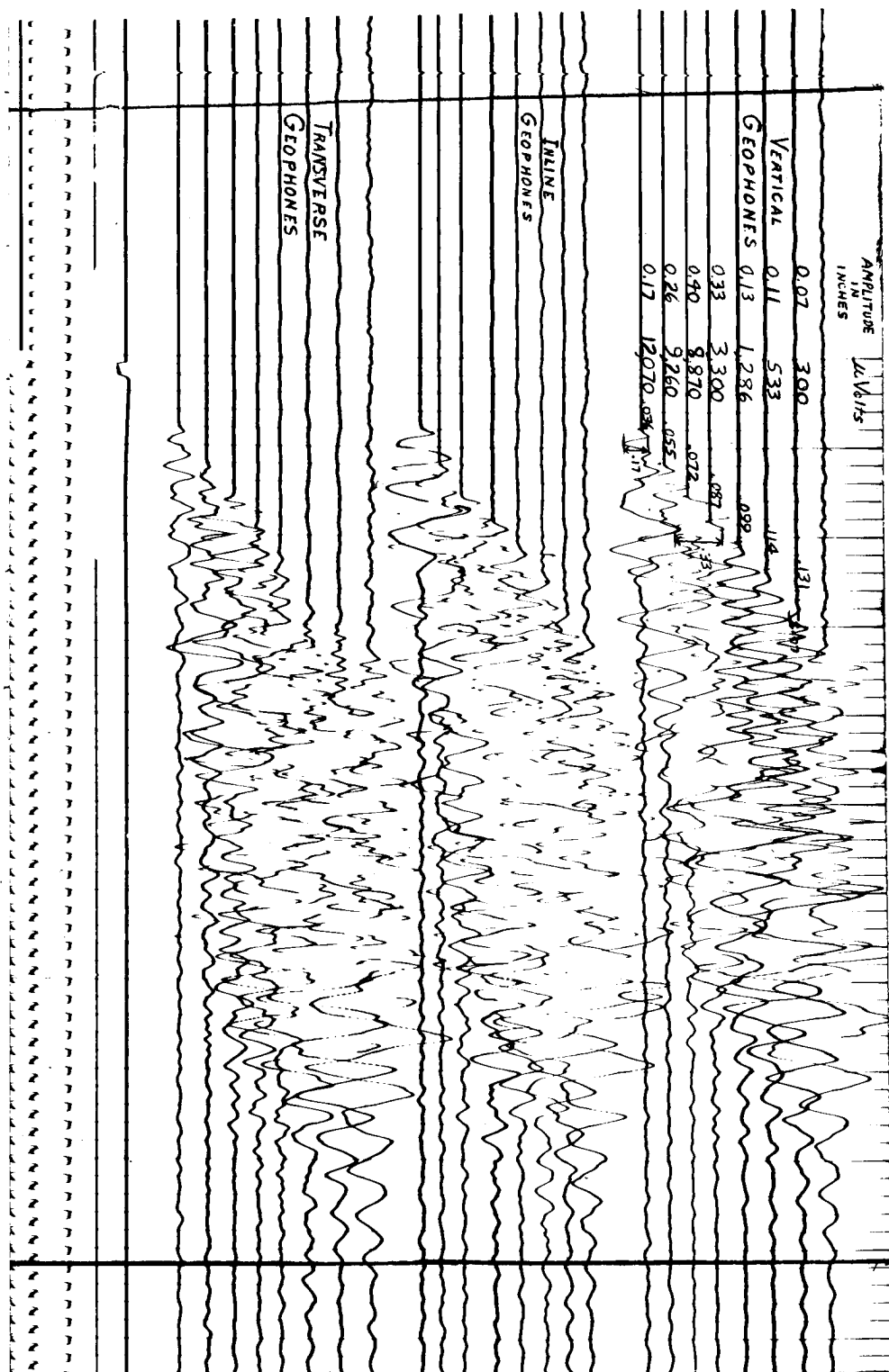Figure 4. Sample field record showing how amplitudes are measured.

Figure 5. Arrival time of head-wave energy as a function of distance on Profile J, Cinder Hills.

KANA-A FLOW PROFILE W

$$A = Ke^{-.02d}$$

Figure 6. Variation of voltage amplitude as a
  function of distance on Profile W, Kana-a Flow.

Figure 7. Arrival time of head-wave energy as a function of distance on Profile A, Southern Coulee.

BISHOP TUFF   PROFILE A

$A = Ke^{-.08d}$

Figure 8.   Variation of voltage amplitude
as a function of distance on Profile A,
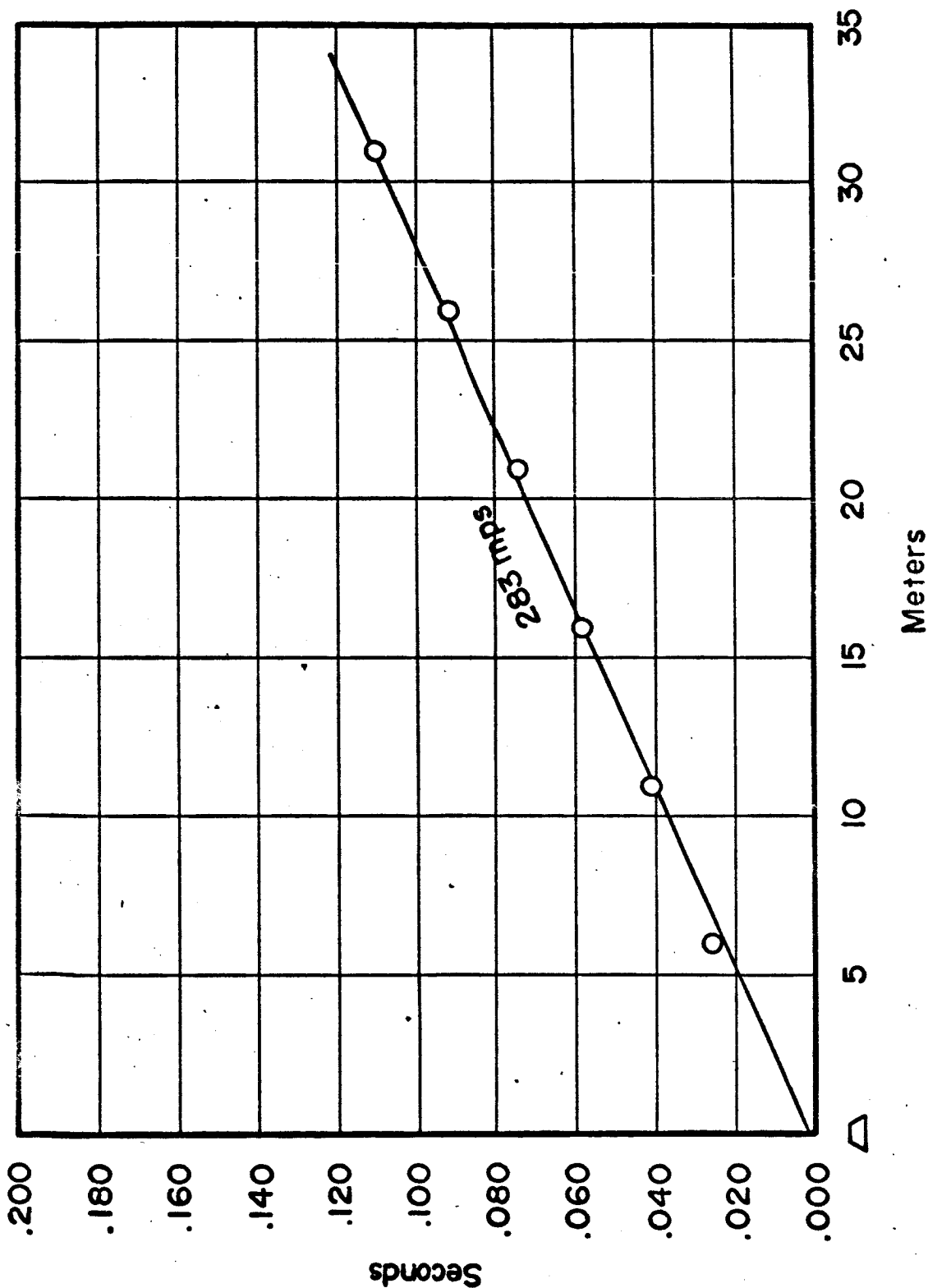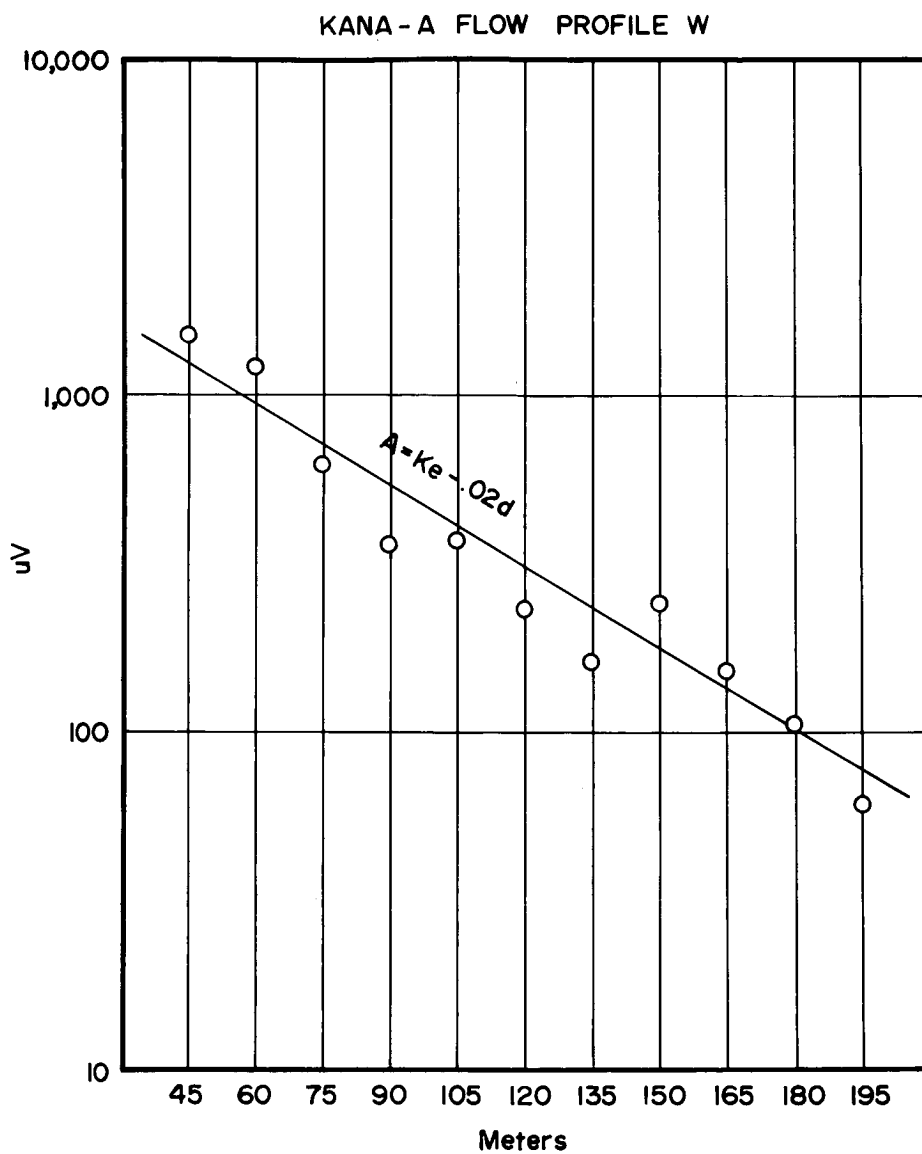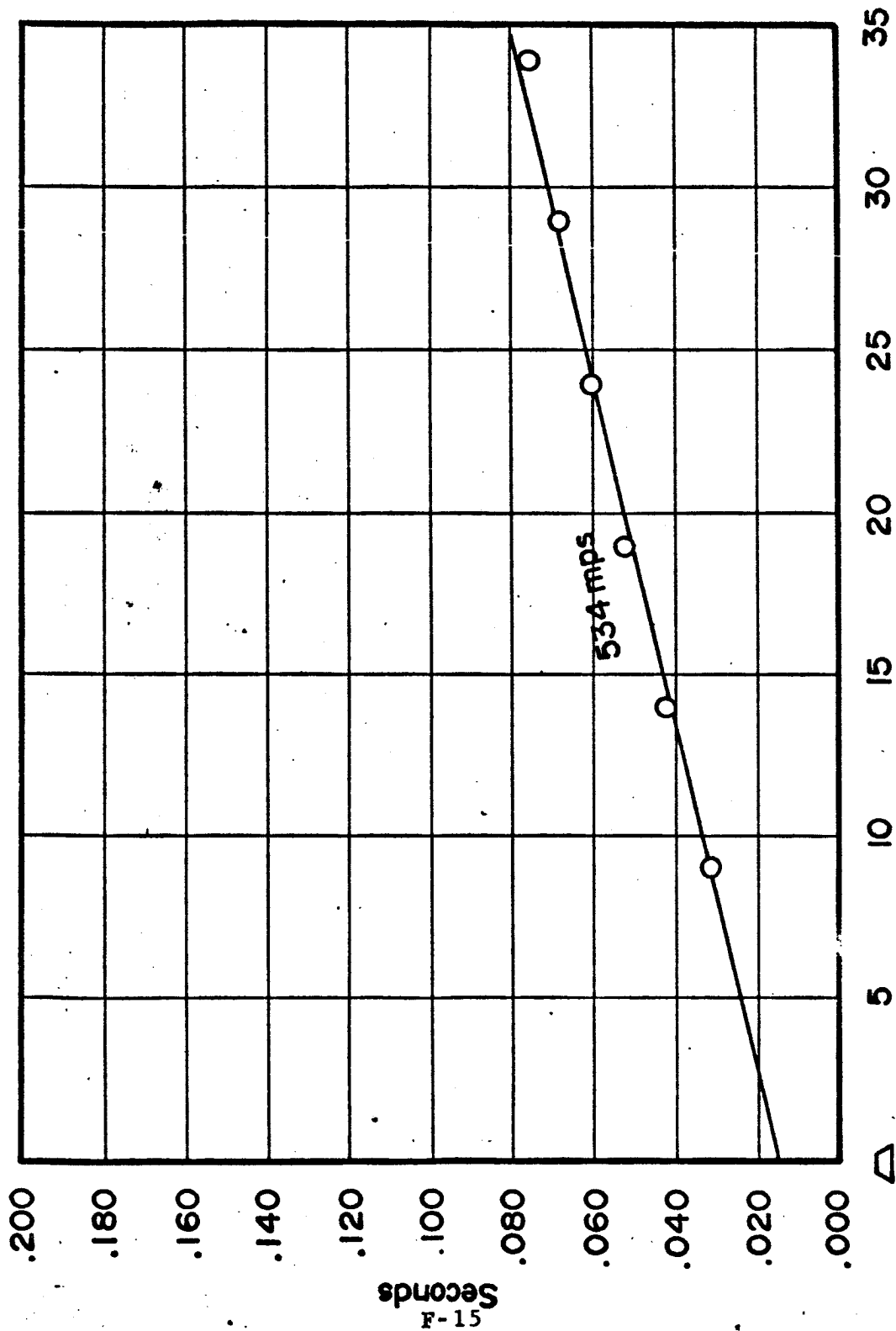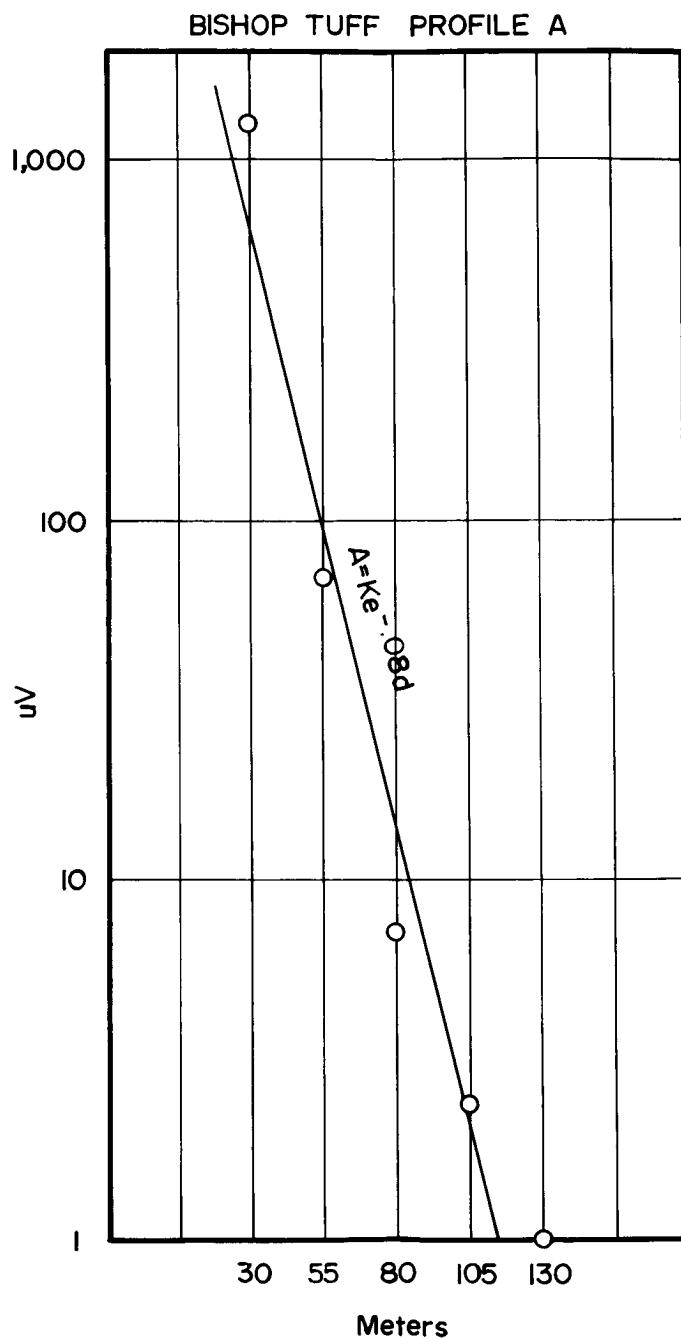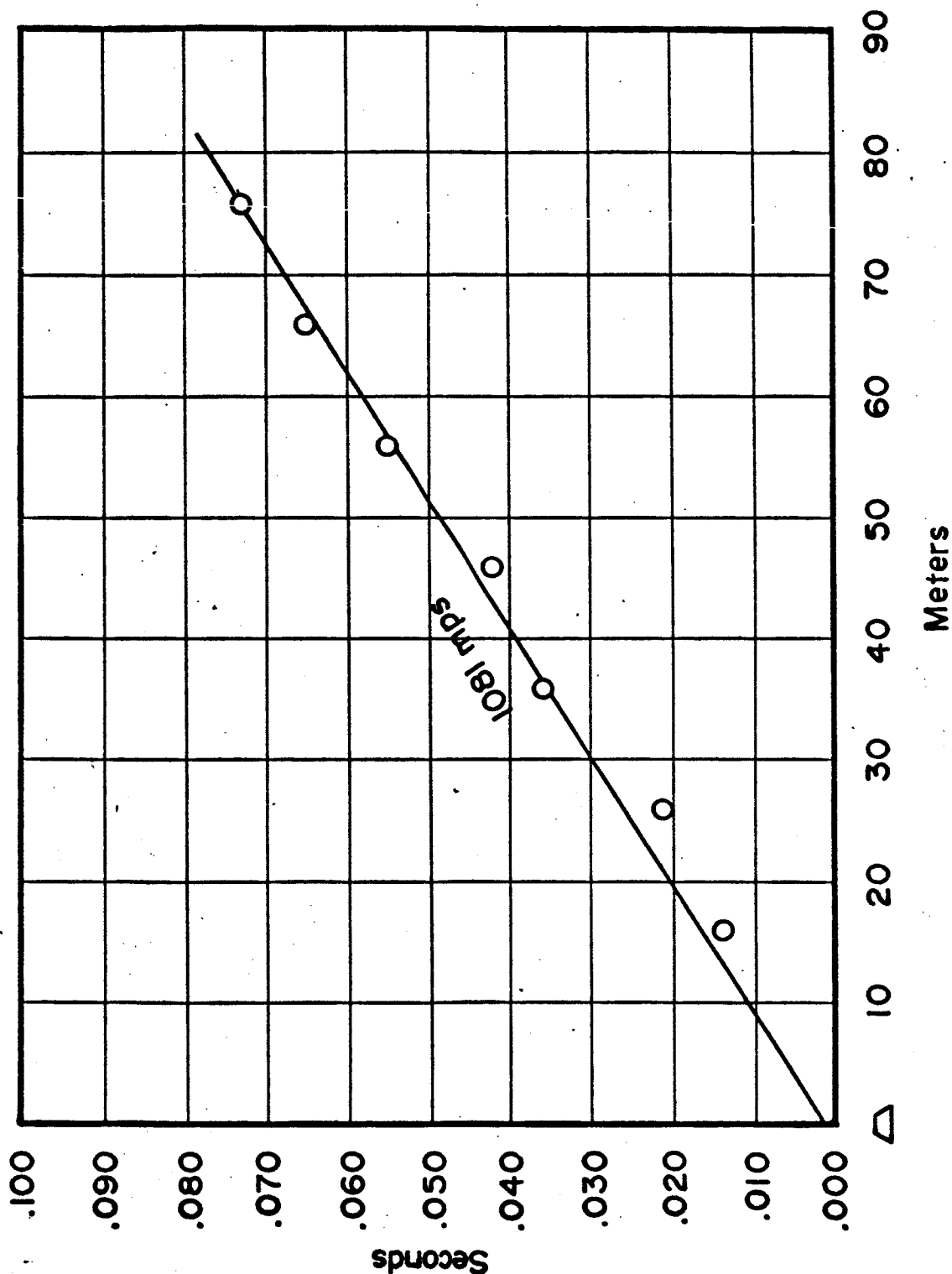Bishop Tuff.

PISGAH FLOW PROFILE T

Figure 9. Arrival time of head-wave energy as a function of distance on Profile T, Pisgah flow.
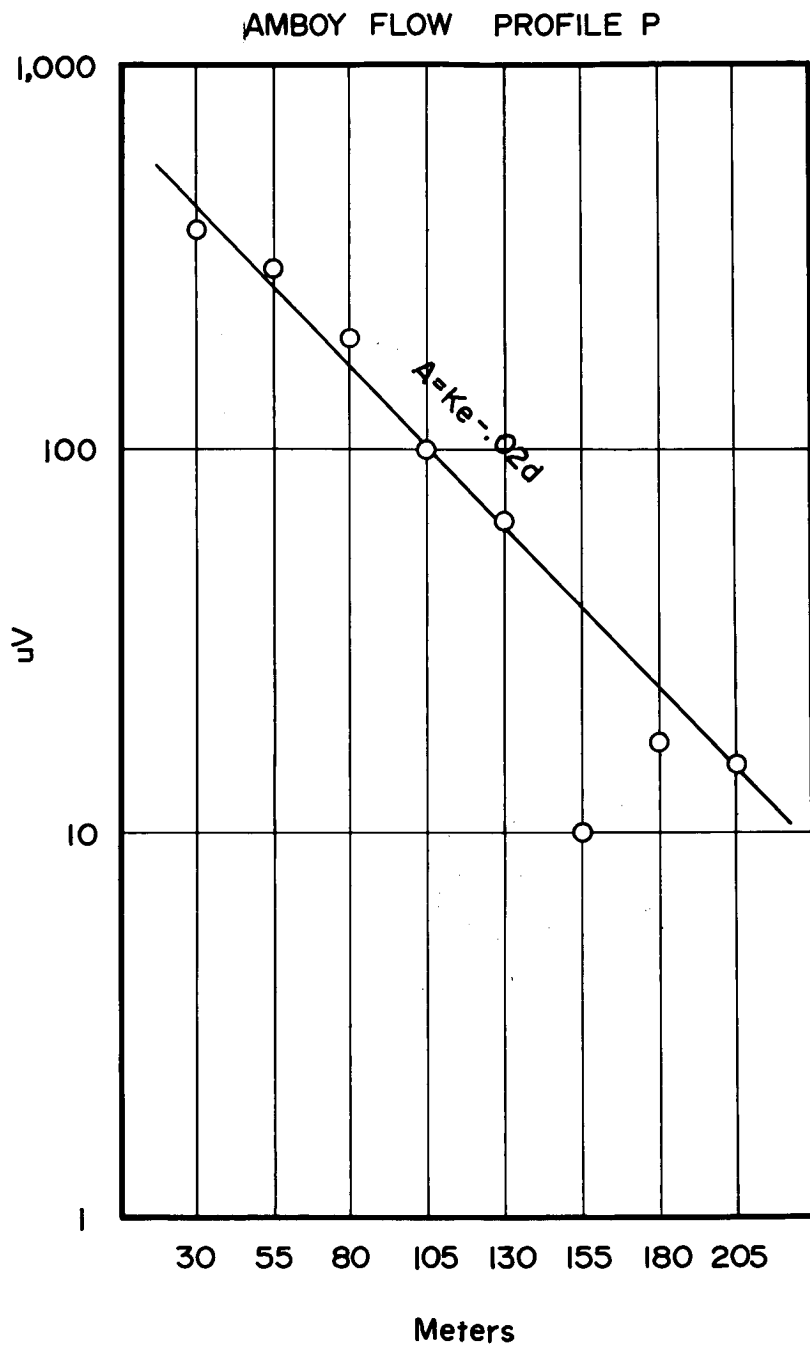
Figure 10. Variation of voltage and amplitude
as a function of distance on Profile P,
Amboy Flow.

include typical data from the Amboy and Pisgah lava flows of
the Mojave desert in southern California. Analysis of Amboy and
Pisgah data, however, is not yet complete and these data are not
included in the tabular and graphical summaries shown in figures
11, 12 and 13.

Figure 11 consists of a tabular summation of data from
spreads shot at the 8 sites mentioned above; figures 12 and
13 consist of graphical presentation of the above data.

Figure 12 shows a plot of Q_α as a function of α. The
data fall into groups when Q_α is plotted as a function of α,
but it is not at all clear what the relationship of Q_α to other
physical properties of the material may be.

Figure 13, which shows $Q_\alpha \alpha$ plotted as a function of α,
although the physical significance of this relationship to
other physical properties is understood no better than the physical
relationship of Q_α and α, is an empirically more useful repre-
sentation. With the exception of the Bishop Tuff, the velocity
appears to be a function of the porosity of the material,
whereas $Q_\alpha \alpha$ is a function of fracturing. When more coring
data are available, we hope to more quantitatively re-
late porosity, fracturing, velocity and $Q_\alpha \alpha$.

KAIBAB		
SPREAD	Qα α	α
E	6,680	2385
F	5,600	2500
G	7,850	2555

S.P. FLOW		
SPREAD	Qα α	α
A	1,950	790
B	2,550	1000
C	2,020	1080
D	2,180	775
E	2,330	1060
F	2,460	1120

KANA-A FLOW		
SPREAD	Qα α	α
N	4,680	872
P	2,540	395*
Q	4,100	1205
R	2,910	309*
T	4,460	769
U	4,900	752
W	4,660	882
X	6,070	1032

CINDER HILLS		

SPREAD	Qα α	α
J	2,640	283
K	2,430	286
K	2,360	319
L	2,580	309
M	2,570	325
N	2,300	366
O	2,440	319

SONORA PASS		
SPREAD	Qα α	α
A	11,800	5000
B&D	12,500	5000
C	17,100	5000
C	12,700	5000
D	12,800	5000

MONO ASH		
SPREAD	Qα α	α
A-1	2,100	525
A-1	7,950	1765
A-2	2,280	547
B	2,470	487
C	2,440	455
D-6	2,516	534
D-8	2,590	487

MONO ASH CONT.		
SPREAD	Qα α	α
E	5,050	1680
E	2,220	458
F	2,640	421
G-11	2,490	611
G-12	2,110	568
H	5,500	2080
H	2,440	512
I	1,900	421
J-2	1,820	512
J-1	1,780	514
K	2,320	460
L	2,620	459
M-8	2,280	510
M-7	5,350	1780
N	2,090	452
O	1,630	473
P-10	2,160	564
Q	2,530	491
R	2,640	455
S-1	2,720	500
T	6,150	2050
T	2,560	434

* SHOT IN CINDERS PLOTTED UNDER CINDER HILLS

Figure 11. Tabular summary of attenuation constants ($Q_\alpha\alpha$) and velocities (α) of records processed through June 30, 1965.

MONO ASH CONT.		
SPREAD	$Q\alpha\alpha$	α
V-5	2,380	567
V-6	2,760	568
W-7	7,180	1640
W-7	2,700	488
W-8	2,450	500
X	2,200	508
Y-11	7,140	2038
Y-12	9,690	2285
Z-15	6,150	2220
Z-16	2,520	536
Z-16	7,500	1839
SOUTHERN COULEE		
SPREAD	$Q\alpha\alpha$	α
A	1,550	534
B-4	1,700	975
B-6	1,290	975
D	1,710	658
E-2	1,760	455
E-3	1,510	541
F	1,510	500
L-1	1,190	476
M-1	2,480	1570

SOUTHERN COULEE CONT.		
SPREAD	$Q\alpha\alpha$	α
M-2	2,010	1570
N	1,740	1280
P-8	1,820	980
S	1,880	768
T	2,070	1345
U	1,360	426
Y	1,250	857
Z	1,930	391
AA	2,610	350
DD	2,180	445
FF-10	3,190	1200
FF-9	2,230	1200
GG-11	1,600	400
GG-12	2,510	1668
BISHOP TUFF		
SPREAD	$Q\alpha\alpha$	α
A-2	5,130	1700
A-4	4,080	1700
B	5,400	1950
C	6,130	1950
D	5,750	1495

BISHOP TUFF CONT.		
SPREAD	$Q\alpha\alpha$	α
E	4,220	1600
F	5,130	1600
G	5,810	1732
H	4,800	1942
I	4,380	1900
J	3,830	1503
K	5,950	1429
L	5,120	1430
M	5,310	1850
N	6,230	2000
O	5,320	1840
P	3,830	1755
Q	4,720	1816
R	4,700	1765
S	5,230	1610
T-6	4,010	1430
T-7	3,960	1430
U	5,300	1430
V	4,230	1515
W	5,450	1820
X	5,820	1665

Figure 11 (continued)
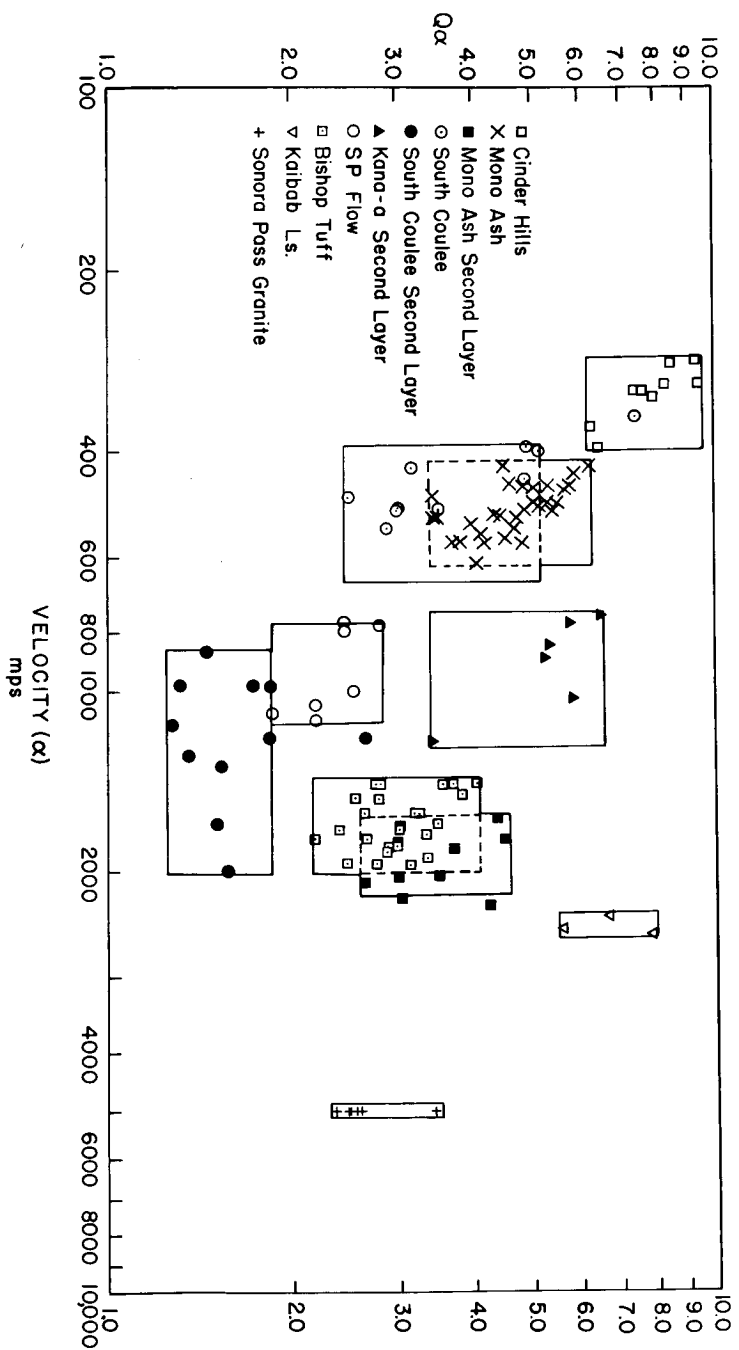
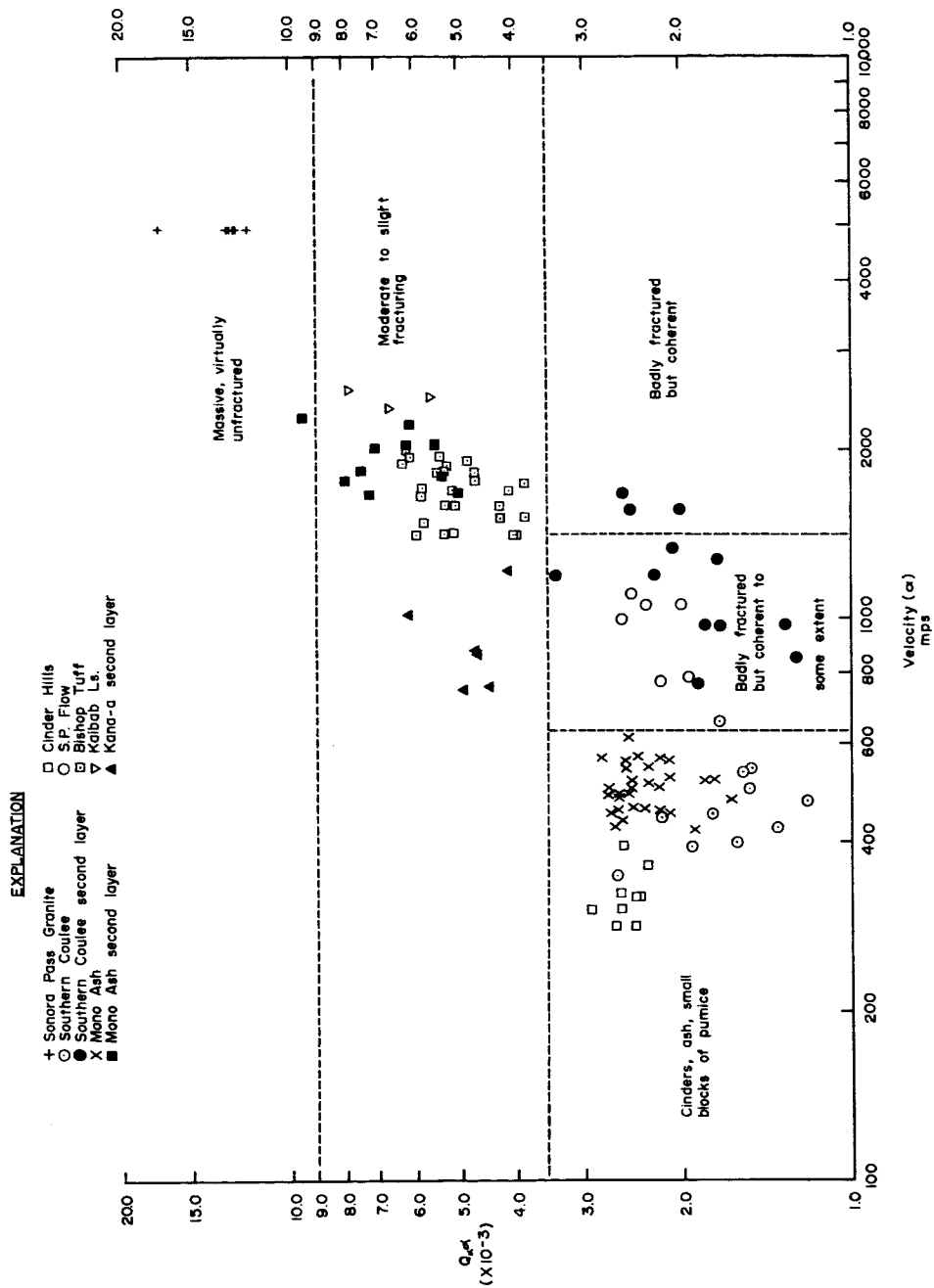Figure 12 Variations of Q_α as a function of velocity for areas studied through June 30, 1965.

Legend:
□ Cinder Hills
× Mono Ash
■ Mono Ash Second Layer
⊙ South Coulee
● South Coulee Second Layer
▲ Kana-a Second Layer
○ SP Flow
□ Bishop Tuff
▽ Kaibab Ls.
+ Sonora Pass Granite

Q_α

VELOCITY (α)
mps

Figure 13. Variation of $Q_\alpha\alpha$ as a function of velocity for areas studied through June 30, 1965.

The sensitivity of $Q_\alpha \alpha$ and the amplitudes in general to fracturing has already lead to the detection of the cone of fracturing above an underground nuclear explosion and may in the future prove valuable for location of fault zones or other fractured areas of the earth's crust.

SUMMARY

A total of 512 recordings at 220 spread locations at 11 sites have been made during fiscal year 1965. Sites include 8 on volcanic terrane, one on limestone, one on granite and one at Meteor Crater, Arizona.

The data suggest that amplitudes of P head-waves in near-surface media are strongly dependent on the degree of fracturing whereas velocities seem more dependent on porosity and degree of cementation.

The data have formed the basis of estimates of amplitude and attenuation incorporated into a proposed lunar engineering seismic experiment and have also been used in the detection of a fractured zone above an underground nuclear explosion.

PART III

Proposed
Work Plan and Operating
Budget, FY-66 and FY-67

"INVESTIGATION OF IN SITU PHYSICAL PROPERTIES
OF SURFACE AND SUBSURFACE SITE MATERIALS BY
ENGINEERING GEOPHYSICAL TECHNIQUES" Project

by

Joel S. Watkins

U. S. Geological Survey
Flagstaff, Arizona

Part III

Proposed
Work Plan and Operating
Budget, FY-66 and FY-67

"Investigation of In Situ Physical Properties
of Surface and Subsurface Site Materials by
Engineering Geophysical Techniques" Project

by

Joel S. Watkins

U. S. Geological Survey
Flagstaff, Arizona

INTRODUCTION

On the basis of project results summarized in Part I and
detailed to some extent in Part II of this report, it is
recommended that the investigation be continued through fiscal
years 1966 and 1967 in order to complete studies in three
areas, (1) attenuation characteristics of seismic energy in
lunar analog materials, (2) shear wave propagation in lunar
analog materials, and (3) geophysical investigations of craters.

Although attenuation of seismic energy in lunar analog
materials has been measured at eleven sites, gaps exist in the
data which we wish to fill. It is thought that five additional
sites will be sufficient. Measurement of shear wave velocities
in lunar analog materials has lagged far behind other measure-
ments because of the inadequacy of conventional detectors but
rotational accelerometers, it was found late in fiscal year 1965,
overcome many problems inherent in translational transducers.
Because of the great potential of simultaneous recording of P-
and S-wave velocities, it is considered essential that the 11
test sites previously used for measurements of P-wave velocities
be reoccupied for S-wave velocity measurements. Measurement of
S-waves with rotational accelerometers will also be included in
studies of the five new sites.

Geophysical studies at Meteor Crater, Arizona, although incomplete, suggest that geophysical studies of lunar impact craters would provide information of significant value about their structure. The next logical step appears to be detailed studies ·of a maar crater such as the Lunar Crater of Nevada or Ubehebe Crater in California. Such a survey would be useful for planning surveys of lunar maar craters, might provide new information about the subsurface structure associated with the maar crater, and might provide data about structural similarities and dissimilarities of impact and maar craters.

During investigation of Meteor Crater and other sites, information has been obtained about optimum conduct of gravity, magnetic, radiation and seismic surveys of lunar structures. Similar data will probably be obtained at Ubehebe and other sites studied during fiscal years 1966 and 1967. Small impact craters created by rocket impacts are available for study at White Sands Proving Grounds. A week may be devoted to study of these craters.

Geologic mapping, petrography and coring of the 11 original and 5 proposed study sites are not yet complete. It is proposed that these efforts also be continued during fiscal years 1966 and 1967.

New study areas.-- As with many investigations, some data collected by this project during fiscal years 1964 and 1965 suggest new and important studies outside the scope of the original work plan. Our cavity data constitute the most obvious case. These data suggest that seismic surveys can locate underground cavities caused by volcanism, fracture zones in the lunar crust, and exposed or buried cracks in the lunar crust. Because underground cavities can provide safe natural shelters for astronauts and their equipment from meteoroid showers or may constitute hazards during traverses of the lunar surface, continued study of seismic phenomena associated with cavities is deemed essential.

It has also been found that frequency and coupling characteristics vary with type and size of source, nature of surface material, and physical configuration of the source-media contact. A topical study of one year's duration at a 3 man-year level seems desirable. These data would permit more efficient use of energy sources on the lunar surface where an excss of explosive can create a hazard or require prohibitively deep shot holes.

The original work plan could be amplified to encompass some but not all the new studies suggested by our data. Therefore, a comprehensive proposal covering new studies such as those outlined in previous paragraphs will be prepared and submitted in the first quarter of fiscal year 1967.

Attenuation characteristics.-- Figure 1 summarizes velocity-attenuation data collected and analyzed during fiscal years 1964 and 1965. $Q_0\alpha$ is an attenuation function defined in Part II of this report. Velocity (α) is that of the head wave.

It can be seen that our data have gaps between massive rocks and fractured rocks, between the fractured rocks and badly fractured rocks, and it is suspected that a fine, dry powder might give data in the very low $Q_0\alpha$ - very low α range such as might exist on the surface of the moon. Five study sites listed below are proposed for fiscal years 1966-67 to fill gaps in these data. Data from these sites would complete the data spectrum. Further attenuation studies are not contemplated beyond FY-67.

1. White Sands, New Mexico--The White Sands consist of fine gypsum sand. The low density of gypsum and the powdery nature of the deposit are expected to provide data in the very low α--low $Q_0\alpha$ range. Quartz sands were considered but rejected because most quartz sands have a thin film of absorbed water around the grains. Gypsum, because of its ability to incorporate water within its crystal structure, is thought to be less likely to have an absorb layer and hence respond as a completely dry material. It may also be possible to collect structural data on small impact craters created by rocket impacts at the White Sands Proving Grounds.

2.. Slightly cemented sandstone--An outcrop of Navajo Sand-stone at Middle Mesa, approximately 25 miles northeast of the junction of Highways U.S. 84 and State 64 in Coconino County, Arizona, has been selected as the second study area. The Navajo Sandstone is slightly cemented and has a porosity of approximately 28 percent.
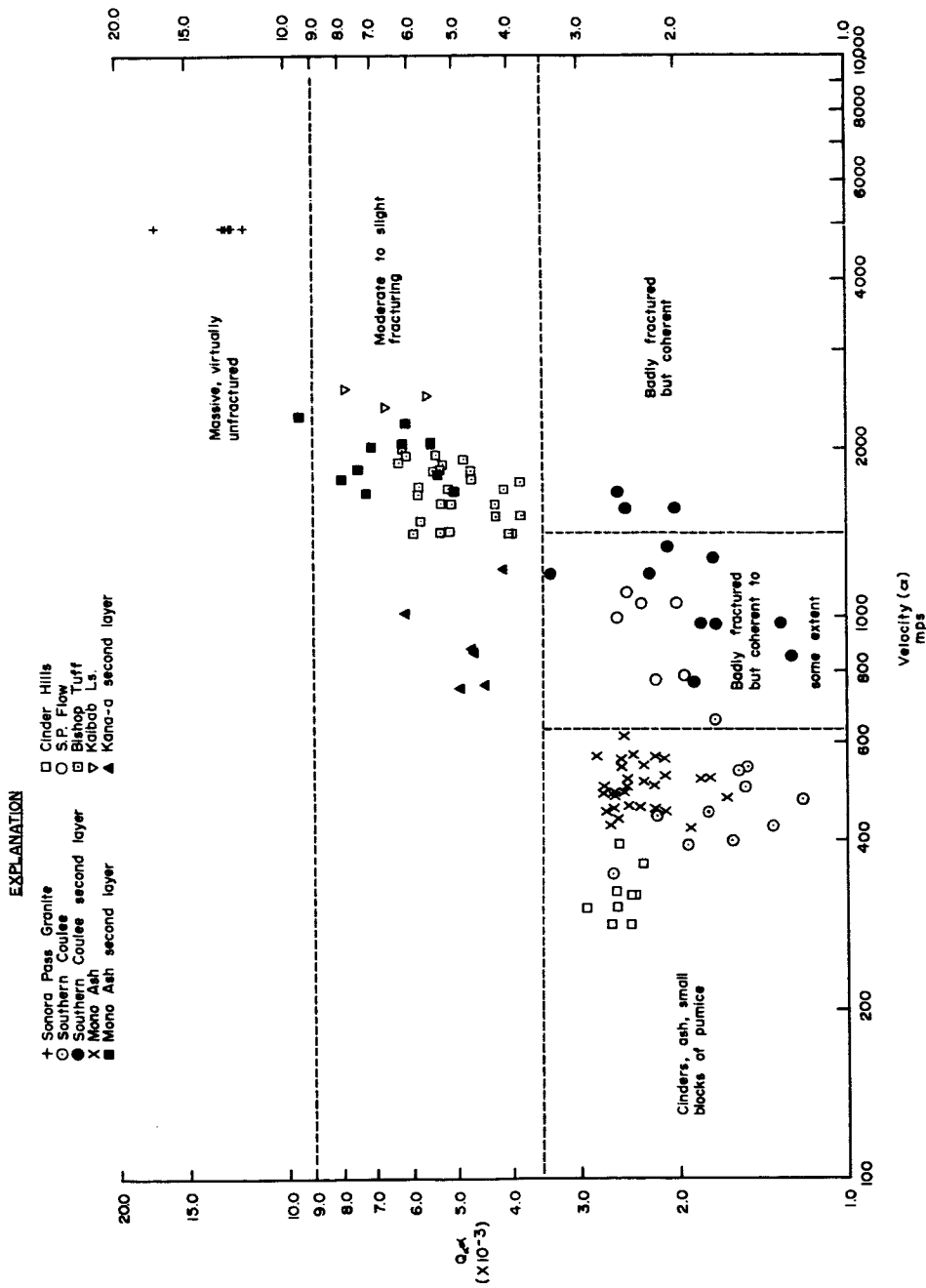
Figure 1. Variation of $Q_\alpha \alpha$ as a function of velocity for areas studied through June 30, 1965.

Data from this site may fill the gap between fractured and badly fractured rocks.

3. Moderately cemented sandstone--The third area consists of an outcrop of Coconino Sandstone, approximately five miles south southeast of Holbrook, Arizona. The Coconino Sandstone is moderately cemented and has porosities ranging from 7 to 14 percent. Data from this site are expected to help fill the gap between massive and fractured rocks.

4. Quartzite--Two localities of strongly cemented quartzite have been selected for study. Both are located between Young, Arizona, and Roosevelt Dam, Arizona. In one area the quartzite is not fractured vertically to any extent but does have prominent bedding planes at intervals of 0.3 - 1.0 m. The second site is massive with respect to bedding, but is vertically fractured to some extent. However, the fractures are filled with soil and may be recemented at depth. Data should fill the gap between massive and fractured rocks.

5. Very weakly cemented sandstone--Subject to the results from the Navajo Sandstone, it may be desirable to obtain data from a very weakly cemented sandstone or conglomerate such as the Tertiary and Quaternary alluvium which fills many of the intermontane basins of Arizona, southern California, and southern Nevada. No specific site has been selected as yet. These data may be necessary to fill the gap between fractured and badly fractured rocks.

Shear wave velocities.-- Simultaneous measurement of shear (S) and compressional (P) wave velocities provides the only direct means of calculating elastic constants in situ. Consequently, a significant part of project effort has been devoted to developing techniques for producing and detecting S-wave motion in lunar analog materials. The only good results to date have been obtained by recording with rotational accelerometers which are

6

sensitive to the rotational component of S-wave motion but in-
sensitive to purely translational motion of P-waves. Details
of our investigations of S-waves are summarized in Part II of
this report. The usefulness of rotational accelerometers was
confirmed late in fiscal year 1965 and no site studies have
been completed yet.

Because of the importance of in situ S-wave velocity
measurements, it is considered necessary to reoccupy each of
the 11 sites studied in fiscal years 1964 and 1965 for shear
wave measurements. Site reoccupations will consume significantly
less time and effort than the original occupations because per-
mitting, geology, surveying, and other peripheral operations need
not be redone. S-wave velocity measurements will be integrated
into field operations at the five new sites.

Crater surveys.-- The geophysical survey of Meteor Crater
has shown that (1) the thickness of the ejecta blanket can be
measured by seismic refraction, (2) the bottom of the ejecta
blanket on the Crater rim and brecciated zone within the Crater
can probably be detected by seismic reflection, and (3) that
radiation and magnetic anomalies exist on the south rim. The
significance of these anomalies cannot be fully evaluated until
the survey and coring operations are completed in fiscal year
1966. Gravity data calculations will also be completed in the
first half of fiscal year 1966. Data analyzed to date give a
reasonably complete picture of the subsurface structure and
complementary radiation, magnetic and gravimetric data promise
to yield information about the distribution of meteoric frag-
ments within the rock as well as additional information about
the extent and degree of brecciation.

The apparent success of geophysical surveys at Meteor
Crater is rewarding not only because of the additional data on
the structure, but most important because success at Meteor
Crater implies that these techniques can be used successfully
to study the larger impact craters of the lunar surface.

7

Successful application of geophysical techniques at
Meteor Crater also suggests that these same techniques should
be applied to study of a maar crater. Final selection of a
site has not been made pending reconnaissance but Ubehebe in
Death Valley, California, is both proximate to project head-
quarters and an excellent example of a maar crater. Lunar
Crater of Nevada is an almost equally atractive alternative
site.

It should also be noted that whereas Meteor Crater has
been drilled and mapped in detail, neither Ubehebe nor Lunar
Crater has. Consequently, in contrast with Meteor Crater
where geophysical data merely confirm previous information,
a geophysical survey of a maar crater will provide a body of
new information about the geologic structure associated with
the crater.

Distribution of effort.-- Figure 2 summarizes the planned
distribution of project manpower during fiscal year 1966, 1967,
and 1968. The manpower commitment to the in situ project
presently stands at 17 man years; of which 9 are committed to
seismic operations including 3/4 of the project chief's time,
two other full-time geophysicists and one quarter-time geo-
physicist. This group is responsible for collection, analyses,
and interpretation of the geophysical data.

The geologic effort consists of a geologist, driller,
and three physical science technicians, one of whom devotes
full-time to measurement of physical properties of rock cores.

The administrative staff consists of a full-time secretary,
1/4 of the project chief's time, and part-time effort of several
members of the Branch of Astrogeology duplicating, photographic,
purchasing, and administrative units.

As shown in figure 2, project manpower commitments will be
gradually reduced during fiscal year 1967 and the project will
be terminated at the middle of fiscal year 1968. Field operations
and the bulk of data analysis will be completed by the end of

8

Figure 2

IN SITU MANPOWER DISTRIBUTION

Fiscal Years 66, 67 and 68

9
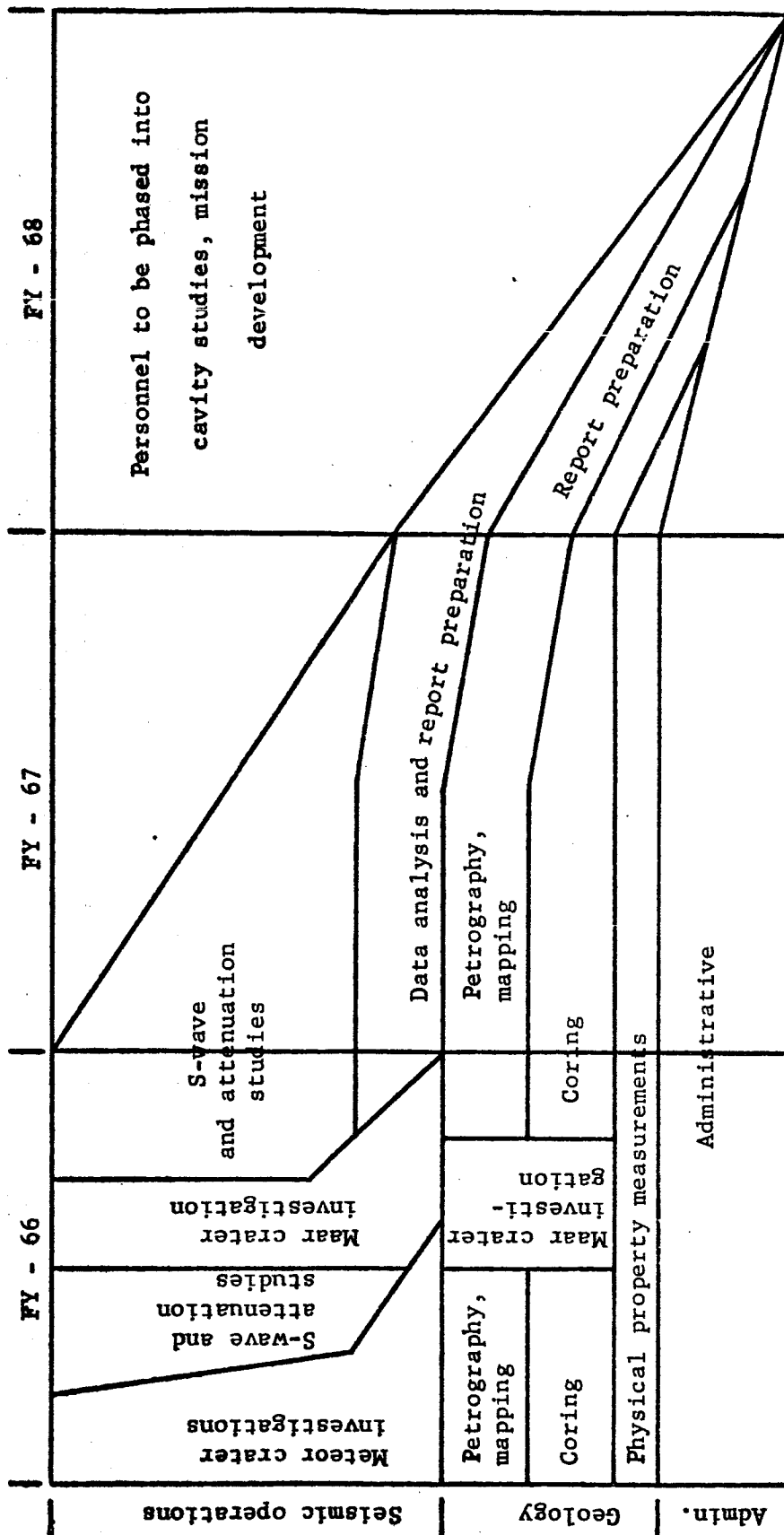
fiscal year 1967 and the small group remaining in fiscal year 1968 will devote almost all of their effort to preparation of a final comprehensive report of project operations.

Personnel phased out of the in situ project will go into the follow-up projects in order to take full advantage of skills developed during the in situ work and to prevent the usual delay initiating a new project.

The in situ project will be terminated with the publication of the final report in fiscal year 1968.

BUDGET

Projected budgets for fiscal years 1966, 1967 and 1968 are as follows:

Fiscal year 1966
(17 man-years)

Salaries	$180,000
Field operations	60,000
Administrative travel	5,000
Computer operations	30,000
Equipment	25,000
	$300,000

Fiscal year 1967
(13 man-years)

Salaries	$127,000
Field operations	43,000
Administrative travel	5,000
Computer operations	30,000
Equipment	10,000
	$215,000

Fiscal year 1968
(4 man-years)

Salaries	$53,000
Administrative travel	5,000
Computer operations	10,000
	$68,000

REPORTS

Progress reports will be submitted to the National Aeronautics and Space Administration within 30 days of the end of each fiscal year; significant scientific discoveries will be reported at national scientific meetings and in appropriate journals; and representatives of the National Aeronautics and Space Administration and the U. S. Geological Survey will meet at least once each quarter to review project progress.